AN ABSTRACT OF THE THESIS OF

Laurie Lynn Broderick for the degree of Doctor of Philosophy

in Civil Engineering presented on July 25, 1991

Title: Interaction of Water Waves and Deformable Bodies

Abstract approved: Redacted for Privacy

Dr. John W. Leonard

A time-domain model was developed to predict the fluid/structure interaction of a three-dimensional deformable body in a fluid domain subject to long-crested finite amplitude waves. These nonlinear waves induce transient motion in the body. In turn, the interaction of the body with the waves modifies the wave field, causing additional motion in the body. A time-domain simulation was required to describe these nonlinear motions of the body and the wave field. An implicit three-dimensional time-domain boundary element model of the fluid domain was developed and then coupled iteratively with a finite element model of the deformable body.

Large body hydrodynamics and ideal fluid flow are assumed and the diffraction/radiation problem solved. Either linear waves or finite amplitude waves can be treated in the model. Thus the full nonlinear kinematic and dynamic free surface boundary conditions are solved in an iterative fashion. To implicitly include time in the governing field equations, Volterra's method was used. The approach is similar to that of the typical boundary element method for a fluid

domain where the boundary element integral is derived from the governing field equation. The difference is that in Volterra's method the boundary element integral is derived from the time derivative of the governing field equation. The transient membrane motions are treated by discretizing the spatial domain with curved isoparametric elements. Newton-Raphson iterations are used to account for the geometric nonlinearities and the equations of motion are solved using an implicit numerical method.

Examples are included to demonstrate the validity of the boundary element model of the fluid domain. The conditions in a wave channel were numerically modeled and compared to sinusoidal waves. The interaction of a submerged rigid horizontal cylinder with water waves was modeled and results compared to experimental and numerical results. The capability of the model to predict the interaction of highly deformable bodies and water waves was tested by comparing the numerical model to large-scale physical model experiment of a membrane cylinder placed horizontally in a wave channel.

Interaction of Water Waves

and

Deformable Bodies

by

Laurie Lynn Broderick

A THESIS

submitted to

Oregon State University

in partial fulfillment of
the requirements for the
degree of

Doctor of Philosophy

Completed July 25, 1991

Commencement June 1992

APPROVED:

Redacted for Privacy

Professor of Civil Engineering in charge of major

Redacted for Privacy

Head of Department of Civil Engineering

Redacted for Privacy

Dean of Graduate School

Date thesis is presented 25 July 1991

Typed by Laurie Lynn Broderick for Laurie Lynn Broderick

ACKNOWLEDGEMENT

I would like to thank my major advisor, Dr. John W. Leonard for his enduring support, encouragement, guidance, understanding and enthusiasm. Thanks are also due to other faculty members who have acted as advisors and committee members; Dr. D. J. Bushnell, Dr. C. J. Garrison, Dr. R. T. Hudspeth, Dr. W. G. McDougal, Dr. C. K. Sollitt and Dr. R. E. Wilson.

Chris Jenkins, a fellow doctoral student, deserves special recognition, especially for his work and support in conduction of the physical model test and for the moral support he constantly provides.

Special thanks go out to Cheryl Zedwick and Naomi Krant, because without their support and guidance this thesis may never have been completed.

Finally, no amount of gratitude can adequately repay my family and friends, for their inspiration, support and sacrifice during the past few years. To all of you I am deeply indebted.

This research is based upon work supported by the USN Office of Naval Research under the University Research Initiative, Contract Number N00014-86-K-0687. Access to the Cray-YMP at the University of Illinois at Urbana-Champaign, National Center of Super Computing Application was made through Grant Number TRA-890382N. I gratefully acknowledge this support.

TABLE OF CONTENTS

LIST OF FIGURES

LIST OF APPENDIX FIGURES

LIST OF APPENDIX TABLES

LIST OF SYMBOLS

$A_{\alpha B}$ metric tensor

A determinant of metric tensor

B_i body force per unit mass of undeformed membrane

C_1 material constant for Hyperelastic material

C_2 material constant for Hyperelastic material

$C(\vec{\xi})$ variable of integration

D water depth

D body diameter (used in Chapter 1)

$e_{\alpha B}$ strain tensor

E Young's modules

F_i concentrated loads

G Green's function

g acceleration due to gravity

g_{ii} metric tensor

H wave height

h thickness of membrane

J_s jacobian

L wave length

M membrane surface

N^{ij} contravariant stress resultant due to static and dynamic load measured with respect to undeformed membrane

$\vec{n}$ unit normal

P,p pressure

Q Bernoulli's constant

$\vec{q}$ fluid velocity

$\vec{r}$ the Green's function vector from the influence point to the source point

S surface

SMS_f Stokes Material Surface of the free surface

SWL Still Water Level

T wave period

T_i traction per unit surface area of undeformed membrane

t_f fluid time scale

t_m membrane time scale

t_r time scale ratio

$\vec{U}$ membrane displacement

$\dot{\vec{U}}$ membrane velocity

$\ddot{U}_i$ membrane acceleration components

V volume

x_i spatial coordinate

γ the angle between the unit normal vector and the Green's Function $-\vec{r}$

δe_{ij} virtual strain tensor

δU_i virtual displacement components

ζ characteristic dimension of membrane

η free surface

Θ wave direction

λ principal extension ratio

μ dynamic viscosity of fluid

σ surface tension of fluid

σ^{ij} contravariant stress due to static and dynamic loads measured with respect to undeformed membrane

${}^{I}\rho$ fluid density - Region I

${}^{II}\rho$ fluid density - Region II

${}^{f}\rho$ fluid density

${}^{m}\rho$ membrane density

ϕ velocity potential

Ψ_i shape functions

INTERACTION OF WATER WAVES AND DEFORMABLE BODIES

CHAPTER 1 INTRODUCTION

1.1 OBJECTIVE AND SIGNIFICANCE

The objective of this study was to develop and verify a numerical model of the interaction between a highly deformable fluid-filled body and ocean waves. This system was conceived as a membrane enclosing a pressurized, incompressible fluid placed in a fluid domain and subjected to long-crested, finite-amplitude waves, i.e. a two-dimensional sea state, with an approach angle Θ. The fluid-structure interaction has been modeled with a coupled boundary element model (BEM) and a finite element model (FEM). The BEM models the fluid domains and the FEM models the structure. The coupling is done through the pressure, velocity, and position of the fluid/structure interface.

The model will permit designers to determine the effectiveness of fluid-filled membranes as engineering structures, i.e. temporary, rapidly-deployable floating breakwaters; semipermanent enhancement of existing fixed breakwaters; and bladder barges or storage depots.

1.2 ASPECTS OF THE PROBLEM

1.2.1 Methods

When a fluid-filled structure is placed in a fluid domain and subjected to long crested, finite-amplitude waves with an approach angle Θ, the structure undergoes large rigid motions and large deformations. The structure's presence

and motions alter the local wave field, producing scattered and radiated waves. These local wave field disturbances will in turn cause additional motions in the structure, and the cycle of wave-structure interaction continues. Figures 1.1 and 1.2 are schematics of the physical problem under study.

The submerged structure was modeled as a membrane enclosing a pressurized, incompressible fluid. Membrane structures are generally considered tension elements and can not support compressive loads. Because their thicknesses are small compared with other dimensions, their stiffnesses in flexure and compression are negligible. They are quite flexible in their unstressed states and obtain rigidity by developing tensile stress under the action of external loads.

Membranes encapsulating a pressurized medium maintain their form and rigidity against external loads because of internal pressure. Rather than point loads, they are best suited for supporting broadly distributed loads and/or dynamic loads such as those encountered in the ocean. Membranes are extremely sensitive to changes in external loadings; to accommodate load changes they simply change shape. Small changes in the loads can result in very large distortions, Leonard (1988). These large distortions present difficulties in the use of conventional linear analysis, which assumes small displacements. Therefore, nonlinear wave theory (finite amplitude wave heights) and nonlinear membrane theory were used in this study of wave-structure interaction.

To estimate the wave-induced hydrodynamic loadings on a structure, either a "small" or "large" body analysis is used, Sarpkaya and Isaacson (1981). The

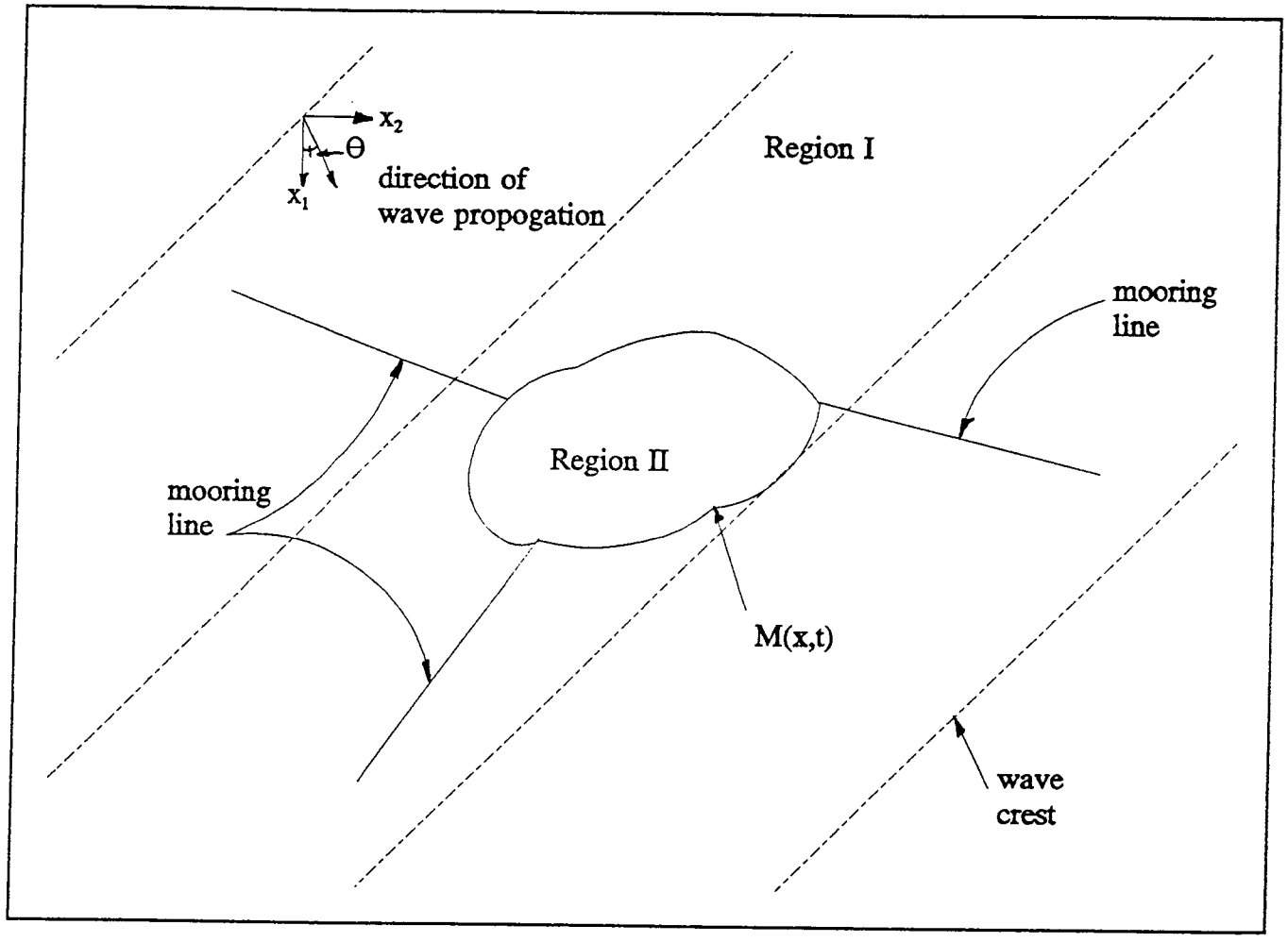

Figure 1.1 Plan View of Problem Under Study

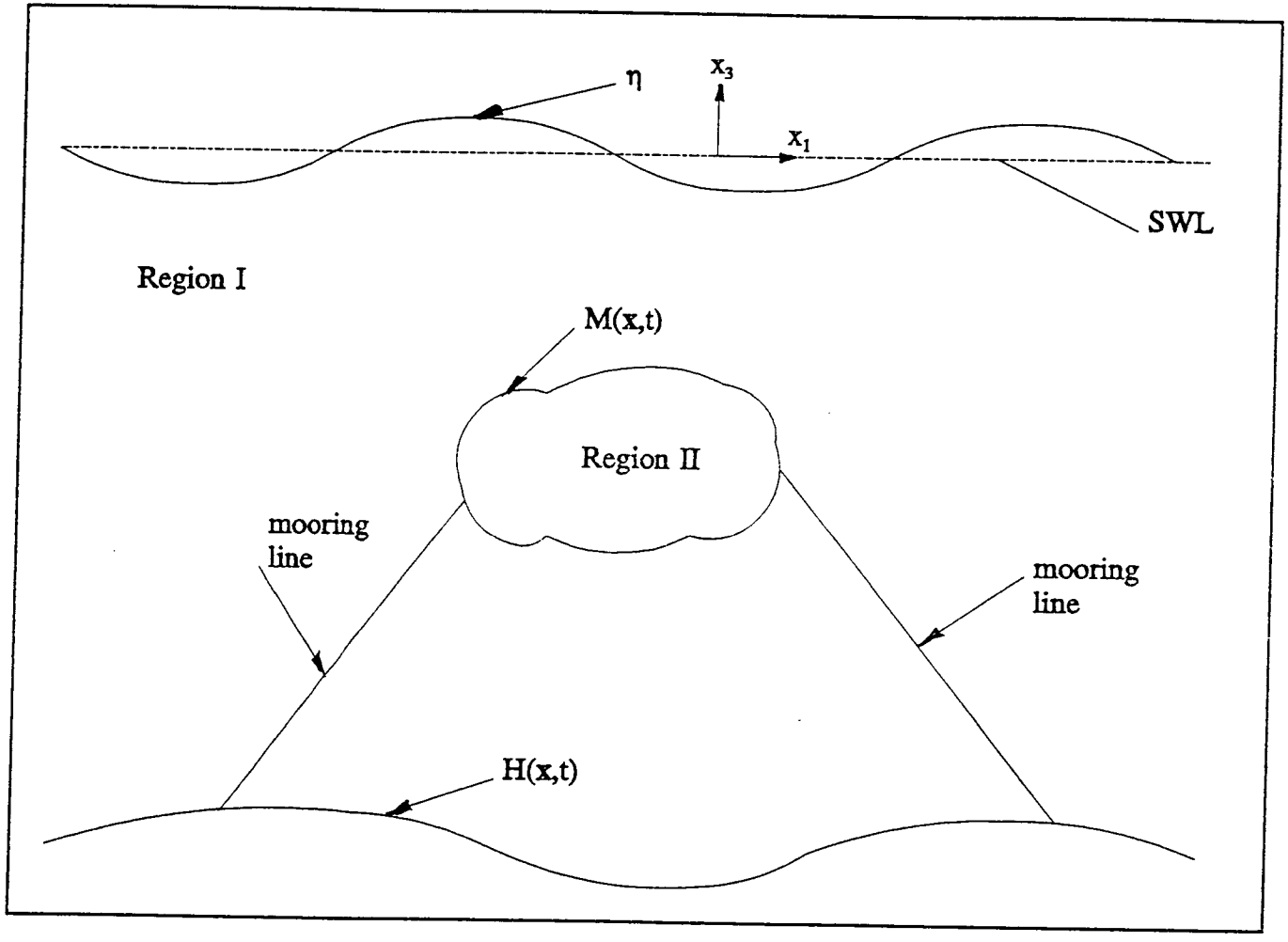

Figure 1.2 Profile of Problem Under Study

categorization is based on the ratio of a characteristic dimension, D, of the structure to a characteristic wave length, L; see Figure 1.3. On one hand, if the body is small, i.e. $D/L < 0.2$, one uses an empirical relationship called the Morison Equation, Sarpkaya and Isaacson (1981), (or a modified version of the Morison Equation). The Morison Equation assumes the force is composed of two components, inertia and drag. The two forces are computed and then added together. If the drag force, which accounts for real fluid effects such as shear, is small and the inertia forces predominate, the Froude-Krylov Theory, Sarpkaya and Isaacson (1981), can be used. When using Froude-Krylov Theory, the assumption is that the structure does not alter the wave field. On the other hand, if the structure is large, e.g. $D/L > 0.2$, and the local wave field is altered, diffraction theory should be used. Diffraction theory assumes that the local wave field is oscillatory, incompressible, and irrotational - an ideal fluid - so that the fluid velocity may be represented solely by the gradient of the velocity potential.

The deformable structure studied in this investigation was large; therefore, diffraction theory was used to estimate the wave loading. Solution techniques were available for the interaction of large rigid bodies and ocean waves, but not for large deformable structures and ocean waves. In general, for a linear analysis of large rigid bodies, the problem is broken down into two parts: a fixed body (diffraction) problem and a moving body (radiation) problem. Then the solutions to the two problems are superimposed, assuming a linear interaction between the body and the waves. The interaction between a deformable membrane and the

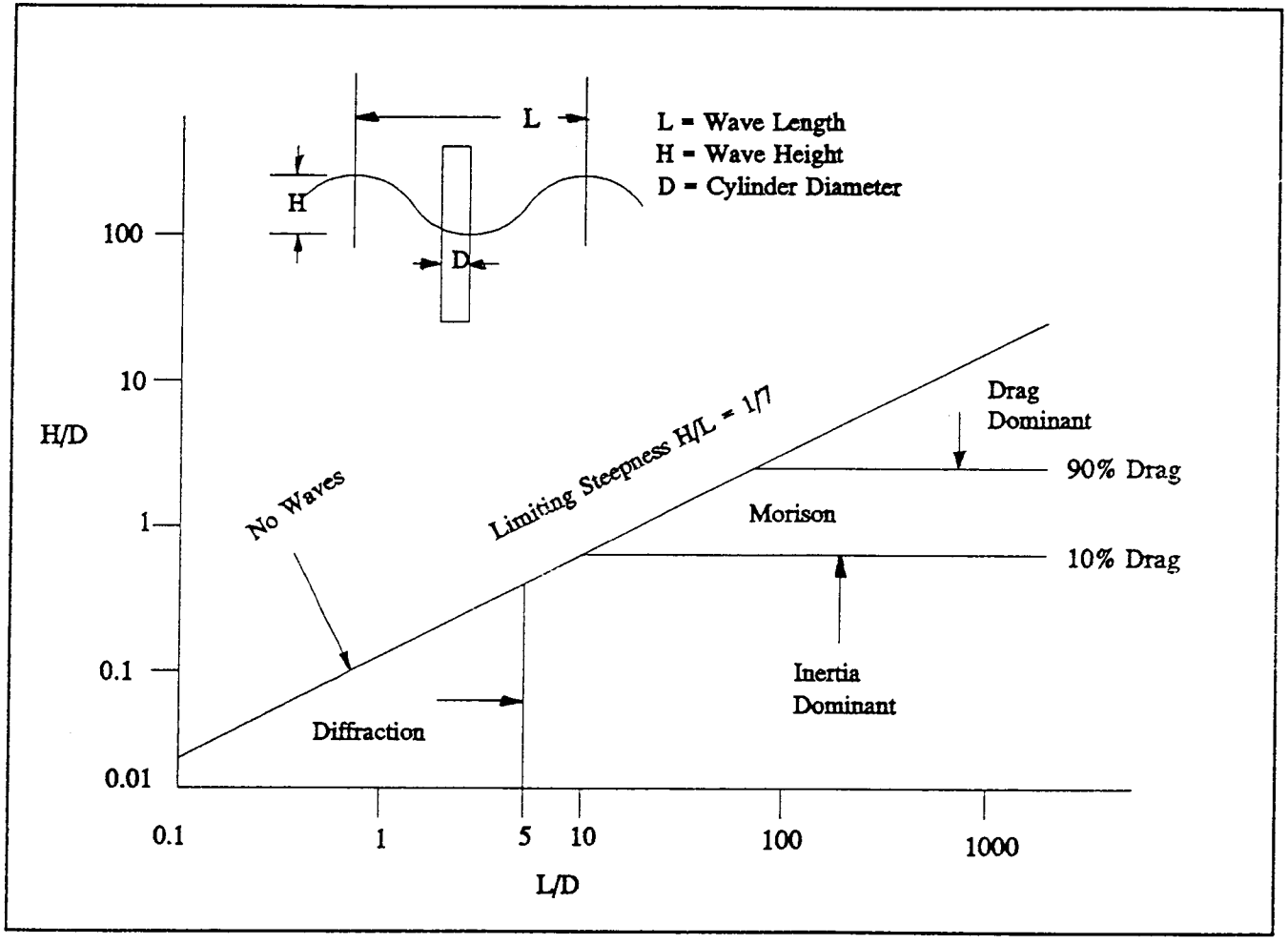

Figure 1.3 Hydrodynamic Flow Regimes, Hudspeth (1988)

ocean waves is nonlinear and coupled. Therefore, in this study, the diffraction and radiation problems were solved simultaneously.

1.2.2 Applications

The potential applications of fluid-filled membrane structures in an ocean environment are suggested by the following:

Floating Breakwaters. A deformable breakwater would be rapidly deployable, provide seasonal coastal protection, create temporary harbors, and provide protection for offshore construction. Floating, inflatable breakwaters would reduce wave impact on coastal shorelines and would provide sacrificial breakwaters for large storm waves. A temporary floating breakwater that is quickly deployable would increase the operational window of dredging operations and other construction activities. There are times when the difference between a safe and unsafe sea state is small and a slight reduction in the sea state possible with a floating breakwater would dramatically increase operation time. Examples of such structures are to be found in Bender (1989), Frederiksen (1971), Lo (1982), Williams and Geiger (1988), Seymour (1976), and Sollitt et al. (1986).

Submerged Breakwaters. As discussed in Frederiksen (1971) and in Iwagaki et al. (1978), inflatable tubes tethered to the bottom could serve as breakwaters for the protection of harbors, jetties, or armored breakwaters. Placement of these inflatable tubes seaward of armored breakwaters would enable them to act as sacrificial breakwaters, reducing the size of storm waves impacting

on the fixed breakwater. The reduction in maximum wave height would reduce the cost of the fixed structure. The tubes could be towed into position and then filled with ballast, and then allowed to settle to the bottom.

Gapped Breakwaters. A combination of submerged and floating breakwaters could be fine-tuned for maximum benefit at a location. The submerged tubes could be placed seaward of the floating breakwater, improving the efficiency of both structures. Larger waves would break on the submerged breakwater, changing the sea state to one that the floating structure is more effective at reducing.

Bladder Barges or Storage Depots. Inflatable membranes could be filled with various cargos, e.g. drinking water, oil, fluidized grain, wood chips, etc. The bladders could serve as temporary storage depots offshore or alongside of ships. They could be towed to offshore sites and deployed at depths below wave effects and then raised as required. The bladders could also be used as deep water storage sites for oil. One difficulty in using rigid structures at great depths is that as the fluid is removed and the internal pressure reduced, the resulting differential pressure could cause collapse. With a flexible-membrane storage container, the shell just changes shape to accommodate the change in pressure.

1.3 PREVIOUS RESEARCH

There has been little research reported on the interaction of water waves and large deformable membrane structures. However, there are several articles

on the following related topics that lend valuable insight into the interaction of water waves and large deformable membrane structures:

- Water waves and large floating rigid structure
- Water waves and small flexible structures
- Water waves and flexible structures
- Acoustic waves and deformable bodies

In addition to conducting a review of the literature on wave-structure interaction, a review was conducted of the viability of using boundary element methods as a modeling technique for the wave-structure interaction. To this end a paper has been published in Engineering Structures entitled "Selective Review of Boundary Element Modeling for Interaction of Deformable Structures with Water Waves" by Broderick and Leonard, October 1990. The information presented in that paper will not be presented here; instead the paper is included in Appendix B.

1.3.1 Water Waves and Large Floating Rigid Structures

In this study, nonlinear wave diffraction theory was used to solve the interaction of water waves and large floating bodies. However, the majority of the results cited in the literature use linear wave theory. Analytical results are limited to those problems where a separation of variables approach can be used, which generally assumes linear wave theory. Numerical solutions generally use boundary element methods or finite element methods. For a summary of the various techniques addressing this interaction, see Mei (1978), Shen (1978), and

Zienkiewics et al. (1975). In those works, the motions of the body are assumed small and the solutions are in the frequency-domain. In a frequency-domain approach the response is assumed periodic and computed for every frequency. Linear superposition is used if more than one frequency exist.

For nonlinear problems, superposition is not valid and a time-domain approach is required. The response is computed at each instance in time using the equations of motion. Time-domain solutions have been obtained for nonlinear interactions with structures by means of the convolution integral of the linear hydrodynamic force coefficients based on the method presented in Cummings (1962). A restriction on this method is that the hydrodynamic force coefficient must be known for all frequencies; however, most numerical methods used to obtained these coefficients break down in the high frequency range.

The following articles deal with the interaction of floating bodies and waves using the BEM. Yeung (1975) solved the two-dimensional problem of a floating body of arbitrary geometry. While the bottom elevation in the area of interest was variable, it had to approach a constant depth in the outer regions (not necessarily the same depth). Yeung assumed the floating body was rigid and not restrained with mooring lines. Linear wave theory was used. Yeung (1982) then extended this work to the time domain using Volterra's method and an unsteady Green's Function. Masuda and Kato (1983) solved a similar problem. They extended their results to three-dimensional bodies in two-dimensional seas, using finite amplitude wave theory. Yamamoto et al. (1980) also solved a problem

similar to that of Yeung, i.e. a two-dimensional body of arbitrary shape. The bottom elevation was allowed to vary in the area of interest but had to reach a constant elevation where the radiation boundary condition was applied. Yamamoto et al. assumed the floating body was restrained by elastic mooring lines. Brevig et al. (1982) were interested in computing the maximum forces on submerged wave energy devices. They used nonlinear wave theory with a time marching process to bring the wave to the point of breaking. The problem was solved in two-dimensions. Isaacson (1982) developed a method for calculating the interaction of steep ocean waves with a fixed or floating structure of arbitrary shape. The problem involved nonlinear wave theory and a time marching process. Several authors have approached the nonlinear problem using a perturbation approach, Sclavounous (1988), Nakayama and Washizu (1981), and Isaacson and Cheung (1990). In particular, Sclavounous (1988) studied the second order radiation and diffraction of surface waves by floating bodies. This was accomplished by deriving a second order Green's Function using an explicit sum-and-difference frequency method.

These articles are typical of what is documented in the literature. Only a couple of the references dealt with deformable structures and waves, Ohyama at al. (1989), Tanaka et al. (1990), Lo (1982) and Leonard and Lo (1987). The work by Ohyama et al. and Tanaka et al. are bottom-mounted flexible mounds. The goal of their work was to evaluate the effectiveness of these structures as wave barriers. They used a two-dimensional linear BEM of the fluid and a two

dimensional linear lump mass model of the membrane (assumes small displacements). They have conducted small-scale physical model tests for numerical model verification and found that the flexible mound breakwater could be an effective wave barrier under certain conditions. In Lo's and Leonard and Lo's studies the structure was modeled using the FEM and only a crude hydrodynamic load model was included. In addition, a series of papers considered the problem of a membrane in air under pneumatic loading: Han and Olson (1987), Han (1986), and Han et al. (1984). The nonlinear interaction of wind-loaded pneumatic membrane structures, Han (1986), involved a BEM of the flow field and a FEM of the membrane. Han solved the coupling problem in an iterative procedure between the boundary element and finite element models. The model was used with good results to model the air-supported roof of a stadium located in Vancouver, British Columbia. This illustrates that the fluid domain is ideally suited for boundary element modeling and the nonlinearity associated with structural motions is more suited to finite element modeling.

1.3.2 Water Waves and Small Flexible Structures

Relevant literature computing the hydrodynamic loadings for small flexible structures in water waves use the Morison Equation with nonlinear coupling effects introduced by the structure's relative deformations. Modi and Mirsa (1980) investigated the general dynamics of a flexible platform formed by three inflated tapered tubes attached to a central head and subjected to linear sinusoidal

standing waves. Milgram (1971) studied the motions and the hydrodynamic forces on a flexible floating barrier subjected to the actions of currents and waves. Interaction between waves and currents was not considered. Small motions of the barrier were assumed, permitting determination of wave effects at the mean position of the barrier.

1.3.3 Water Waves and Flexible Barrier Structures

Several published studies reported model tests of flexible barrier structures and linear water waves. Sollitt et al. (1986) conducted small-scale experiments in a wave tank on hinged buoyant flap breakwaters, i.e. membrane structures filled with air and hinged to the tank floor. Modeling the flap-barrier as an elastic beam, Kerper (1988) conducted large-scale tests and developed a theory describing the structural behavior of a hinged flap-barrier. Bender (1989) extended Kerper's theory to evaluate large-scale experiments of a breakwater consisting of a thin membrane extending through the water column. The membrane was fixed at the tank floor and tensioned by a cylinder buoy at the surface. A structure very similar to that of Bender's was modeled numerically by Williams and Geiger (1988). Williams and Geiger modeled the fluid-structure interaction with a boundary element model.

1.3.4 Acoustic Waves and Deformable Bodies

When the external loading on the body is acoustic pressure waves, the

methods of analysis typically adopted are similar to that for water waves but without free surface effects, Shaw and Friedman (1975). A basic assumption concerning the linear aspects of the problem is that the total velocity potential is composed of an incident potential, a reflected potential, and a radiated potential. Four basic techniques have been used for solving the problem: (1) series expansion, Geers (1975), Huang (1970); (2) integral transformations, Berger (1969); (3) spatial discretization, Friedman and Shaw (1962), Shaw and Friedman (1962); and (4) surface interaction approximations, Haywood (1958), Geers(1971). Only spatial discretization and surface interaction approximation methods were extended to treat most nonlinear problems. A general review and extensive references can be found in Geers (1975).

1.4 SCOPE OF STUDY

1.4.1 Selected Method

In prior analyses of the interactions between waves and large structures, a frequency-domain approach has been extensively used to pose and solve a linear boundary value problem describing the interactions under steady state conditions. However, in the class of problems considered in this work transient motions and localized deformations of the structure are expected; thus the radiated waves in the fluid possess unsteady features. The time-dependent wave loadings induced by unsteady flow in turn affect the structural motions. To account for such time-dependent behaviors, it was necessary to use a time-domain simulation for the

wave-structure interaction.

Mathematically, the localized deformations of the membrane were modeled using a time-domain FEM adapted from Lo (1982). The hydrodynamic loadings in Lo's FEM were simplistic, however, so a BEM was developed to model the fluid domain, thus providing better hydrodynamic loadings for the FEM. The fluid domain has been modeled using a BEM that utilized the complete boundary conditions. Thus, since no assumptions were made on the linearity of the free surface and nonlinear waves can be modeled. Volterra's method was used to develop an implicit time domain BEM.

The performance of the BEM and the FEM were assessed on independent flow and structure problems. Once the models established satisfactory accuracies, they were coupled in an iterative procedure to solve the wave-structure interaction. The coupling at each time step was as follows: (1) the hydrodynamic loads were computed based on an assumed membrane profile in the BEM; (2) with the loading stipulated, a new membrane profile was obtained from the FEM; (3) the new profile was entered into the BEM to compute new loadings. This iterative process was continued until an equilibrium profile consistent with the hydrodynamic loading at that time was attained.

Model verification has been conducted in several steps. The BEM was evaluated independently by comparing the BEM model to other numerical and physical models of the interaction of water waves and a submerged horizontal cylinder. The FEM was evaluated previously, Lo (1982). The coupled FEM and

BEM were evaluated by comparison to a physical model test conducted in conjunction with the development of the numerical model.

1.4.2 Organization of This Study

In Chapter 2 the governing field equations and boundary conditions for the membrane and the fluid domain are presented. In addition, Chapter 2 contains a discussion on dimensional analysis and scaling factors. Chapter 3 covers the development of the BEM; Chapter 4 a brief discussion of the FEM. The coupling of the BEM and FEM is presented in Chapter 5. The numerical results of the BEM and the coupled model are given in Chapter 6. Results from the physical model are also presented in Chapter 6. Chapter 7 provides a summary of the accomplishments of this research, conclusions, and needs for future research.

Flow diagrams for the computer algorithms in the BEM and the coupled BEM and FEM can be found in Appendix A. The previously published review of literature on the acceptability of the boundary element method as a modeling technique for predicting fluid-structure interaction is reproduced in Appendix B. Appendix C contains a description of the large-scale wave tank experiments conducted for model verification.

CHAPTER 2 PROBLEM FORMULATION

2.1 METHODOLOGY

A schematic of the problem under investigation in this study was shown in Figures 1.1 and 1.2. There are three areas of interest: the membrane; the fluid surrounding the membrane, Region I; and the fluid enclosed by the membrane, Region II. The motion and location of the two fluid regions are coupled through the motion and location of the membrane, which in turn are forced by the difference in hydrodynamic pressures between the two regions. To develop an algorithm to predict the fluid-structure interaction, governing field equations and boundary conditions are necessary. These will be presented in this chapter. The solution algorithm will be presented in later chapters. Prior to presenting the governing field equations and boundary conditions, however, assumptions inherent in the system under study will be presented.

2.2 ASSUMPTIONS/IMPLICATIONS

2.2.1 Membrane, $M(\vec{x},t)$

The membrane is modeled using a previously-developed finite element model (FEM) based on the principle of virtual work. The model is for cable and membrane structures. Cables are assumed to be in a state of uniaxial stress, while the curved membranes are assumed to be in a state of plane stress. The thickness of the membrane is assumed small compared to other membrane dimensions, such

that lines normal to the undeformed membrane midsurface remain normal to the deformed midsurface and inextensible; the motion of the membrane is characterized by the motion of the midsurface. Membrane stress is assumed constant through the thickness, which implies that the flexural rigidity is negligible. No assumptions are made on the magnitudes of the displacements and strains. Mooring line loads are applied to the membrane through linear springs or nonlinear cables. The membrane material is considered isotropic and hyperelastic.

2.2.2 Region I (fluid domain)

The fluid is assumed incompressible and inviscid, and the flow irrotational. The fluid motion can therefore be described by a velocity potential, ϕ, which satisfies the Laplace Equation within the fluid domain. The bottom is assumed rigid and satisfies a kinematic boundary condition. If the bottom were deformable, then the appropriate sediment transport models would be coupled with the kinematic bottom boundary conditions and an appropriate dynamic boundary condition. An equilibrium condition between the velocity at the bed, suspended sediment, and bed load transport would be sought. At this time no attempt will be made to model a deformable bottom. Dynamic and kinematic boundary conditions are satisfied on the body and on the free surface. Only one medium is assumed to exist in the fluid, thus no stratified flow occurs. To include stratified flow, each layer would become a subdomain and at each interface kinematic and dynamic boundary conditions would need to be satisfied.

2.2.3 Region II (enclosed by membrane)

The assumptions that apply to this region are similar to those for Region I. The fluid is assumed incompressible and inviscid, and the flow irrotational. The fluid motion can therefore be described by a velocity potential, ϕ, which satisfies the Laplace Equation within the fluid domain. Dynamic and kinematic boundary conditions are satisfied on the body. Several materials, e.g., wood pulp, that could be in Region II would not fit the above assumptions. This research concentrates on the nonlinear interaction of the fluid domain, Region I, and the membrane. Region II is important to the interaction, but the additional complications of different materials in Region II needs to be addressed after an accurate model of the interaction is developed.

2.3 MEMBRANE GOVERNING EQUATIONS AND BOUNDARY CONDITIONS

The dynamic equilibrium equations are obtained from the principle of virtual work, Green and Adkins (1960). In a Total Lagrangian Reference Frame, the principle of virtual work done by stresses, σ^{ij}, accelerations, $\ddot{U}_i$, and loads B_i, T_i, and F_i, acting through virtual strains, δe_{ij}, and displacements, δU, can be stated as

$$\underset{(i)}{\int_V \sigma^{ij}\delta e_{ij}dV} - \underset{(ii)}{\int_V {}^m\rho B_i\delta U_i dV} + \underset{(iii)}{\int_V {}^m\rho \ddot{U}_i\delta U_i dV} - \underset{(iv)}{\int_S T_i\delta U_i dS} - \underset{(v)}{F_i\delta U_i} = 0 \qquad 2.1$$

where the quantities are referenced to the undeformed condition of the membrane and where repeated indices denote summation over the range 1,2,3 of the lower case indices.

σ^{ij} = contravariant tensor component of stress due to static and dynamic load measured with respect to undeformed membrane

δe_{ij} = covariant tensor component of virtual strain

${}^m\rho$ = initial density

B_i = body force per unit mass of undeformed membrane

δU_i = virtual displacements

$\ddot{U}_i$ = material acceleration

T_i = traction per unit surface area of undeformed membrane

F_i = concentrated loads

V = Volume of membrane embedded in a three-dimensional cartesian space with Lagrangian coordinated y_i, i = 1,2,3

S = mid-surface area of membrane

The terms in Equation 2.1 are the contributions to the virtual work from the following

(i) virtual work of internal stresses

(ii) body forces

(iii) inertia forces

(iv) difference in surface pressures and surface stresses

(v) mooring or other concentrated loads

In Equation 2.1, term (iv), the difference in surface pressures, is the coupling term between the fluid domain and the membrane.

Because the stress is assumed constant throughout the membrane and the thickness is assumed small, Equation 2.1 can be integrated through the thickness and rewritten replacing volume integrals with an equivalent surface integral, where **h** is the initial thickness:

$$\underset{(i)}{\int_S N^{\alpha\beta}\delta e_{\alpha\beta} h dS} - \underset{(ii)}{\int_S {}^{m}\rho B_i \delta U_i h dS} + \underset{(iii)}{\int_S {}^{m}\rho \ddot{U}_i \delta U_i h dS} - \underset{(iv)}{\int_S T_i \delta U_i dS} - \underset{(v)}{F_i \delta U_i} = 0 \qquad 2.2$$

where $N^{\alpha\beta}$ are the contravariant components of the stress resultant; $\delta e_{\alpha\beta}$ are the mid-surface virtual strain. Greek indices denote curvilinear Lagrangian surface coordinate attached to the undeformed membrane. Equation 2.2 is the dynamic boundary condition between Region I and Region II.

When a fluid boundary is deformable, two boundary conditions are needed to describe the boundary: kinematic and dynamic. The dynamic boundary

condition is obtained from Equation 2.2. The kinematic boundary condition is that the normal component of the velocity of any point on the membrane, $\vec{\dot{U}}$, must equal the normal component of the fluid velocity, $\vec{q}_I$ for Region I or $\vec{q}_{II}$ for Region II, at the same location.

$$\vec{q}_I \bullet \vec{n} = \dot{U} \bullet \vec{n} \qquad on\ M \qquad 2.3$$

or alternatively

$$-\vec{\nabla}\phi_I \bullet \vec{n} = \dot{U} \bullet \vec{n} \qquad on\ M \qquad 2.4$$

and

$$\vec{q}_{II} \bullet \vec{n} = \dot{U} \bullet \vec{n} \qquad on\ M \qquad 2.5$$

or alternatively

$$-\vec{\nabla}\phi_{II} \bullet \vec{n} = \dot{U} \bullet \vec{n} \qquad on\ M \qquad 2.6$$

where $\vec{n}$ is the unit normal, ϕ_I and ϕ_{II} are the velocity potential, in Regions I and II respectively, and $\vec{q}_I$ and $\vec{q}_{II}$ are defined as $-\vec{\nabla}\phi_I$ and $-\vec{\nabla}\phi_{II}$, as described in Section 2.4.

2.4 FLUID REGION GOVERNING FIELD EQUATIONS AND BOUNDARY CONDITIONS

The governing field equations and boundary conditions will be presented for a fluid region governed by the Laplace Equation. If a subscript f or no subscript appears the derivation applies for both Regions I and II. An Eulerian coordinated system, x_i, is defined for the fluid regions. The x_3 origin is located at the still water level and directed in opposition to the direction of gravity, see Figure 1.2. Irrotational flow implies:

$$\vec{q} = -\vec{\nabla}\phi \tag{2.7}$$

Conservation of mass implies, Yuan (1967):

$$\frac{D^f\rho}{Dt} + {}^f\rho\,\vec{\nabla q} = 0 \tag{2.8}$$

where $D^f\rho/Dt$ is the total derivative of the fluid density, ${}^f\rho$. Thus for an incompressible fluid, Equations 2.7 and 2.8 yield the governing field equation in the fluid domain as the Laplace Equation

$$\nabla^2\phi = 0 \tag{2.9}$$

Once the velocity potential, ϕ is known, the flow kinematics can be computed using Equation 2.7.

The flow dynamics are computed from the Navier-Stokes Equation, Yuan (1967). For an inviscid and incompressible fluid, the Navier-Stokes Equation simplifies to Euler's Equation:

$$\frac{\partial \vec{q}}{\partial t} + \vec{q} \cdot \nabla \vec{q} = \vec{F} - \frac{\nabla \vec{p}}{\rho} \qquad 2.10$$

Where p is pressure, F is a body force per unit mass (0,0,-g) and g is the acceleration of gravity.

The boundary conditions for the four fluid boundaries - the membrane, the free surface, the radiation boundary (far field interface), and the bottom are assumed below:

2.4.1 Membrane Boundary Conditions

There are two boundary conditions on the membrane, kinematic and dynamic. The kinematic boundary condition has already been stated as

$$-\nabla \vec{\phi} \cdot \vec{n} = \dot{U} \cdot \vec{n} \qquad 2.4$$

This condition requires the fluid and the membrane remain in contact. There are two locations where this boundary condition becomes difficult, when the

membrane pierces the free surface or when the membrane rolls along the bottom. Equation 2.4 is valid for the contact points but when the membrane moves the contact points will change. The dynamic boundary condition is included in Equation 2.2, which is the dynamic equilibrium equation for the membrane. The dynamic loading applied to the membrane is computed from Euler's Equation

$$\frac{\partial \vec{q}}{\partial t} + \vec{q} \cdot \nabla \vec{q} = \vec{F} - \frac{\nabla \vec{p}}{f_\rho} \qquad 2.10$$

which can be modified with the following vector identity

$$\vec{q} \cdot \nabla \vec{q} = \frac{1}{2} \nabla (\vec{q} \cdot \vec{q}) - \vec{q} \times (\nabla \times \vec{q}) \qquad 2.11$$

noting that due to the assumption of irrotational flow the second term on the right side of the identity is zero. Thus, Equation 2.10 can be written as:

$$\frac{\partial \vec{q}}{\partial t} + \frac{1}{2} \nabla (\vec{q} \cdot \vec{q}) = \vec{F} - \frac{\nabla \vec{p}}{f_\rho} \qquad 2.12$$

Equation 2.12 is integrated to solve for the pressure:

$$-\frac{\partial \phi}{\partial t} + \frac{p}{f_\rho} + \frac{1}{2} q^2 + g x_3 = Q(t) \qquad 2.13$$

where Q(t) = Bernoulli's constant. The only constant force included in this

derivation is that due to gravity. In Equation 2.13 the x_3 could be modified in Region II to include an overburden pressure on the internal fluid. Thus, the pressures exerted on the membrane by the fluid is:

$$p = {}^f\rho\frac{\partial\phi}{\partial t} - \frac{{}^f\rho}{2}q^2 + {}^f\rho Q(t) - {}^f\rho g x_3 \qquad 2.14$$

2.4.2 Free Surface Boundary Conditions

The free surface boundary has two boundary conditions, a kinematic and a dynamic. The kinematic boundary condition can be derived in two ways: 1) knowing that the velocity of the free surface and the fluid velocity at the free surface are the same or 2) by a Stokes Material Surface. The second method, Stokes Material Surface, will be presented here. The Stokes Material Surface, SMS_f, for the free surface is:

$$SMS_f = \eta - x_3 = 0 \qquad on\ x_3 = \eta \qquad 2.15$$

where η is the location of the free surface. The kinematic boundary condition is derived by taking the total derivative of the SMS_f.

$$\frac{D}{Dt}SMS_f = 0 = \left[\frac{\partial}{\partial t} + q_i\frac{\partial}{\partial x_i}\right]\eta - \left[\frac{\partial}{\partial t} + q_i\frac{\partial}{\partial x_i}\right]x_3 \qquad 2.16$$

$$0 = \frac{\partial \eta}{\partial t} + q_1 \frac{\partial \eta}{\partial x_1} + q_2 \frac{\partial \eta}{\partial x_2} - q_3 \qquad 2.17$$

$$-\frac{\partial \phi}{\partial x_3} = \frac{\partial \eta}{\partial t} - \frac{\partial \phi}{\partial x_1}\frac{\partial \eta}{\partial x_1} - \frac{\partial \phi}{\partial x_2}\frac{\partial \eta}{\partial x_2} \qquad 2.18$$

Thus the kinematic boundary condition is:

$$-\frac{\partial \phi}{\partial x_3} = \frac{D\eta}{Dt} \qquad 2.19$$

The dynamic free surface boundary condition is derived from Euler's Equation. On the free surface $x_3 = \eta$ and $p = 0$. Equation 2.14 reduces to:

$$\eta = \frac{1}{g}\left[Q(t) + \frac{\partial \phi}{\partial t} - \frac{1}{2}q^2 \right] \qquad 2.20$$

The free water surface, η, can be eliminated from the boundary condition by combining the kinematic and dynamic free surface boundary conditions. The left side of Equation 2.19

$$-\frac{\partial \phi}{\partial x_3} = \frac{D\eta}{Dt} \qquad 2.19$$

is equated to the total derivative of the right-hand side of Equation 2.20

$$\eta = \frac{1}{g}\left[Q(t) + \frac{\partial\phi}{\partial t} - \frac{1}{2}q^2\right] \qquad 2.20$$

Assuming g is a constant, one obtains

$$\frac{\partial^2\phi}{\partial t^2} + g\frac{\partial\phi}{\partial x_3} + \frac{\partial Q}{\partial t} - \frac{\partial}{\partial t}q^2 - \frac{1}{2}(\vec{q}\cdot\vec{\nabla})q^2 = 0 \qquad 2.21$$

Thus for the free water surface, the kinematic free surface boundary condition (KFSBC) is stated in Equation 2.19, the dynamic free surface boundary condition (DFSBC) is stated in Equation 2.20, and the combine free surface boundary condition (CFSBC) is stated in Equation 2.21.

2.4.3 Radiation Boundary Condition

The radiation boundary condition is easy to define theoretically but difficult to implement. The radiation boundary condition can be stated as follows: the radiated and scattered waves are local effects and in the far field only the incident wave field is present. In this model, initial conditions are chosen such that still water exists in the area of the structure and a known incident wave field is approaching at time t=0. The scattered waves generated by the wave-structure interaction travel only a short distance over the time duration analyzed. Thus, providing that the far field boundary lies sufficiently far from the body, the scattered waves will not reach the boundary during the time period analyzed.

Consequently, at the boundary the values of the velocity potential and the normal derivative of the velocity potential correspond to those of the incident wave field which are known at all times for any chosen wave theory. The location of the far field boundary can be estimated using the time interval to be analyzed and the speed of the scattered wave energy propagation. The propagation of the scattered wave can be estimated from the group velocity calculated by linear wave theory. With this in mind, the far field boundary should extend several wavelengths from the structure.

2.4.4 Bottom Boundary Condition

The bottom boundary condition can be described by one boundary condition, the kinematic boundary condition, since the bottom boundary is assumed to be rigid. The kinematic boundary condition is:

$$\frac{\partial \phi}{\partial n} = 0 \qquad 2.22$$

where $\vec{n}$ is the unit normal. If the bottom is approximately horizontal the kinematic boundary condition can be stated as:

$$\frac{\partial \phi}{\partial n} = \frac{\partial \phi}{\partial x_3} = 0 \qquad 2.23$$

2.5 REGION I GOVERNING FIELD EQUATIONS AND BOUNDARY CONDITIONS

The governing field equation in Region I is the Laplace Equation

$$\nabla^2 \phi_I = 0 \tag{2.24}$$

All four boundaries conditions; membrane, free surface, radiation and bottom, exist in Region I. The membrane kinematic boundary condition is stated in Equations 2.3 and 2.4. The dynamic boundary conditions is

$$p_I = {}^I\rho \frac{\partial \phi_I}{\partial t} - \frac{{}^I\rho}{2} q_I^2 + {}^I\rho Q(t)_I - {}^I\rho g x_3 \tag{2.25}$$

The free surface boundary conditions are

$$-\frac{\partial \phi_I}{\partial x_3} = \frac{D\eta}{Dt} \tag{2.26}$$

$$\eta = \frac{1}{g}\left[Q_I(t) + \frac{\partial \phi_I}{\partial t} - \frac{1}{2} q_I^2 \right] \tag{2.27}$$

$$\frac{\partial^2 \phi_I}{\partial t^2} + g\frac{\partial \phi_I}{\partial x_3} + \frac{\partial Q_I}{\partial t} - \frac{\partial}{\partial t} q_I^2 - \frac{1}{2}(\vec{q}_I \bullet \vec{\nabla}) q_I^2 = 0 \tag{2.28}$$

The bottom boundary condition is

$$\frac{\partial \phi_I}{\partial n} = \frac{\partial \phi_I}{\partial x_3} = 0 \qquad 2.29$$

2.6 REGION II GOVERNING FIELD EQUATIONS AND BOUNDARY CONDITIONS

The governing field equation in Region II is the Laplace Equation

$$\nabla^2 \phi_{II} = 0 \qquad 2.30$$

Region II has only one boundary, the membrane. The kinematic boundary is stated in Equations 2.5 and 2.6. The dynamic boundary condition is

$$p_{II} = {}^{II}\rho \frac{\partial \phi_{II}}{\partial t} - \frac{{}^{II}\rho}{2} q_{II}^2 + {}^{II}\rho Q_{II}(t) - {}^{II}\rho g x_3 \qquad 2.31$$

An additional constraint needs to be imposed on Region II, based on the assumptions of incompressibility and conservation of mass: the volume must be conserved.

CHAPTER 3 BOUNDARY ELEMENT MODEL OF FLUID DOMAIN

3.1 BOUNDARY ELEMENT METHOD

A common approach to develop models for most engineering systems is based on an infinitesimally small element in which the relationships between the major variables can be developed, thus creating a series of differential equations. In the case of finite element or finite difference methods, the differential equations are left in this form, Banerjee and Butterfield (1981). These equations are approximated discretely over the domain by functions which fully or partially satisfy the boundary conditions. This is accomplished by discretizing the domain and then simultaneously solving the systems of equations while imposing the boundary conditions.

In the boundary element method an attempt is made to integrate the differential equations prior to discretizing the domain. These equations, called boundary element integrals, exactly satisfy the conditions in the domain. Boundary element integrals only involve variables on the boundaries, which means that only the boundaries need to be discretized. The solution variables will then vary continuously throughout the domain, and all approximations of geometry will occur on the boundaries.

The boundary element method utilizes the principle of superposition and thus is only applicable to linear systems or to those nonlinear systems that can be approximated in an incremental sense using linear systems. Because of the "linear

systems" requirement, the domain must be homogenous. If the domain is not homogenous, it must be divided into regions that are homogenous, or can be approximated as homogenous.

There are two major classes of boundary element models (BEMs), indirect and direct, Banerjee and Butterfield (1981) and Brebbia (1978). The indirect method starts with a solution that satisfies the governing equations in the spatial domain but has unknown coefficients. The coefficients are evaluated by imposing the boundary conditions in some sense, like least squares. Generally, the solution used is the unit singular solution of the differential equations and the unknown coefficients are the specific densities over the boundaries. Once the coefficients are determined, the values of the physical variables can be determined using a simple integration procedure. In the direct method, the physical variables are the unknown functions appearing in the integral equations. The direct method is generally presented in terms of Green's identity. Both the indirect and the direct method can be equated to the weighted residual formulation, Brebbia (1978).

In the boundary element method there are two approximations made to obtain the boundary values:

1) Integrating in a piecewise manner

2) Solving the integral in a weighted residue sense (on the boundary)

The integration can be extremely difficult to perform because the functions tend to be singular. The singular nature of the functions does allow BEM to effectively model problems with high gradients.

In general, the advantages of using a BEM are as follows, Kuich (1984):

1) For homogeneous material, only the boundary needs to be discretized.
2) Infinite boundaries are easier to model in the BEM than in the FEM.
3) The order of nodes and elements is not critical to the efficiency of the computer solution.
4) Once a solution for the boundary is established, solving for any interior point is straightforward.

On the other hand, disadvantages include:

1) Off-the-shelf computer codes are not yet commonly available.
2) The solution matrix is fully populated.
3) Internal forces other than those that can be related to a surface integral can not be applied.
4) If the surface-area-to-volume ratio is large, the solution technique will not be economical.
5) If the material is nonhomogeneous the inner region will need to be discretized.

3.2 BOUNDARY ELEMENT INTEGRAL

Figure 3.1 is a schematic of the problem under study. In Regions I and II the governing field equation is the Laplace Equation,

$$\nabla^2\phi = 0 \tag{3.1}$$

which is easily transferred to a boundary element integral. Equation 3.1 can be multiplied by any function G, here selected to be the fundamental solution to the Laplace Equation, to obtain

$$G\nabla^2\phi = 0 \tag{3.2}$$

In three-dimensional problems the fundamental solution

$$G = \frac{1}{4\pi r} \tag{3.3}$$

is the influence at a field point ξ_i of a source at point x_i, where $r = [(\xi_i - x_i)(\xi_i - x_i)]^{1/2}$ is the distance between the point $\vec{x}$ and $\vec{\xi}$. The function G satisfies the Laplace Equation except at the singularity (r = 0), Tang (1988). Thus

$$\nabla^2 G(\vec{\xi},\vec{x}) = -\delta(\vec{\xi},\vec{x}) \tag{3.4}$$

where

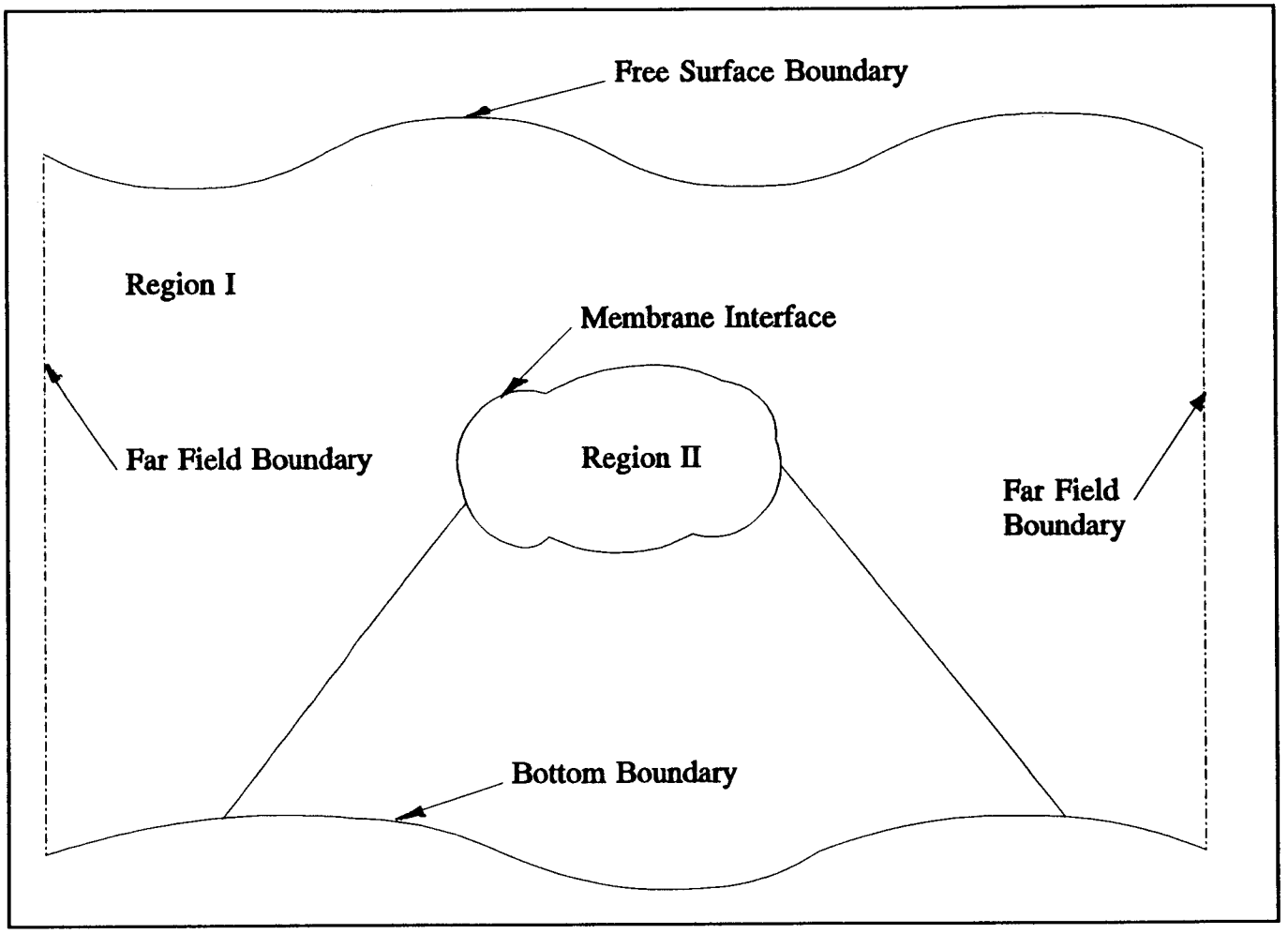

Figure 3.1 Schematic of Boundary Element Model Boundaries

$$\delta(\vec{\xi},\vec{x}) = \left\{ \begin{array}{ll} 0 & \vec{\xi} \neq \vec{x} \\ \infty & \vec{\xi} = \vec{x} \end{array} \right\} \qquad 3.5$$

Multiplying Equation 3.4 by ϕ and subtracting Equation 3.2, one obtains

$$\phi\nabla^2 G - G\nabla^2\phi = 0 \qquad 3.6$$

Equation 3.6 is valid over the domain, V, and by Green's Second Identity, Guenther and Lee (1988), the following is derived:

$$\int_v \left(\phi\nabla^2 G - G\nabla^2\phi \right) dV = \int_s \left[\phi\frac{\partial G}{\partial n} - G\frac{\partial \phi}{\partial n} \right] dS \qquad 3.7$$

where n is the surface normal and directed out of the fluid domain.

Incorporate Equations 3.2 and 3.4 into the left hand side of Equation 3.7 to obtain

$$-\int_v \phi(\vec{x})\delta(\vec{\xi},\vec{x})dV = -\phi(\vec{\xi}) \qquad 3.8$$

Equation 3.7 can then be written as:

$$\phi(\vec{\xi}) = \int_s \left[G\frac{\partial \phi}{\partial n} - \phi\frac{\partial G}{\partial n} \right] dS \qquad 3.9$$

Equation 3.9 is only valid for $\vec{\xi}$ inside the fluid domain. If Equation 3.9 is extended to include points on the boundary, the equation becomes, Tang (1988):

$$C(\vec{\xi})\phi(\vec{\xi}) = \int_s \left[G\frac{\partial \phi}{\partial n} - \phi\frac{\partial G}{\partial n} \right] dS \qquad 3.10$$

Where the value of $C(\vec{\xi})$ depends on the position of $\vec{\xi}$, that is

$$\begin{aligned} C(\vec{\xi}) &= 1 && \text{for } \vec{\xi} \text{ inside the domain} \\ C(\vec{\xi}) &= 0 && \text{for } \vec{\xi} \text{ outside the domain} \\ C(\vec{\xi}) &= 1 + \lim_{\epsilon \to 0} \int_{S_\epsilon} \frac{\partial G}{\partial n} dS && \text{for } \vec{\xi} \text{ on the boundary} \end{aligned} \qquad 3.11$$

Equation 3.10 is the boundary element integral for a domain where the Laplace Equation is the governing differential equation. In general, the resulting boundary element integral can not be solved analytically, so a numerical technique is used. The numerical technique normally involves discretization of the boundaries. With the appropriate boundary conditions applied, a solvable system of equations can be developed.

Since time only appears in the boundary conditions, time would be modeled explicitly, as done by Isaacson (1982). To implicitly include time in the governing field equation Volterra's method is used, Yeung (1982). The approach is similar to the one already presented except the time derivative of the governing field equation becomes the starting point for the derivation. Take the time derivative of Equation 3.1

$$\left[\frac{\partial}{\partial t}\right] \nabla^2\phi = 0 \qquad 3.12$$

which can be written as:

$$\nabla^2\dot{\phi} = 0 \qquad 3.13$$

Where an overdot denotes a partial time derivative, not a total derivative. Thus, following the earlier argument, one obtains

$$\begin{aligned} \nabla^2\dot{\phi} &= 0 & \nabla^2 G &= 0^* \\ G\nabla^2\dot{\phi} &= 0 & \dot{\phi}\nabla^2 G &= 0^* \end{aligned} \qquad 3.14$$

$$\dot{\phi}\nabla^2 G - G\nabla^2\dot{\phi} = 0 \qquad 3.15$$

where $\nabla^2 G$ is zero except for the singularity which exists at $\vec{\xi} = \vec{x}$. The definition for the Green's Function, G, used in the previous derivation still holds but time must be introduced,

$$\nabla^2 G(\vec{\xi},\vec{x},\tau-t) = -\delta(\vec{\xi},\vec{x},\tau-t) \qquad 3.16$$

where G

$$\delta(\vec{\xi},\vec{x},\tau-t) = \begin{cases} 0 & \vec{\xi} \neq \vec{x} \text{ or } \tau \neq t \\ \infty & \vec{\xi} = \vec{x} \text{ and } \tau = t \end{cases} \qquad 3.17$$

After integration over the domain and use of Green's Second Identity:

$$\begin{aligned} &\int_V \left(G(\vec{\xi},\vec{x},\tau-t)\nabla^2\dot{\phi}(\vec{x}) - \dot{\phi}(\vec{x})\nabla^2 G(\vec{\xi},\vec{x},\tau-t)\right) dV \\ &= \int_S \left[G(\vec{\xi},\vec{x},\tau-t)\frac{\partial}{\partial n}\dot{\phi}(\vec{x}) - \dot{\phi}(\vec{x})\frac{\partial}{\partial n}G(\vec{\xi},\vec{x},\tau-t)\right] dS \end{aligned} \qquad 3.18$$

As with the preceding section the left hand side of Equation 3.18 is equated to, the expression derived by Tang (1988) which includes points on the boundaries (see Equation 3.11)

$$\int_V \left(G(\vec{\xi},\vec{x},\tau-t)\nabla^2\dot{\phi}(\vec{x}) - \dot{\phi}(\vec{x})\nabla^2 G(\vec{\xi},\vec{x},\tau-t)\right) dV = C(\vec{\xi})\dot{\phi}(\vec{\xi}) \qquad 3.19$$

Thus, Equation 3.18 can be written as:

$$C(\vec{\xi})\dot{\phi}(\vec{\xi}) = \int_S \left[G(\vec{\xi},\vec{x},\tau-t)\frac{\partial}{\partial n}\dot{\phi}(\vec{x}) - \dot{\phi}(\vec{x})\frac{\partial}{\partial n}G(\vec{\xi},\vec{x},\tau-t)\right] dS \qquad 3.20$$

Equation 3.20 is first integrated with respect to time,

$$C(\vec{\xi},\tau)\phi(\vec{\xi},\tau) - C(\vec{\xi},0)\phi(\vec{\xi},0) = \int_0^t \int_S \left[G(\vec{\xi},\vec{x},\tau-t)\frac{\partial}{\partial n}\dot{\phi}(\vec{x}) - \dot{\phi}(\vec{x})\frac{\partial}{\partial n}G(\vec{\xi},\vec{x},\tau-t) \right] dSdt \qquad 3.21$$

and then the right side of the equation is evaluated by integrating by parts to arrive at the implicit time-domain boundary integral equation for the fluid domain governed by the Laplace Equation

$$\begin{aligned} C(\vec{\xi},\tau)\phi(\vec{\xi},\tau) - C(\vec{\xi},0)\phi(\vec{\xi},0) = & \int_S \left[\phi(\vec{x},0)\frac{\partial}{\partial n} - \frac{\partial}{\partial n}\phi(\vec{x},0) \right] G(\vec{\xi},\vec{x},\tau)\, dS \\ & - \int_S \left[\phi(\vec{x},\tau)\frac{\partial}{\partial n} - \frac{\partial}{\partial n}\phi(\vec{x},\tau) \right] G(\vec{\xi},\vec{x},0)\, dS \\ & + \int_0^t \int_S \left[\phi(\vec{x},\tau)\frac{\partial}{\partial n} - \frac{\partial}{\partial n}\phi(\vec{x},\tau) \right] \dot{G}(\vec{\xi},\vec{x},\tau-t)\, dSdt \end{aligned} \qquad 3.22$$

Since an analytical solution to Equation 3.22 is not likely for any practical problem, Equation 3.22 will be approximated by discretizing the boundary into J elements. The discretization of the problem changes the integral over the boundary to a summation over the number of elements. By shifting from the integral to the summation, Equation 3.22 can be written as:

$$C_l(\tau)\phi_l(\tau) - C_l(0)\phi_l(0) =$$

$$\sum_{j=1}^{J} \left\{ \int_{\Delta S_j} \frac{\partial}{\partial n}\phi_j(\tau)G_{lj}(0)dS(x) \right.$$

$$- \int_{\Delta S_j} \phi_j(\tau)\frac{\partial}{\partial n}G_{lj}(0)dS(x) + \int_{\Delta S_j} \phi_j(0)\frac{\partial}{\partial n}G_{lj}(\tau)dS(x) \qquad 3.23$$

$$- \int_{\Delta S_j}\frac{\partial}{\partial n}\phi_j(0)G_{lj}(\tau)dS(x) + \int_0^t \int_{\Delta S_j} \phi_j(\tau)\frac{\partial}{\partial n}\dot{G}_{lj}(\tau-t)dS(x)dt$$

$$\left. - \int_0^t \int_{\Delta S_j}\frac{\partial}{\partial n}\phi_j(\tau)\frac{\partial}{\partial n}G_{lj}(\tau-t)dS(x)dt \right\}$$

where the subscript l represents the point of interest ($\vec{\xi}$); the subscript j represents the source location ($\vec{x}$); and $\int_{\Delta S_j}(....)dS_j$ denotes the integral over the area of the jth element, j = 1,2,...,J and l = 1,2,...,J.

In Equation 3.23, each element could be approximated by a constant value. This amounts to approximating the boundary by a series of step functions. A better approximation is achieved by using shape functions based on nodal values. Any variable, p, can be approximated by:

$$p_i(x) = \psi_N(x)P_{iN} \qquad 3.24$$

where $p_i(x)$ is the ith component of the variable, Ψ_N is the shape function for node N, and P_{iN} is the ith component of the variable at node N, Leonard (1988). Isoparametric interpolation functions will be used which will be consistent with the interpolation functions used in the FEM. Isoparametric functions imply that the

interpolation functions for both the geometry and the dynamic unknowns are the same. These isoparametric shape functions have the property that their numerical value is unity at node N and zero at other nodes. In addition, the polynomial shape functions used map the general quadrilateral surface element curved in three-dimensional space onto two-dimensional squares. The squares have local coordinates ζ_1 and ζ_2, with each ranging from -1 to 1.

The choice of shape functions, i.e., order of interpolation, has a significant effect on the accuracy and efficiency of the numerical solution. With the simplest linear shape functions, flat elements are obtained and numerous elements are needed. Using higher-order shape functions generally means less elements are needed but the computational effort is more. Table 3.1 is the isoparametric shape functions used in the BEM, Leonard (1988).

Incorporating the interpolation functions one can write Equation 3.23 as

Table 3.1 Quadrilateral Isoparametric Shape Function

Element	Number of nodes	Shape functions
Linear	4	$\Psi_1 = (1 + \zeta_1)(1 + \zeta_2)/4$ $\Psi_2 = (1 - \zeta_1)(1 + \zeta_2)/4$ $\Psi_3 = (1 - \zeta_1)(1 - \zeta_2)/4$ $\Psi_4 = (1 + \zeta_1)(1 - \zeta_2)/4$
Quadratic	8	$\Psi_1 = (1 + \zeta_1)(1 + \zeta_2)(\zeta_1 + \zeta_2 - 1)/4$ $\Psi_2 = (1 - \zeta_1)(1 + \zeta_2)(-\zeta_1 + \zeta_2 - 1)/4$ $\Psi_3 = (1 - \zeta_1)(1 - \zeta_2)(-\zeta_1 - \zeta_2 - 1)/4$ $\Psi_4 = (1 + \zeta_1)(1 - \zeta_2)(\zeta_1 - \zeta_2 - 1)/4$ $\Psi_5 = (1 - \zeta_1)(1 - \zeta_2)(1 + \zeta_2)/2$ $\Psi_6 = (1 - \zeta_1)(1 + \zeta_2)(1 + \zeta_2)/2$ $\Psi_7 = (1 - \zeta_1)(1 + \zeta_2)(1 - \zeta_2)/2$ $\Psi_8 = (1 - \zeta_1)(1 + \zeta_2)(1 - \zeta_2)/2$
Cubic	12	$\Psi_1 = (1 + \zeta_1)(1 + \zeta_2)(9\zeta_1 + 9\zeta_2 - 10)/32$ $\Psi_2 = (1 - \zeta_1)(1 + \zeta_2)(9\zeta_1 + 9\zeta_2 - 10)/32$ $\Psi_3 = (1 - \zeta_1)(1 - \zeta_2)(9\zeta_1 + 9\zeta_2 - 10)/32$ $\Psi_4 = (1 + \zeta_1)(1 - \zeta_2)(9\zeta_1 + 9\zeta_2 - 10)/32$ $\Psi_5 = (1 + \zeta_1)(1 - \zeta_2^2)(1 - 3\zeta_2)9/32$ $\Psi_6 = (1 + \zeta_2)(1 - \zeta_1^2)(1 + 3\zeta_2)9/32$ $\Psi_7 = (1 - \zeta_1)(1 - \zeta_2^2)(1 + 3\zeta_2)9/32$ $\Psi_8 = (1 - \zeta_2)(1 - \zeta_1^2)(1 - 3\zeta_1)9/32$ $\Psi_9 = (1 + \zeta_1)(1 - \zeta_2^2)(1 + 3\zeta_2)9/32$ $\Psi_{10} = (1 + \zeta_2)(1 - \zeta_1^2)(1 - 3\zeta_1)9/32$ $\Psi_{11} = (1 - \zeta_1)(1 - \zeta_2^2)(1 - 3\zeta_2)9/32$ $\Psi_{12} = (1 - \zeta_2)(1 - \zeta_1^2)(1 - 3\zeta_1)9/32$

$$C_M(\tau)\phi_M(\tau) - C_M(0)\phi_M(0) =$$

$$\sum_{j=1}^{J} \left\{ \int_{\Delta S_j} \psi_N \frac{\partial}{\partial n}\phi_N(\tau) G_{MN}(0) dS(x) \right.$$

$$- \int_{\Delta S_j} \psi_N \phi_N(\tau) \frac{\partial}{\partial n} G_{MN}(0) dS(x) + \int_{\Delta S_j} \psi_N \phi_N(0) \frac{\partial}{\partial n} G_{MN}(\tau) dS(x) \qquad 3.25$$

$$- \int_{\Delta S_j} \psi_N \frac{\partial}{\partial n}\phi_N(0) G_{MN}(\tau) dS(x) + \int_0^t \int_{\Delta S_j} \psi_N \phi_N(\tau) \frac{\partial}{\partial n} \dot{G}_{MN}(\tau - t) dS(x) dt$$

$$\left. - \int_0^t \int_{\Delta S_j} \psi_N \frac{\partial}{\partial n}\phi_N(\tau) \dot{G}_{MN}(\tau - t) dS(x) dt \right\}$$

where the subscript M represents the node of interest ($\vec{\xi}$) and the subscript N represents the nodes of the jth element; j = 1,2,...,J J = number of elements; M = 1,2,...,NN; NN = number of nodes; N = 1,2,...,NN; $\phi_i = \Psi_N \phi_{iN}$ and $(\partial\phi/\partial n)_i = \Psi_N (\partial\phi/\partial n)_{iN}$.

For ease of numerical integration, Equation 3.25, which is in global coordinates, will be transformed to local coordinates, (ζ_1, ζ_2). The transformation, Zienkiewicz and Taylor (1989), is based on the vector algebra equation:

$$dS(x) = |a_1 x a_2| (d\zeta_1 d\zeta_2) \qquad 3.26$$

In terms of the unit base vectors $\vec{a}$ and $\vec{c}$ shown in Figure 3.2.

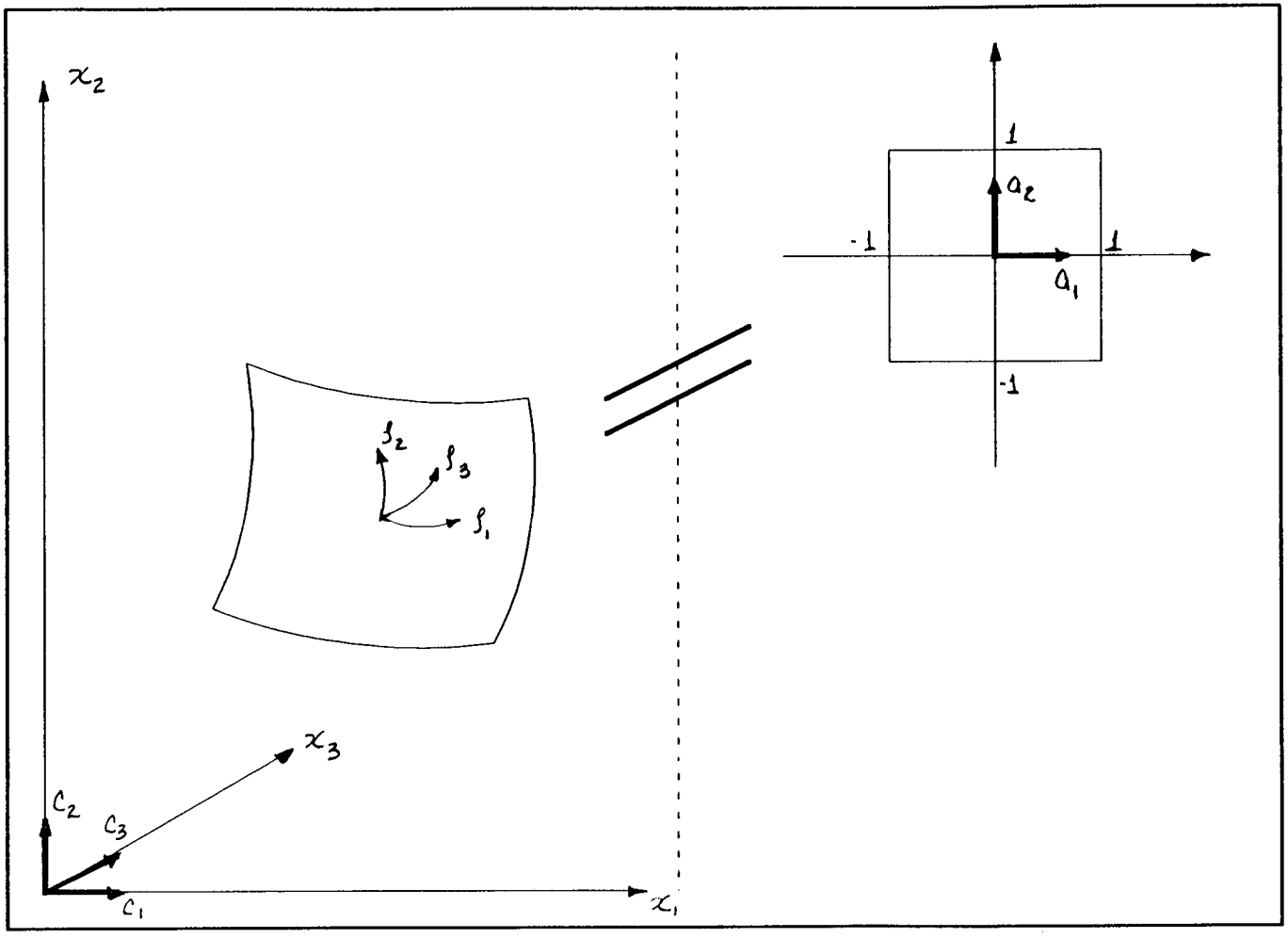

Figure 3.2 Mapping of $\vec{x}$ to $\vec{\zeta}$

$$a_1 = \left[c_1 \frac{\partial x_1}{\partial \zeta_1} , c_2 \frac{\partial x_2}{\partial \zeta_1} , c_3 \frac{\partial x_3}{\partial \zeta_1} \right] \qquad 3.27a$$

$$a_2 = \left[c_1 \frac{\partial x_1}{\partial \zeta_2} , c_2 \frac{\partial x_2}{\partial \zeta_2} , c_2 \frac{\partial x_3}{\partial \zeta_2} \right] \qquad 3.27b$$

one obtains

$$[dS(x)]^2 = [J_s \partial \zeta_1 \partial \zeta_2]^2 \qquad 3.28a$$

where J_s is the Jacobian of the transformation given by

$$J_s = \left\{ \left[\frac{\partial x_2}{\partial \zeta_1} \frac{\partial x_3}{\partial \zeta_2} - \frac{\partial x_3}{\partial \zeta_1} \frac{\partial x_2}{\partial \zeta_2} \right]^2 + \left[\frac{\partial x_1}{\partial \zeta_1} \frac{\partial x_3}{\partial \zeta_2} - \frac{\partial x_3}{\partial \zeta_1} \frac{\partial x_1}{\partial \zeta_2} \right]^2 + \left[\frac{\partial x_1}{\partial \zeta_1} \frac{\partial x_2}{\partial \zeta_2} - \frac{\partial x_2}{\partial \zeta_1} \frac{\partial x_1}{\partial \zeta_2} \right]^2 \right\} \qquad 3.28b$$

Upon the transformation to local coordinates, Equation 3.25 becomes

$$C_M(\tau)\phi_M(\tau) - C_M(0)\phi_M(0) =$$

$$\sum_{j=1}^{J} \left\{ \int J_s \psi_N \frac{\partial}{\partial n}\phi_N(\tau) G_{MN}(0) d\zeta_1 d\zeta_2 \right. \tag{3.29}$$

$$- \int J_s \psi_N \phi_N(\tau) \frac{\partial}{\partial n} G_{MN}(0) d\zeta_1 d\zeta_2 + \int J_s \psi_N \phi_N(0) \frac{\partial}{\partial n} G_{MN}(\tau) d\zeta_1 d\zeta_2$$

$$- \int J_s \psi_N \frac{\partial}{\partial n}\phi_N(0) G_{MN}(\tau) d\zeta_1 d\zeta_2 + \int_0^t \int J_s \psi_N \phi_N(\tau) \frac{\partial}{\partial n} \dot{G}_{MN}(\tau - t) d\zeta_1 d\zeta_2 dt$$

$$\left. - \int_o^t \int J_s \psi_N \frac{\partial}{\partial n}\phi_N(\tau) \dot{G}_{MN}(\tau - t) d\zeta_1 d\zeta_2 dt \right\}$$

The last two expressions in Equations 3.29 involve integrals in time and will be approximated linearly in the time interval. With these approximations Equation 3.29 becomes:

$$\underset{(1)}{C_M(\tau)\phi_M(\tau)} - \underset{(2)}{C_M(0)\phi_M(0)} =$$

$$\sum_{j=1}^{J} \left\{ \underset{(3)}{\int J_s \psi_N \frac{\partial}{\partial n}\phi_N(\tau) G_{MN}(0) d\zeta_1 d\zeta_2} \right. \tag{3.30}$$

$$- \underset{(4)}{\int J_s \psi_N \phi_N(\tau) \frac{\partial}{\partial n} G_{MN}(0) d\zeta_1 d\zeta_2} + \underset{(5)}{\int J_s \psi_N \phi_N(0) \frac{\partial}{\partial n} G_{MN}(\tau) d\zeta_1 d\zeta_2}$$

$$- \underset{(6)}{\int J_s \psi_N \frac{\partial}{\partial n}\phi_N(0) G_{MN}(\tau) d\zeta_1 d\zeta_2} + \frac{\Delta t}{2} \int J_s \psi_N \underset{(7a)}{(\phi_N(\tau)} - \underset{(7b)}{\phi_N(0)) \frac{\partial}{\partial n} \dot{G}_{MN}(0) d\zeta_1 d\zeta_2}$$

$$\left. - \frac{\Delta t}{2} \int J_s \psi_N \left[\underset{(8a)}{\frac{\partial}{\partial n}\phi_N(\tau)} - \underset{(8b)}{\frac{\partial}{\partial n}\phi_N(0)} \right] \dot{G}_{MN}(0) d\zeta_1 d\zeta_2 \right\}$$

The normal derivative of G is defined as:

$$\frac{\partial G}{\partial n} = \left\{ \frac{\partial \left[\frac{1}{4\pi r} \right]}{\partial r} \right\} \cos\gamma \tag{3.31}$$

$$\frac{\partial G}{\partial n} = \frac{-\cos\gamma}{4\pi r^2} \tag{3.32}$$

where γ = angle between $\vec{n}$ and $\vec{r}'$, $\vec{r}' = -\vec{r}$ and $\cos\gamma = (\vec{n} \bullet -\vec{r})/ r$.

In addition, there are time derivatives of the Green's Function and the normal derivative of the Green's Function.

$$\frac{\partial G}{\partial t} = \frac{\partial}{\partial t}\frac{1}{4\pi r} \tag{3.33}$$

$$\frac{\partial G}{\partial t} = \frac{-1}{4\pi r^2}\,\dot{r} \tag{3.34}$$

and

$$\frac{\partial}{\partial t}\frac{\partial}{\partial n}G = \frac{\partial}{\partial n}\left[\frac{-1}{4\pi r^2}\,\dot{r}\right] \tag{3.35}$$

$$\frac{\partial}{\partial t}\frac{\partial}{\partial n}G = \frac{1}{2\pi r^3}\cos\gamma\,\dot{r} \tag{3.36}$$

3.3 BOUNDARY ELEMENT MODEL

The boundary element integral in discretized form, Equation 3.30, becomes the BEM. After some rearrangement, Equation 3.30 can be written in matrix form

$$[H]|_{t=0}\,\{\phi\}|_t - [G]|_{t=0}\left\{\frac{\partial\phi}{\partial n}\right\}|_t = [H]|_t\,\{\phi\}|_{t=0} - [G]|_t\left\{\frac{\partial\phi}{\partial n}\right\}|_{t=0} \tag{3.36}$$

where [H] at time t=0, are the surface integrals found in terms (1), (4), and (7) of

Equation 3.30; [G] at time t=0 are the surface integrals found in terms (3) and (8a) of Equation 3.30; [H] at time t are the surface integrals found in terms (2), (5), and (7b); and [G] at time t are the surface integrals found in terms (6) and (8b). Equation 3.36 can be expanded to account for the various boundaries and the first term of Equation 3.36 is as follows:

$$\begin{bmatrix} H_{(fs)(fs)} & H_{(fs)(m)} & H_{(fs)(s)} & H_{(fs)(b)} & H_{(fs)(ff)} \\ H_{(m)(fs)} & H_{(m)(m)} & H_{(m)(s)} & H_{(m)(b)} & H_{(m)(ff)} \\ H_{(s)(fs)} & H_{(s)(m)} & H_{(s)(s)} & H_{(s)(b)} & H_{(s)(ff)} \\ H_{(b)(fs)} & H_{(b)(m)} & H_{(b)(s)} & H_{(b)(b)} & H_{(b)(ff)} \\ H_{(ff)(fs)} & H_{(ff)(m)} & H_{(ff)(s)} & H_{(ff)(b)} & H_{(ff)(ff)} \end{bmatrix} \begin{Bmatrix} \phi_{(fs)} \\ \phi_{(m)} \\ \phi_{(s)} \\ \phi_{(b)} \\ \phi_{(ff)} \end{Bmatrix} \qquad 3.37$$

where fs = free surface boundary, m = membrane boundary, s = solid boundaries ($\partial\phi/\partial n = 0$), b = bottom boundary, and ff = the far field boundary.

In the boundary element integral there are three variables that are defined on the boundaries; the velocity potential, the normal derivative of the velocity potential, and the location of the boundary. At time t=0, the variables are known and at time t they are known or unknown, depending on the boundary, see Figure 3.3. Of the unknowns some are estimated in order to establish a system of equations that can be solved. In this model, the normal derivative of the velocity potential on the location of all boundaries except the free surface are known. The velocity potential is unknown everywhere except on the far field boundaries. On the free surface none of the variables are known *a priori*, thus an iterative

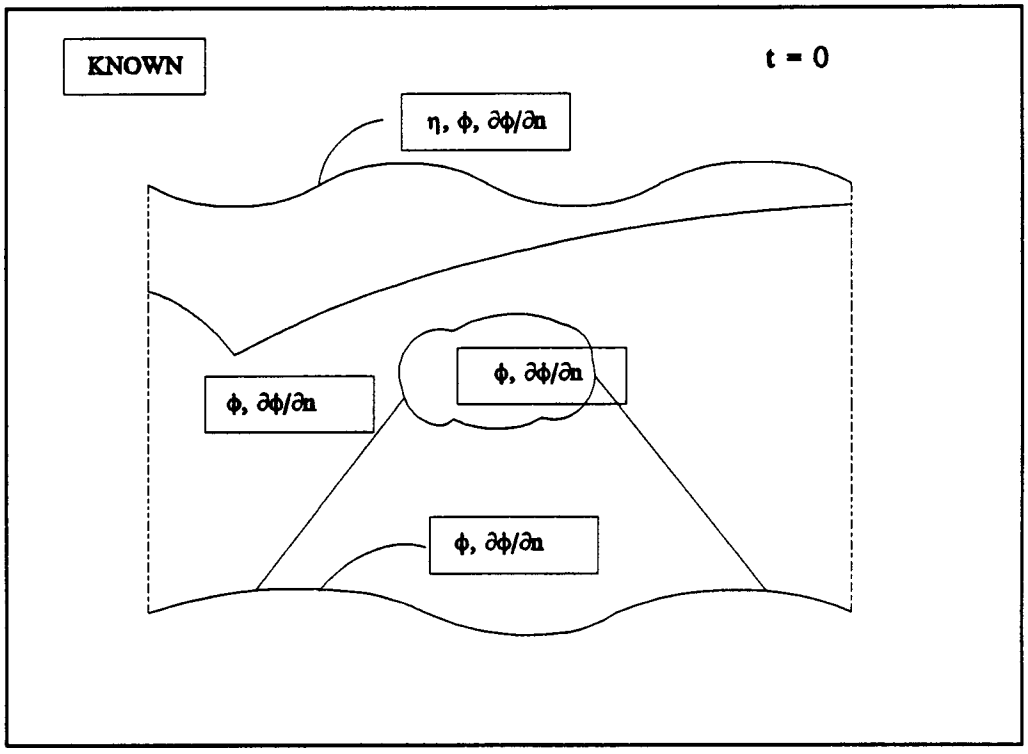

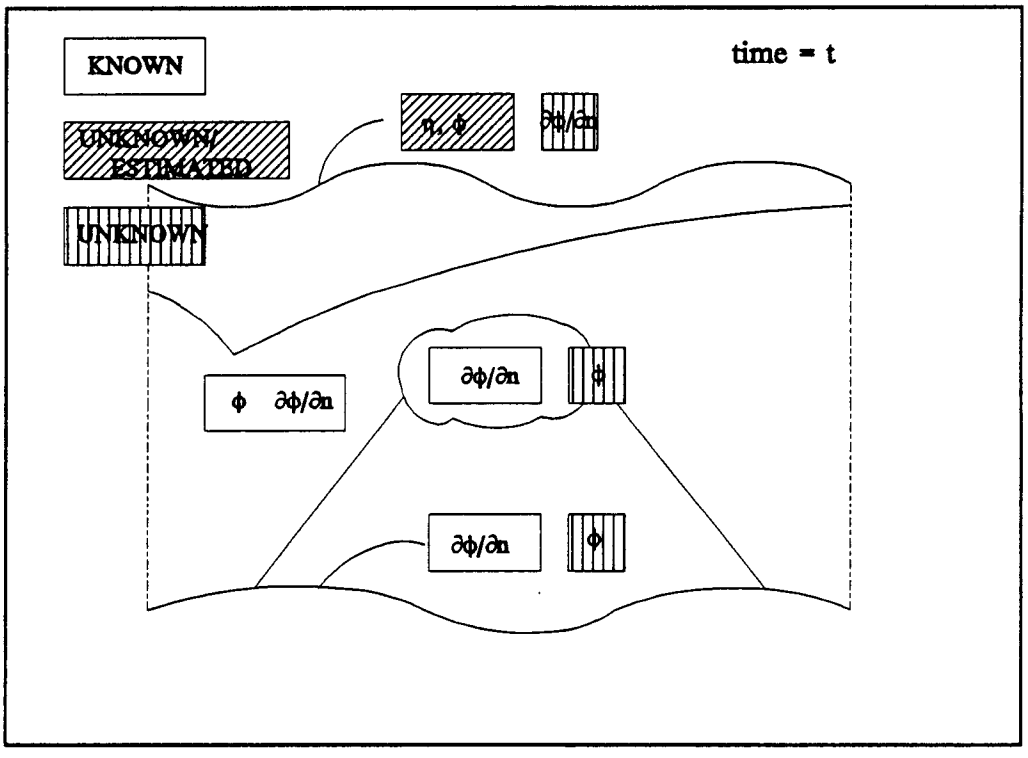

Figure 3.3 Known and Unknown Variables

procedure is required as follows: first, estimate the location of and velocity potential on the free surface; second, solve for the unknown velocity potential on all boundaries except the free surface and the far field boundary and the normal derivative of the velocity potential on the free surface; third, re-compute the location of and the velocity potential on the free surface using the results from the second step; and fourth, compare the computed and estimated values. If the two are not equivalent to within some tolerance use the computed values and re-solve for the unknowns.

The matrix equation, Equation 3.36, can be rearranged to generate the following solvable system of equations

$$\begin{bmatrix} G_{(fs)(fs)} & H_{(fs)(m)} & H_{(fs)(s)} & H_{(fs)(b)} & H_{(fs)(ff)} \\ G_{(m)(fs)} & H_{(m)(m)} & H_{(m)(s)} & H_{(m)(b)} & H_{(m)(ff)} \\ G_{(s)(fs)} & H_{(s)(m)} & H_{(s)(s)} & H_{(s)(b)} & H_{(s)(ff)} \\ G_{(b)(fs)} & H_{(b)(m)} & H_{(b)(s)} & H_{(b)(b)} & H_{(b)(ff)} \end{bmatrix} \begin{Bmatrix} \frac{\partial \phi}{\partial n}_{(fs)} \\ \phi_{(m)} \\ \phi_{(s)} \\ \phi_{(b)} \end{Bmatrix} = \begin{Bmatrix} B_{(fs)} \\ B_{(m)} \\ B_{(s)} \\ B_{(b)} \end{Bmatrix} \qquad 3.38$$

where, for an example,

$$
\begin{aligned}
B_{(fs)} = \{ & H_{(fs)(fs)}|_t \, \phi_{(fs)}|_{t=0} + H_{(fs)(m)}|_t \, \phi_{(m)}|_{t=0} + H_{(fs)(s)}|_t \, \phi_{(s)}|_{t=0} \\
& + H_{(fs)(b)}|_t \, \phi_{(b)}|_{t=0} + H_{(fs)(ff)}|_t \, \phi_{(ff)}|_{t=0} - G_{(fs)(fs)}|_t \, \frac{\partial \phi}{\partial n_{(fs)}}|_{t=0} \\
& - G_{(fs)(m)}|_t \, \frac{\partial \phi}{\partial n_{(m)}}|_{t=0} - G_{(fs)(s)}|_t \, \frac{\partial \phi}{\partial n_{(s)}}|_{t=0} - G_{(fs)(b)}|_t \, \frac{\partial \phi}{\partial n_{(b)}}|_{t=0} \\
& - G_{(fs)(ff)}|_t \, \frac{\partial \phi}{\partial n_{(ff)}}|_{t=0} - H_{(fs)(fs)}|_{t=0} \, \phi_{(fs)}|_t + G_{(fs)(m)}|_{t=0} \, \frac{\partial \phi}{\partial n_{(m)}}|_t \\
& + G_{(fs)(s)}|_{t=0} \, \frac{\partial \phi}{\partial n_{(s)}}|_t + G_{(fs)(b)}|_{t=0} \, \frac{\partial \phi}{\partial n_{(b)}}|_t + G_{(fs)(ff)}|_{t=0} \, \frac{\partial \phi}{\partial n_{(ff)}}|_t \; \}
\end{aligned}
$$

Although the location of the free surface and the velocity potential on the free surface are unknown, they must be estimated to generate a solvable system of equations.

The location of the free surface is computed from

$$\dot{\eta} n_{x_3} = -\frac{\partial \phi}{\partial n} \qquad 3.39$$

which is derived from the Stokes Material Surface for the free surface as follows: Given

$$SMS_f = \eta - x_3 = 0 \qquad on \; x_3 = \eta \qquad 2.15$$

$$\dot{\eta} = \frac{\partial \eta}{\partial t} = \frac{\partial \phi}{\partial x_1}\frac{\partial \eta}{\partial x_1} + \frac{\partial \phi}{\partial x_2}\frac{\partial \eta}{\partial x_2} - \frac{\partial \phi}{\partial x_3} \qquad 2.18$$

The unit normal for the free surface is

$$\vec{n} = \left[n_{x_1},\ n_{x_2},\ n_{x_3}\right] = \frac{\nabla SMS_f}{|\nabla SMS_f|} \qquad 3.40$$

and, therefore

$$\vec{n} = \frac{1}{A}\left[\frac{\partial \eta}{\partial x_1},\ \frac{\partial \eta}{\partial x_2},\ -1\right] \qquad 3.41$$

where

$$A = \left[\left(\frac{\partial \eta}{\partial x_1}\right)^2 + \left(\frac{\partial \eta}{\partial x_2}\right)^2 + 1\right]^{\frac{1}{2}}$$

Then,

$$\frac{\partial \phi}{\partial n} = \vec{\nabla}\phi \cdot \vec{n} = \frac{1}{A}\left[\frac{\partial \phi}{\partial x_1}\frac{\partial \eta}{\partial x_1} + \frac{\partial \phi}{\partial x_2}\frac{\partial \eta}{\partial x_2} - \frac{\partial \phi}{\partial x_3}\right] \qquad 3.42$$

and thus

$$\dot{\eta} n_{x_3} = -\frac{\partial \phi}{\partial n} \qquad 3.39$$

The velocity potential on the free surface is estimated from the dynamic free surface boundary condition, Equation 2.20

$$\dot{\phi} = \frac{\partial \phi}{\partial t} = g\eta + \frac{1}{2}q^2 - Q(t) \qquad 2.20$$

The time derivatives of η and ϕ are approximated by a finite difference scheme which symbolically is expressed as

$$\dot{f} = \frac{\partial f}{\partial t} = g(t) \qquad 3.43$$

where $\partial f/\partial t$ represents $\partial \eta/\partial t$ or $\partial \phi/\partial t$ and g(t) is the right hand side of Equation 3.39 or Equation 2.20. Given solutions at time t_p, solutions at time t are sought. Integration of Equation 3.43 from t_p to t can be performed symbolically to obtain

$$f_t = f_p + \int_{t_p}^{t} g(t)dt = f_p + C \qquad 3.44$$

where f_p and f_t are solutions at time t_p and t, respectively and C is the area under the g(t) versus t curve between t_p and t. The area, C, can be approximated in several ways one of which is

$$C = g_p \Delta t + c\Delta t(g_t - g_p) \qquad 3.45$$

where g_p and g_t are g evaluated at the two time points, t_p and t, respectively, and c is a parameter. Different approximation rules are obtained from different values of c. If c is less that 0.5 the integration rule is explicit; a forward difference rule is obtained with c=0. If c is equal to or greater than 0.5, the integration rule is implicit; a backward difference rule is obtained with c=1. With a value of c greater than 0.5 the solution will be artificially damped. With c=0.5, an average acceleration method, the solution will be implicit and undamped, Hildebrand (1974). In the present method, during the first pass in solving Equation 3.38 c = 0 and in subsequential passes c = 0.5.

The iterative procedure continues until the estimated values on the free water surface match the recomputed values. Once the estimated and re-computed values agree to the specific tolerance, time is incremented and solutions at the new time are sought. Flow charts and algorithms for the BEM are in Appendix A.

3.4 COUPLED BOUNDARY ELEMENT MODEL AND FINITE ELEMENT MODEL

3.4.1 Region I

In Region I there are four types of boundary conditions: the bottom boundary condition, the fluid/structure interface, the free surface boundary condition, and the radiation boundary condition. Everything at time t=0 is

known. At time t the following are known:

1. The normal derivative of the velocity potential on the bottom boundary conditions is zero.
2. The location of the bottom boundary condition is known since the bottom is assumed non-erodible and impermeable.
3. The velocity potential on the far field boundary.
4. The normal derivative of the velocity potential on the far field boundary.
5. The location of the far field boundary.

At time t the following are unknown but estimated:

1. The normal derivative of the velocity potential of the fluid/structure interface.
2. The location of the fluid/structure interface.
3. The location of the free water surface, η.
4. The velocity potential on the free surface.

At time t the unknowns are:

1. The velocity potential on the bottom boundary.
2. The velocity potential on the fluid/structure interface.
3. The normal derivative of the velocity potential on the free water surface.

Of the estimated values, Items 1 and 2 serve as input to the BEM and verification of these items comes through the coupling of the FEM and the BEM.

Once the velocity potential is computed, the pressure field acting on the fluid/structure interface is computed. The values calculated for the pressure field then serve as input into the FEM, where the velocity and location of the membrane are computed. An iterative procedure follows until the assumed values in the BEM match those computed in the FEM to some tolerance. The procedure described in the preceding section is used to estimate the location of the free surface and the velocity potential on the free surface.

3.4.2 Region II

In Region II there is only one boundary, the fluid/structure interface. As with Region I, the location and the normal derivative of the velocity potential are assumed and the velocity potential computed. Once the velocity potential is computed, the pressure field is computed and used as input into the FEM. The FEM computes the velocity and location of the structure. An iterative procedure between the two models will continue until the assumed and computed values are the same to within some tolerance.

CHAPTER 4 FINITE ELEMENT MODEL OF DEFORMABLE BODY

4.1 SUMMARY OF FINITE ELEMENT MODEL

The membrane is modeled using a finite element model (FEM) previously developed, Lo (1982). Modifications were required to couple the FEM and boundary element model (BEM). Although a complete description of the FEM can be found in Lo (1982), a summary of the model will be presented here. Portions of the material in this chapter were presented in Chapter 2 but are repeated for completeness. The model has the following capabilities:

- Develops initial static configuration
- Develops nonlinear static configuration
- Analyzes the modal behavior of the body
- Solves the dynamic equilibrium equations by direct time integration technique

The feature of the FEM that will be utilized in the coupled model is the solution of the dynamic equilibrium equations by direct time integration.

The FEM accounts for tension structures: cables and membranes. Cables are assumed to be in a state of uniaxial stress, while the membranes are assumed to be in a state of plane stress in local surface coordinates. This implies that the normal component of stress is negligible. The thickness of the membrane is assumed small, such that lines normal to the undeformed membrane midsurface remain normal to the deformed midsurface and the motion of the membrane is

characterized by the motion of the midsurface. Membrane stress is assumed constant throughout the thickness, which implies that the flexural rigidity is negligible. No assumptions are made on the magnitudes of the displacements and strains.

The dynamic equilibrium equation in a Total Lagrangian Reference Frame for the membrane from the Principle of Virtual Work is:

$$\underset{(i)}{\int_S N^{\alpha\beta}\delta e_{\alpha\beta} h dS} - \underset{(ii)}{\int_S {}^m\rho B_i \delta U_i h dS} + \underset{(iii)}{\int_S {}^m\rho \ddot{U}_i \delta U_i h dS} - \underset{(iv)}{\int_S T_i \delta U_i dS} - \underset{(v)}{F_i \delta U_i} = 0 \qquad 2.2$$

It should be noted that the formulation is based on curvilinear coordinates embedded in an arbitrarily selected reference surface and tensor notation is used. Equation 2.2 is referenced to the unstrained surface (a Total Lagrangian Reference Frame) but it could have been referenced to a static equilibrium surface (an Updated Lagrangian Reference Frame).

If the static equilibrium state were the reference frame and the dynamic motions were limited to small unforced excursions about this reference frame, the resulting equations would be the linear equations of free vibration of the membrane. These equations could be solved for modal responses (frequencies and shape), which could then be used for a modal superposition solution for small forced vibrations. Alternatively, if the unstrained state were the reference frame,

a total Lagrangian description of the nonlinear equations of motion would be obtained. An implicit integration technique could then be used to develop numerical solutions at discrete times for nonlinear motions.

Since an analytical solution to Equation 2.2 is not likely for any practical problem, the equation was approximated by discretizing the membrane into J finite elements. The discretization is accomplished by using isoparametric interpolation functions, which means that the same interpolation function is used for both the geometry and the displacements. The curvilinear coordinates (ζ_1, ζ_2) on the surface of the element are specified to be nondimensional natural coordinates that range from -1.0 to 1.0. The coordinates and displacements at a generic point (ζ_1, ζ_2) are given in terms of shape functions $\Psi(\zeta_1, \zeta_2)$ by

$$x_i(\zeta_1, \zeta_2) = \Psi_N(\zeta_1, \zeta_2) x_{iN} \qquad 4.1a$$

and

$$u_i(\zeta_1, \zeta_2) = \Psi_N(\zeta_1, \zeta_2) u_{iN} \qquad 4.1b$$

where x_{iN} is the ith cartesian coordinate of node N and u_{iN} is the ith cartesian component of displacement of node N. Repeated capital letters used as indices denote summation over the nodes or an element. Polynomial shape functions have been used, which map a general quadrilateral surface element curved in three-dimensional space onto two-dimensional squares.

The choice of shape functions has a significant effect on the accuracy and efficiency of the numerical solutions. With the simplest linear shape functions, flat elements are obtained and numerous element are needed. Discontinuities in strain and hence stresses will be predicted at element boundaries. However, less nodes are required per element and the resulting finite element model will be seen to be less stiff than those obtained using higher-order shape functions. With higher-order shape functions, more accurate results can be obtained because they provide better predictions of the equilibrium shape and discontinuities in the stresses are eliminated. They do require an intensive computational effort at the element level and lead to stiffer results.

With Equation 4.1a the various geometric parameters of Equation 2.2 can be written as:

$$A_{\alpha\beta} = \text{metric tensor} = \Psi_{N,\alpha}\, \Psi_{M,\beta}\, x_{Ni}\, x_{Mi} \qquad 4.2$$

where $A_{\alpha\beta}$ accounts for the transformation of the element in cartesian coordinates to curvilinear coordinates so the integration can be conducted. The determinant of $A_{\alpha\beta}$ is:

$$\begin{aligned} A = & \left(\Psi_{M,1}\Psi_{N,1}\, x_{Mi}\, x_{Ni}\right)\left(\Psi_{Q,2}\Psi_{S,2}\, x_{Qj}\, x_{Sj}\right) \\ & - \left(\Psi_{M,1}\Psi_{N,2}\, x_{Mi}\, x_{Ni}\right)\left(\Psi_{Q,2}\Psi_{S,1}\, x_{Qj}\, x_{Sj}\right) \end{aligned} \qquad 4.3$$

and the normal to the surface is:

$$\hat{n} = \frac{e_{ijk}\,\Psi_{M,1}\Psi_{N,2}\,x_{Mj}\,x_{Nj}}{\sqrt{A}}\,\hat{e}_i \qquad 4.4$$

The other parts of Equation 2.2 need to be discretized using the interpolation function. They will be presented here, but for their development see Lo (1982). The strain tensor is written as

$$'e_{\alpha\beta} = \frac{1}{2}\,\Psi_{N,\alpha}\Psi_{M,\beta}\left(x_{iN}\,'u_{iM} + x_{iM}\,'u_{iN} + 'u_{iN}\,'u_{iM}\right) \qquad 4.5$$

where the ' implies the condition at time t and no superscript before the variable means that the variable is based on the reference frame (unstrained state). The stress resultants for a Hookean material are

$$'N^{\alpha\beta} = C^{\alpha\beta\lambda\mu}\,'e_{\lambda\mu} \qquad 4.6$$

where for an isotropic material

$$C^{\alpha\beta\lambda\mu} = \frac{hE\nu}{(1+\nu)(1-2\nu)}\,A^{\alpha\beta}A^{\lambda\mu} + \frac{hE\nu}{1+\nu}\left(A^{\alpha\lambda}A^{\beta\mu} + A^{\alpha\mu}A^{\beta\lambda}\right) \qquad 4.7$$

where E = Young's modulus and ν = Poisson's ratio.

Alternatively, for rubber-like Mooney material which is isotropic and incompressible,

$$'N^{\alpha\beta} = 2'\lambda \left\{ A^{\alpha\beta}\left[C_1 + C_2 '\lambda^2\right] + A^{\alpha\beta}\left[\frac{C_2}{'\lambda^2} - '\lambda^2\left(C_1 + C_2 A^{\eta\rho} 'A_{\eta\rho}\right)\right]\right\} \qquad 4.8$$

where C_1 and C_2 are material constants

$$\begin{aligned} 'A_{\eta\rho} &= A_{\eta\rho} + 'e_{\eta\rho} \\ 'A &= 'A_{11}'A_{22} - 'A_{12}'A_{21} \\ \lambda &= \sqrt{\frac{A}{'A}} \end{aligned} \qquad 4.9$$

Using the above Equations 4.1-4.9, one can write Equation 2.2 in the discretized form:

$$\begin{aligned} &\int_{-1}^{1}\int_{-1}^{1} \frac{1}{2} 'N^{\alpha\beta}\left(\Psi_{M,\alpha}\Psi_{N,\beta} + \Psi_{N,\alpha}\Psi_{M,\beta}\right)\left(x_{Mi} + 'u_{Mi}\right) h\sqrt{A}\, d\zeta_1 d\zeta_2 \\ &\qquad (i) \\ &- \int_{-1}^{1}\int_{-1}^{1} {}'\rho h' B_i \Psi_N \sqrt{A} d\zeta_1 d\zeta_2 + \int_{-1}^{1}\int_{-1}^{1} {}'\rho h \Psi_N \Psi_M '\ddot{U}_{M,i}\sqrt{A} d\zeta_1 d\zeta_2 \\ &\qquad (ii) \qquad\qquad (iii) \\ &- \int_{-1}^{1}\int_{-1}^{1} T_i \Psi_N \sqrt{a}\, d\zeta_1 d\zeta_2 - \underset{(v)}{F_i \delta U_i} = 0 \\ &\qquad (iv) \end{aligned} \qquad 4.10$$

Equation 4.10 represents a set of ordinary differential equations of dynamic equilibrium at time t. The equation is nonlinear in that:

- Material nonlinearities are possible in the restoring force, term i, since $'N^{\alpha\beta}$ can be replaced by nonlinear (Mooney) constitutive equations.

- The restoring force is nonlinear even if a linear constitutive relation is used, since the work of the restoring force includes products of finite displacement components, $'u_{Mi}$.
- Nonconservative loads are possible in the external traction force, T_i, if the magnitude or direction of the force is dependent on displacements, e.g., pressure.

The integrals in Equation 4.10 are computed numerically using Gaussian quadrature.

Equation 4.10 forms the basis for the finite element model. To solve for the nonlinear dynamic equilibrium equation a combined incremental and iterative scheme is used, for more information see Lo (1982).

4.2 HYDRODYNAMIC LOADING

As stated earlier, one of the primary aims of this research was to improve the computed hydrodynamic loads used in the FEM. To this end, the FEM has been coupled with a BEM of the fluid domain. The coupling is done iteratively with the hydrodynamic pressure being computed in the BEM and then used as input into the FEM, term (iv) in Equation 2.2. The FEM then computes the location and velocity of the membrane. Iteration is required since the pressure is computed assuming a position and velocity of the membrane. Iteration continues until the computed and assumed values are within a certain tolerance.

Pressures induced by hydrodynamic loads are nonconservative, the forces

change direction and magnitudes when the body undergoes deformation. It is computationally inconvenient to include external loads that are dependent on the displacements, since a nonsymmetric matrix is generated. In the present study, symmetry is preserved and effects of nonconservative loads are accounted for by iterations and by using an approximation for the external load vector, see Lo (1982).

CHAPTER 5 COUPLING OF BOUNDARY ELEMENT MODEL AND FINITE ELEMENT MODEL

5.1 NUMERICAL COUPLING OF MODELS

There are numerous approaches to coupling the boundary element model (BEM) and finite element model (FEM), Zienkiewicz and Taylor (1989). The models could be directly coupled during the formulation of the problem, providing BEM-hosted models or FEM-hosted models. The models could be incrementally coupled at different time steps or iteratively coupled at each time step. Or a combination of above could be used. For this work, iteratively coupling at each time step has been chosen, although in this chapter each method is briefly presented.

In the numerical discretization of a physical problem there are three basic solution techniques: finite difference, finite element, and boundary element. These three techniques are based on defining an engineering problem three different mathematical ways, Zienkiewicz and Taylor (1989):

- Finite difference. The physical system characteristics may be described by formulating the appropriate partial difference equations by considering some elemental portion of the domain and applying some physical law (conservation of mass). The particular solution is then found by applying the boundary conditions.
- Finite element. The physical problem can be described by applying

the variational principle or a weak integral form over the domain. The boundary conditions can be satisfied implicitly within this procedure or explicitly after the procedure has been applied.

- Boundary element. The physical problem can also be described using singular solutions of the governing differential equations. In this case, the boundary conditions are satisfied when solving the problem: indirectly by solving for the unknown distributions of the singular solutions, or directly by solving for the unknown "potentials."

Although these three procedures have been developed as unrelated numerical procedures, they in fact can be described as special cases of a weighted residual process.

The link between the procedures can be achieved in several ways. The problem may be one that has an inner region with nonlinearities and nonhomogeneities and an outer region where the problem is linear and homogeneous. The inner region is then discretized in some weighted residual process - finite element or finite difference - and the outer region is approximated by a boundary integral equation around the inner/outer interface in terms of the dependent variables and their derivatives. This integral relationship becomes the boundary condition for the inner region. In another case, an energy function may be introduced as the link between two models. The energy function enforces compatibility in some integral sense along the interface. Finally, the systems of

equations for each procedure could be linked prior to solving. The differences among these various coupling techniques is the treatment of the interface between the regions.

Care must be taken when using a coupled model to ensure that fictitious gaps between the elements do not affect the results. These numerical gaps are due to the way that the BEM satisfies the boundary conditions. In the BEM formulations, the governing equations are satisfied exactly in the domain but the boundary conditions are only approximately satisfied. The shape functions used for the BEM do not constrain the displacement field, but are merely an approximation of the boundary values for integration, Cox (1988).

5.2 DIRECT COUPLING

A symmetric or nonsymmetric approach can be taken to link a system of equations. The symmetric formulation gives rise to a symmetric and sometimes banded system of equations, which, in general, is computationally more efficient. When using this approach, compatibility is either forced explicitly or satisfied in some integral sense by modifying the variational or weighted residual procedure being used. Equilibrium in this formulation is satisfied in a nodal force sense. In the direct, nonsymmetric, mechanical form of coupling, compatibility is satisfied explicitly at the nodes. Equilibrium is achieved by nodal force matching, or a linking of the nodal tractions, or fluxes on the interface.

If the problem is dominated by a region where FEM is used, a FEM-hosted

model should be used. In a FEM-hosted model, the BEM subdomain is treated as one or several finite elements. In this approach, the boundary integral equations are the equivalent stiffness of the subdomain and can be assembled in the FEM. The stiffness can be obtained by a variational approach or a direct approach. In the variational approach the stiffness relationship is derived from a boundary variational equation. In the direct approach the boundary element equations are manipulated into a stiffness form. Generally in FEM models the system of equations is symmetric and banded, which is efficient to solve numerically. Thus care should be taken to keep the resulting stiffness matrices symmetric and banded. While it is possible to create symmetric and banded matrices using the direct method, Brebbia (1978), it is more straightforward to use the variational approach to do so.

In the case where the domain is dominated by BEM, the FEM subdomain becomes a boundary element region, and equilibrium and compatibility are approximately enforced along the interface. This is similar to breaking up a nonhomogeneous domain into several homogeneous domains. This method will result in equations that are nonsymmetric, which are not as efficiently solved as symmetric and banded matrices. The choice of which method, BEM or FEM, should be the host depends on which region predominates.

5.3 INCREMENTAL COUPLING

In this approach, the problem is leap-frogged through time. At time T, the

FEM is solved and those conditions are used at time T + Δt in the BEM. This step is repeated until the desired time is reached. This process is especially useful for systems where the time scales of the two models being coupled are different and different time steps are required for each model. In such a case, several time steps may be computed in one model before jumping to the other.

5.4 ITERATIVE COUPLING

In this approach, the FEM and BEM are solved at each time step and compatibility on the interface is insured in an iterative process. The position of the interface is assumed in the BEM and the forcing on the interface is computed. The computed conditions are then used in the FEM to compute the position of the interface. The computed and assumed positions are compared and an iterative procedure follows until the desired accuracy is achieved.

A successful example of an iterative approach was presented by Han (1986), who developed a numerical model to study the nonlinear interaction of wind-loaded pneumatic membrane structures. The membrane was modeled using a FEM and the medium surrounding the membrane was modeled using a BEM.

5.5 COUPLING IN THE DEFORMABLE BODY MODEL

In the model developed in this study, the BEM and FEM were coupled using the iterative coupling procedure. The process was as follows:

1) Using the FEM, a static equilibrium position is computed.

2) Assuming the position and velocity of the membrane, the BEM is used to compute the hydrodynamic pressures on the membrane. In the BEM, the model must iterate to the true position of the free surface.
3) With the hydrodynamic loads as input into the FEM, the position and velocity of the membrane are computed.
4) The assumed and computed values are compared and an iterative procedure follows until they were within a certain tolerance limit of each other.
5) At the next time step, the process is repeated from Step 2.

The procedure continues until the desired time is reached. Flow charts on the coupled model are shown in Appendix A.

CHAPTER 6 NUMERICAL RESULTS

Three examples are given in this chapter to demonstrate and validate aspects of the methodology and algorithm presented in Chapters 3 and 4. The examples considered involve the prediction of: 1) transient motions of the free surface when no structure is present; 2) the motions of the free water surface and the transient hydrodynamic forces on a rigid horizontal cylinder; and 3) the motions of the free water surface and transient deformations of a flexible horizontal membrane cylinder. Before results for the three examples are given, some general comments on the computer code and its implementation in Fortran are warranted.

6.1 COMMENTS ON THE NUMERICAL CODE

The ultimate aim of this research is to develop a time-domain numerical model of the nonlinear interaction of water waves and membrane structures. In particular, the goal is to improve the hydrodynamic load model used in the finite element model (FEM) previously developed, Lo (1982). To improve the hydrodynamics of the FEM a boundary element model (BEM) was developed to be coupled with the FEM. The resulting BEM is a valuable tool, independent of the coupled model, for evaluating water wave problems, such as wave/structure interaction where the structure is fixed.

The flow charts for the BEM and the coupled BEM and FEM are found in

Appendix A. The BEM is computationally intensive and has been implemented in Fortran on a Cray YMP super computer at the University of Illinois at Urbana-Champaign, National Center of Super Computing Application. The use of a super computer is required for two reasons: memory and number of computations. The memory requirements are based on the number of elements/nodes required to adequately model a problem. In general, a substantial number (1000 or more) of elements are needed to adequately model the domain. The numerical model is currently set up to store everything in the main memory, although it is possible that other machines could be used if out-of-core solvers were incorporated in the code.

Regarding the number of computations, the majority of the computational effort required is in generating the system of equations to be solved. The [H] and [G] matrices, Equation 3.36, must be re-computed at each iteration because of the deformable surfaces (the free water surface and the membrane boundary), which result in constantly changing distances between the source and the field points in the Green's Function, (see Section 3.2). If the deformable surfaces are eliminated or assumed to be fixed, the [H] and [G] matrices need only be computed once. In linear wave/rigid structure interaction problems this is in fact done, the free water surface is assumed to be at the still water surface and the structures to be stationary. When one of the surfaces is highly deformable, like the membrane boundary, the [H] and [G] matrices must be recomputed. Allowing the free surface to deform does not adversely affect the computational effort. Once the

[H] and [G] matrices are computed and the system of equations is generated, portions of the [H] and [G] matrices are arranged into the left hand side of Equation 3.38 and the necessary multiplications conducted to generate the right hand side of Equation 3.38. Then, the system of equations is solved using a LINPAK matrix solver resident on the Cray YMP. Although, the BEM appears as one step in the flow chart for the coupled model, Appendix B, the majority (in excess of 80 percent) of the computational effort is in the BEM. It should also be noted that the FEM can be executed on some personal computers at reasonable speeds, but a major increase in computational effort is required to include diffraction effects in the hydrodynamic loads. This can partly be seen by examining the numerical grids of the BEM and FEM, in Section 6.4

Care should be exercised when generating the numerical grids, in particular, in selecting aspect ratios and relative sizes of individual elements. There are standard guidelines on selecting shapes of elements, Zienkiewicz (1989). Besides avoiding sharp corners, one should grid the domain such that the elements approach rectangles with aspect ratios of no more than 4. One should avoid abruptly changing the relative size of an element in comparison to its neighbors. This proved to be particularly troublesome in the present work when the rigid cylinder (Section 6.3) was first modeled. The overall grid spacing was at first selected to be the same as for the no-structure model (Section 6.2), but several long/slender rectangles were added at and around the cylinder. Numerical instabilities developed in the area of the cylinder causing the model to diverge.

The numerical instabilities were eliminated by changing the grid spacing and by removing abrupt changes in the grid pattern.

Another difficulty that appeared when first modeling the rigid cylinder was the selection of an appropriate time step. For the free surface the desired accuracy requires ten data points per wave length and this accuracy should be carried over to the time domain. If ten data points are collected per wave length, ten data points should be collected per wave period. This is reasonable when the grid is uniform, but the time step is controlled by the smallest element of the grid. Isaacson and Cheung (1990) show a graph for the required minimum ratio of wave period to time step, $T/\Delta t$, as a function of the ratio of wave length to element size, $L/\Delta s$, for a stable solution. For a $L/\Delta s$ of ten, the $(T/\Delta t)_{min}$ should be approximately twelve and for a $L/\Delta s$ of twenty, the $(T/\Delta t)_{min}$ should be approximately eighteen. The important thing to note is that it is the smallest element that controls the time step required for a stable solution rather than the global accuracy desired for the model. In the present study, when the rigid cylinder example was first considered, the time step that provided approximately ten data points was used. This ignored the fact that the elements around the cylinder were smaller then the average free surface element and, consequently, numerical instabilities developed. When the time step was changed, a stable solution was obtained.

The difficulty of selecting an appropriate time step takes on a different aspect in the coupled model. The membrane and the fluid can have very different

time scales. In the fluid domain, the change in pressure can be adequately modeled with ten to twenty data points over a wave period. On the other hand, to adequately model the response of the membrane approximately one hundred data points per wave period are required. Thus, if the overall model time step is based on modeling the membrane response, there is an "overkill" in providing a stable solution for the fluid domain. This is particular troublesome since the majority of the computational effort is in the BEM. To reduce the computational effort, while still using a time step based on the membrane response, the hydrodynamic loads are re-computed at a different time step based on the BEM.

There are some basic questions that any numerical model needs to address: numerical stability, conservation of mass and energy and model sensitivity. The last issue, sensitivity has been addressed in the preceding paragraphs, and the model is sensitive to both the time step and the relative size of neighboring elements. Numerical stability is typically addressed by running long simulation times. During the developmental stages of the BEM long simulation runs were ran on a small problem in open water and stability of the BEM verified. Long simulation times were not typically ran on the BEM because of computer time limitations. For wave channel problems the simulation is stopped when wave reflection from the far wall reaches the structure, thus simulation times were typically eight cycles long.

Conservation of energy was also verified during the developmental stages of the BEM. Verification was on an open water problem where the initial

conditions were a fully developed sea surface. The energy content within the domain remained the same to ± three percent. The energy in the sea surface was also computed for an open water problem where at time zero the still water level was at elevation zero. The energy increased with time until the domain was fully developed and it reached a constant (± three percent).

Conservation of mass (volume) is an internal check within the numerical model. The volume contained within the fluid domain is computed at each time step. If the volume is not within ± five percent of the starting volume an error message is printed in the output file. Computations continue even though an error has been detected. Currently the check for the conservation of mass is based on a horizontal sea floor where each surface element is considered a cube of water. Submerged objects were ignored when computing the total volume. The error was detected once when the BEM grid had a gap and water was leaking out of the fluid domain.

The Bernoulli constant was computed at each time step and assumed constant throughout the domain. The Bernoulli constant is zero with linear wave theory and is computed on the far field boundary with finite amplitude wave theory. This method of computing the Bernoulli constant is based on steady state conditions and no fluid/structure interaction. How the Bernoulli constant develops during the initiation of waves and how it is altered when the waves interact with a structure is unknown and guidance was not available. For this reason, the Bernoulli constant was assumed constant throughout the fluid domain at each time step.

6.2 BOUNDARY ELEMENT MODEL - NO STRUCTURE

The numerical results that will be presented in this chapter are based on a three-dimensional model of a wave channel, see Appendix D for specifics of the wave channel. The wave channel is a two-dimensional basin with unidirectional waves and normally would be modeled using a two-dimensional approach. Since this example is the first step towards the solution of a cylindrical membrane problem, the wave channel was modeled in three-dimensions. The three-dimensional approach was desired since the anticipated motions of the cylinder are three-dimensional.

Figure 6.1 is a schematic of the large wave channel at the O.H. Hinsdale Wave Research Laboratory at Oregon State University. The channel is 342 feet long, 12 feet wide and 15 feet deep. A 100 foot section of the main testing area of the wave channel has been modeled in the BEM. The BEM grid is shown in Figure 6.2, and consisted of 1090 nodes and 1048 four-noded quadrilateral elements. The grid size and spacing were selected to provide an adequate representation of the free surface, given the incident wave. The incident wave conditions modeled were for a water depth of 9 feet, a wave period of 2 seconds, and a wave height of 1 foot.

The boundary conditions of the free surface and the bottom boundaries are described in Sections 2.4.2 and 2.4.4, respectively. The side walls and beach face have a similar kinematic boundary condition as the bottom boundary, i.e. $\partial\phi/\partial n = 0$. Only a single condition is required on each of these boundaries since the

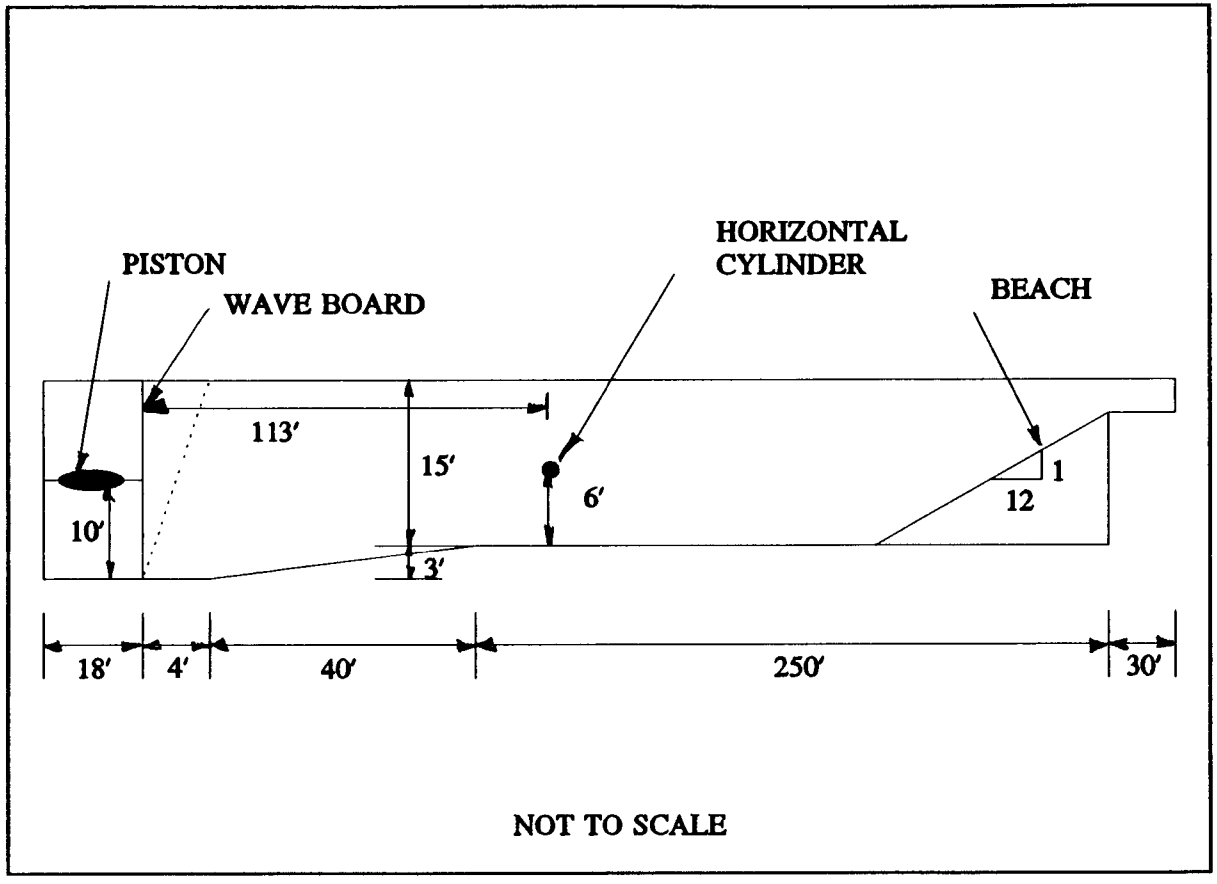

Figure 6.1 Schematic of Wave Channel

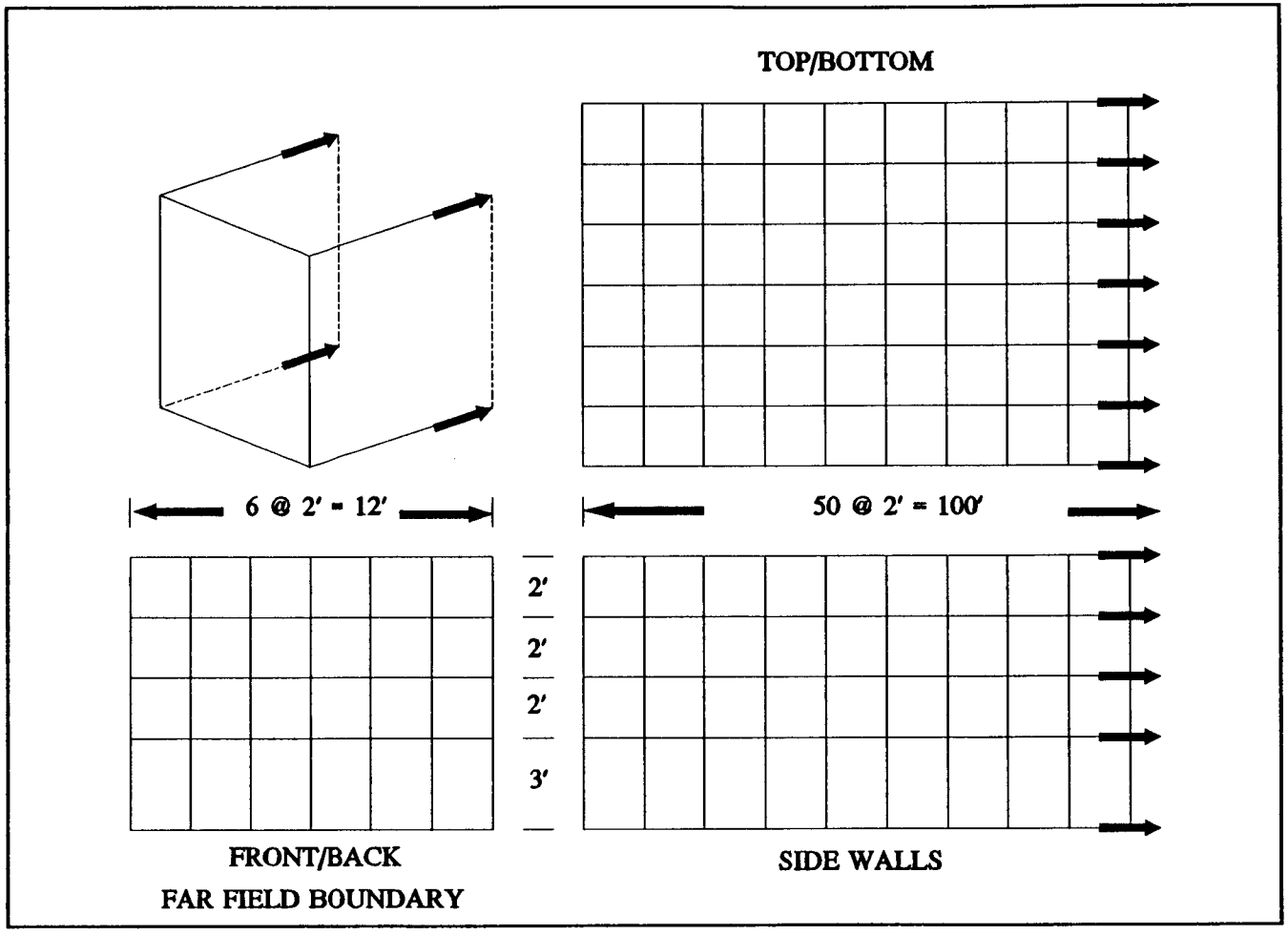

Figure 6.2 BEM Grid of Wave Channel

boundaries are non-deformable and fixed. On the far field boundary (wave maker) the location of, the velocity potential on, and the normal derivative of the velocity potential on the boundary can be computed using either linear wave theory or Stokes Finite Amplitude Wave Theory, Chakrabarti (1987). If finite amplitude wave theory is used the Bernoulli constant is computed on the far field boundary and assumed to be the same throughout the domain at that instant in time.

Figures 6.3 and 6.4 show the water surface elevation (non-dimensionalized by the wave amplitude) along the centerline of the wave channel (non-dimensionalized by the wave length) at selected times, 5 seconds and 6 seconds into the simulation, respectively. The water surface elevation predicted by the numerical model (solid line) is shown along with the incident wave (dashed line) which is inputted at $x/L = 0$. Inspection of these two figures shows that the generated waves are transforming from unsteady to steady waves and the first wave is a long stretched wave. The time history of the water surface elevation (non-dimensionalized by the wave amplitude) is shown in Figure 6.5. The data in Figure 6.5 is for a location a half a wave length into the BEM grid.

One concern with modeling the two-dimensional channel with a three-dimensional model was the accuracy in predicting the water surface elevation across the channel. In general, wave measurements are not taken across the width of the channel and a two-dimensional wave is assumed to have a constant wave height across the channel. Would this condition be shown in the numerical model? Figure 6.6 displays the surface elevation across the wave channel at the

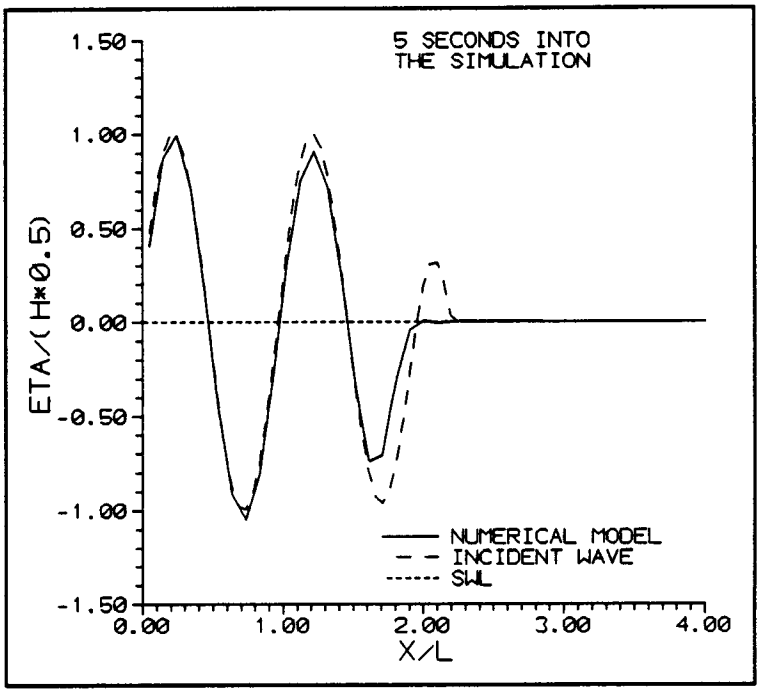

Figure 6.3 Water Surface Elevation Along the Wave Channel

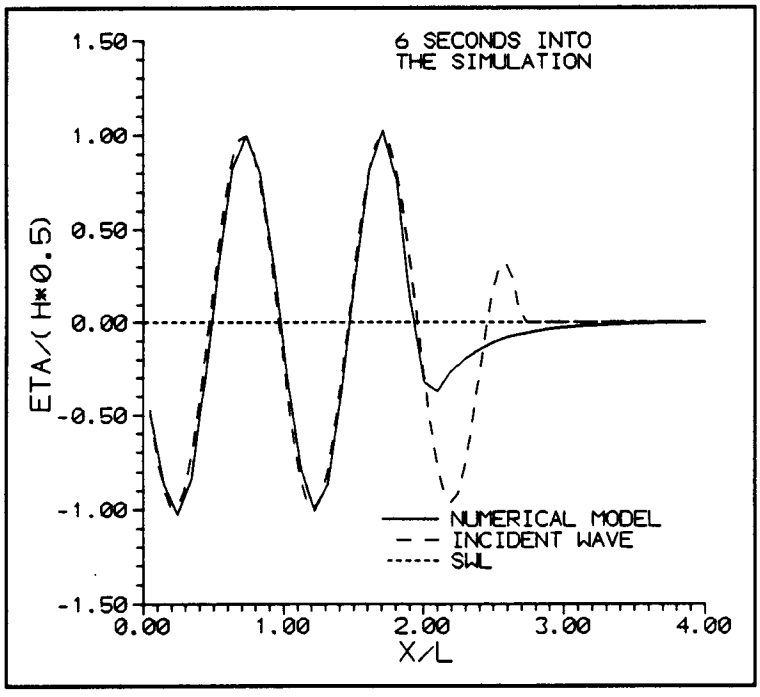

Figure 6.4 Water Surface Elevation Along the Wave Channel

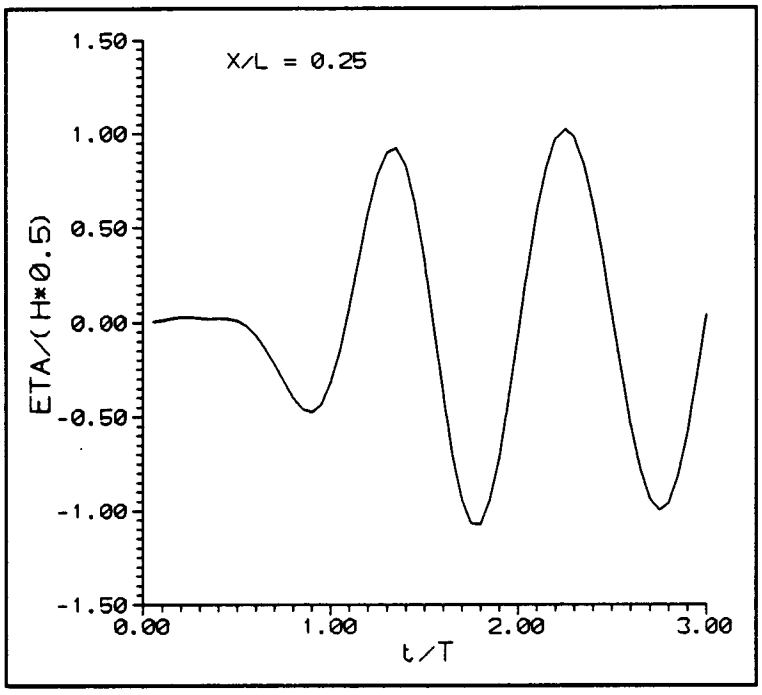

Figure 6.5 Water Surface Elevation

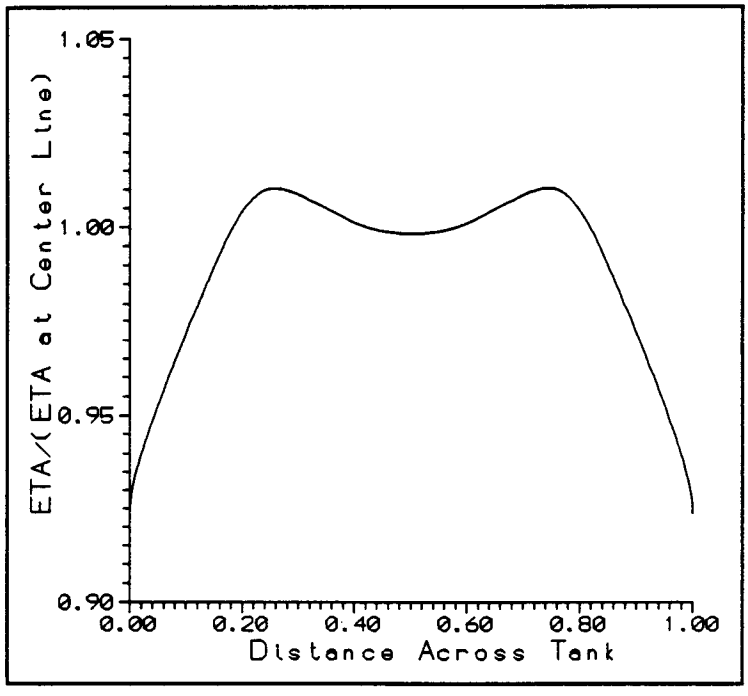

Figure 6.6 Water Surface Elevation Across the Wave Channel

center of the BEM grid. There is a slight symmetrical change in the water surface across the wave channel. The BEM grid in Figure 6.2, was selected so as to reduce the change across the wave channel to less than 8 percent.

6.3 BOUNDARY ELEMENT MODEL - RIGID CYLINDER

The next example problem considered was evaluation of the wave/structure interaction of a horizontal rigid circular cylinder submerged with its axis parallel to the wave crests, see Figure 6.7. The effects of submerged cylinders have been well studied, Chaplin (1984), Vada (1987), McIver and McIver (1990) and Isaacson and Cheung (1988 and 1990) to name a few. One of the most interesting characteristics about the flow about a submerged circular cylinder is that the reflection coefficient is zero, Isaacson and Cheung (1988). The reflection coefficient squared and transmission coefficient squared must sum to unity if there is no loss in energy. This implies that for a submerged circular cylinder the transmission coefficient should be unity and that the wave train should experience no change as it passes over the cylinder. In fact, the transmission coefficient is unity, the wave train undergoes a phase shift as it passes over the cylinder. The next step in verifying the BEM is to reproduce these results.

In Figure 6.1, the center of the cylinder was shown 113 feet from the wave board, which is 40 feet into the BEM grid. The cylinder has a 3-foot diameter and the center of the cylinder is 6 feet above the floor. The water depth is 9 feet providing 1.5 feet of submergence at the still water level. The incident wave has

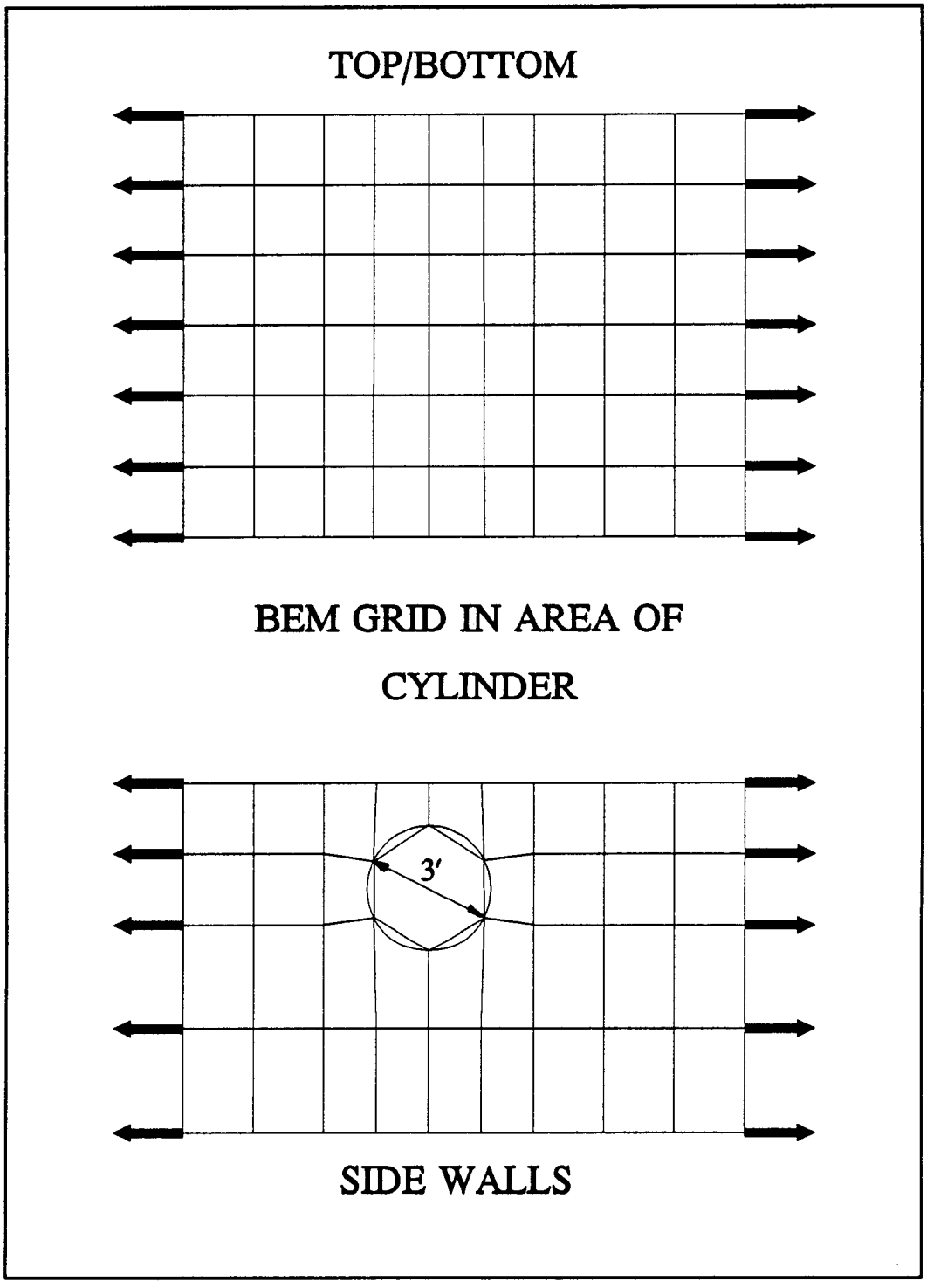

Figure 6.7 BEM Grid for the Rigid Cylinder

a wave period of 2 seconds and a wave height of 2 feet. The wave channel and BEM grid described in Section 6.2 were used for the submerged cylinder but the BEM grid was modified in the area of the cylinder. Figure 6.7 shows the refined BEM grid in the vicinity of the cylinder. After modifications, the BEM grid consists of 1151 nodes and 1102 four-noded quadrilateral elements. The cylinder surface is modeled using six elements circumferentially and six elements axially, for a total of 36 elements, see Figure 6.8.

The numerical results are shown in Figures 6.9 - 6.17. Figures 6.9 and 6.10 show the non-dimensionalized water surface elevation along the channel a quarter of a wave period apart. The centerline of the cylinder is located at x/L = 0. The solid line depicts the numerical results of the flow about a submerged horizontal cylinder and the dashed line depicts the numerical results without the cylinder. A small phase shift in the wave train as it passes over the cylinder can be seen in both Figures 6.9 and 6.10, but the wave height is approximately the same. The scattered wave train lags the incident wave train by approximately a tenth of a wave length, or approximately 36 degrees. Similar results have been shown by Isaacson and Cheung (1988) and are reproduced in Figure 6.11. The water surface elevations at points a quarter of a wave length fore and aft of the cylinder are shown in Figures 6.12 and 6.13, respectively. Again it can be seen that the wave amplitude is approximately the same fore and aft of the structure, with a phase shift aft of the structure.

The pressure on the cylinder is computed at each time step (see Section

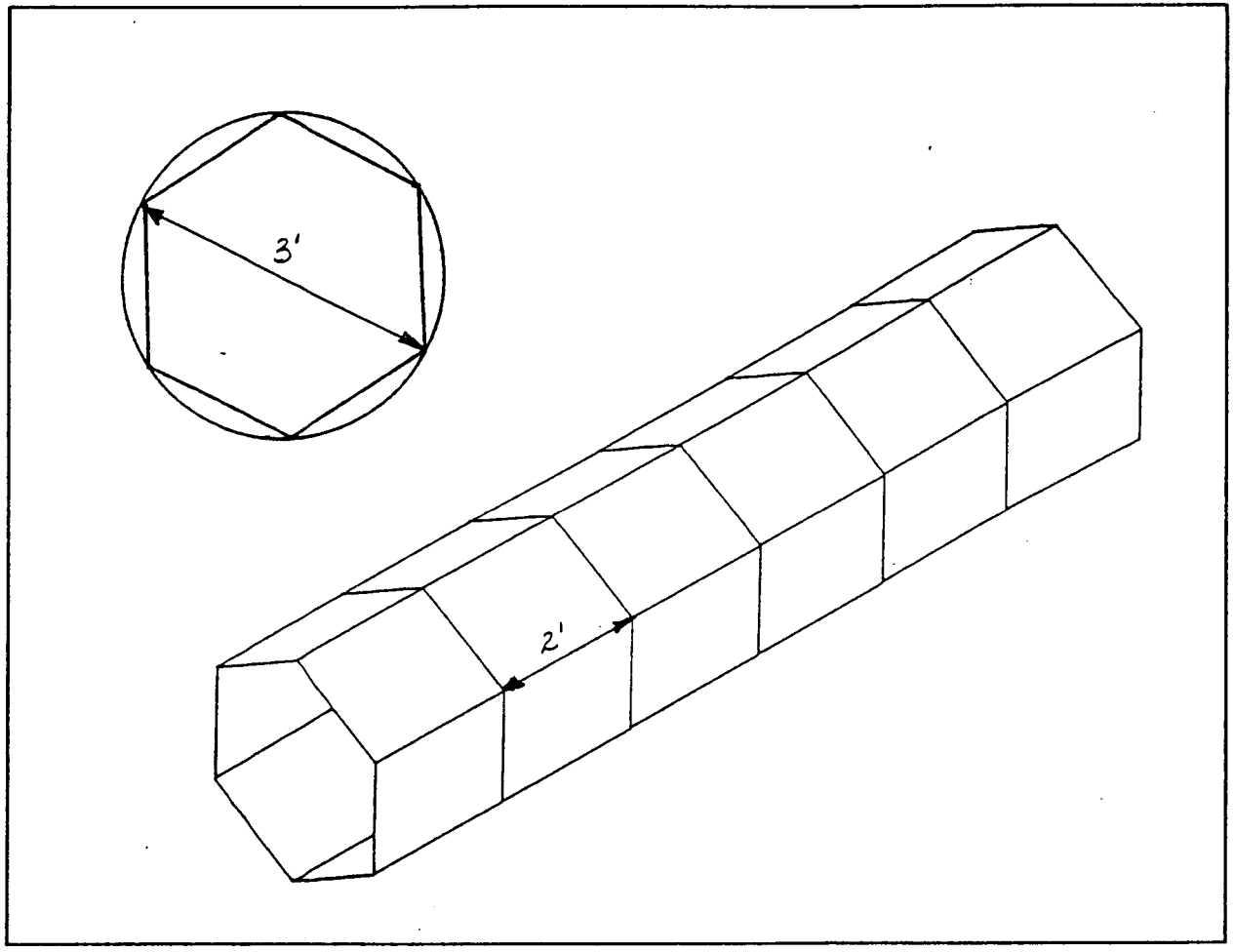

Figure 6.8 Schematic of the Rigid Cylinder

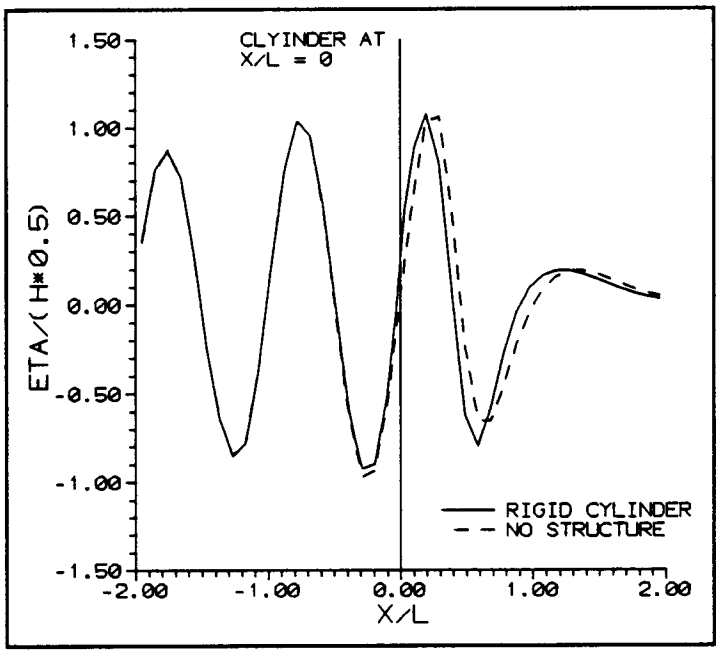

Figure 6.9 Water Surface Elevation Along the Wave Channel with a Rigid Cylinder at X/L = 0

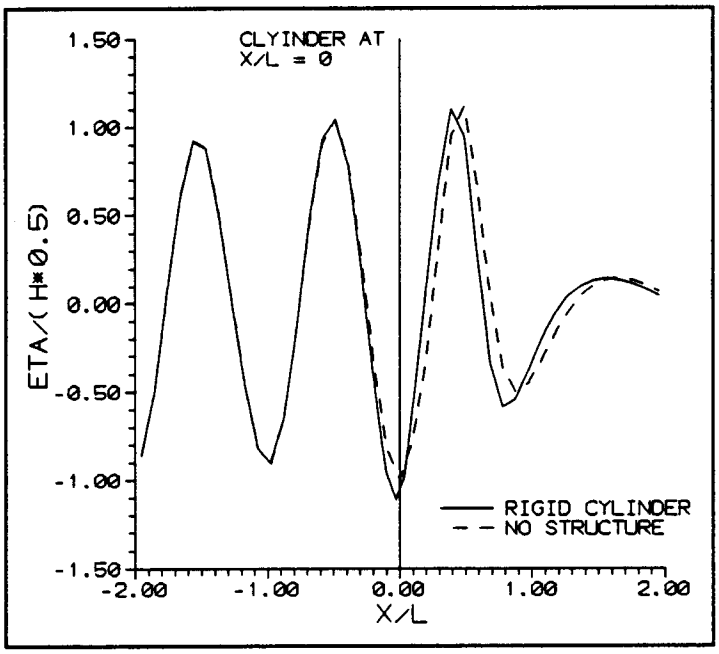

Figure 6.10 Water Surface Elevation Along the Wave Channel with a Rigid Cylinder at X/L = 0

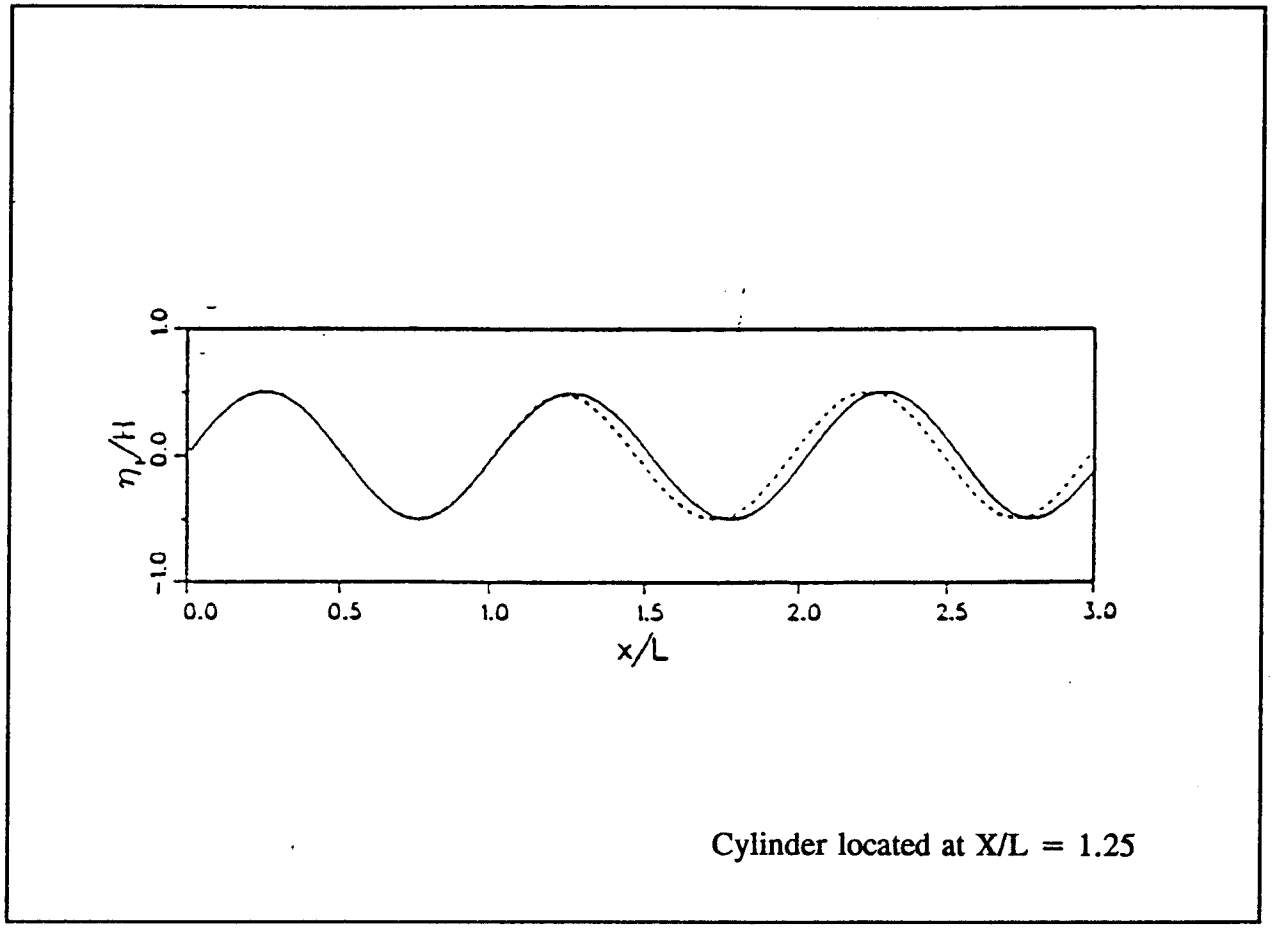

Figure 6.11 Phase Shift of Scattered Waves as Shown by Isaacson and Cheung (1988)

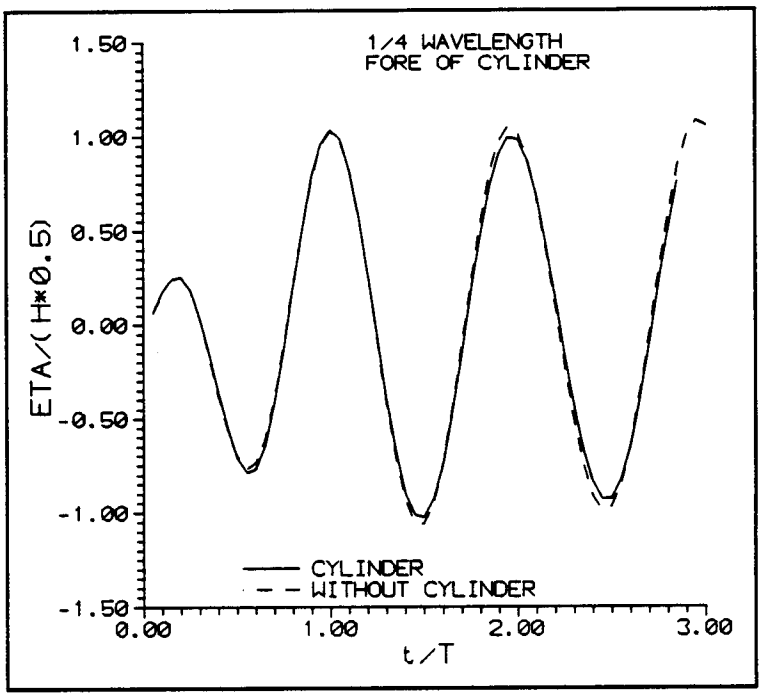

Figure 6.12 Water Surface Elevation Fore of the Clyinder

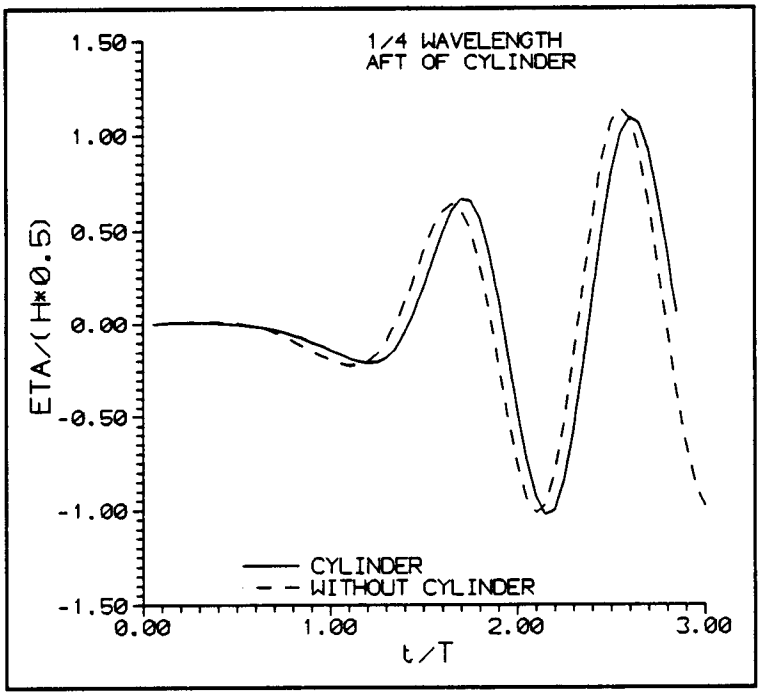

Figure 6.13 Water Surface Elevation Aft of the Cylinder

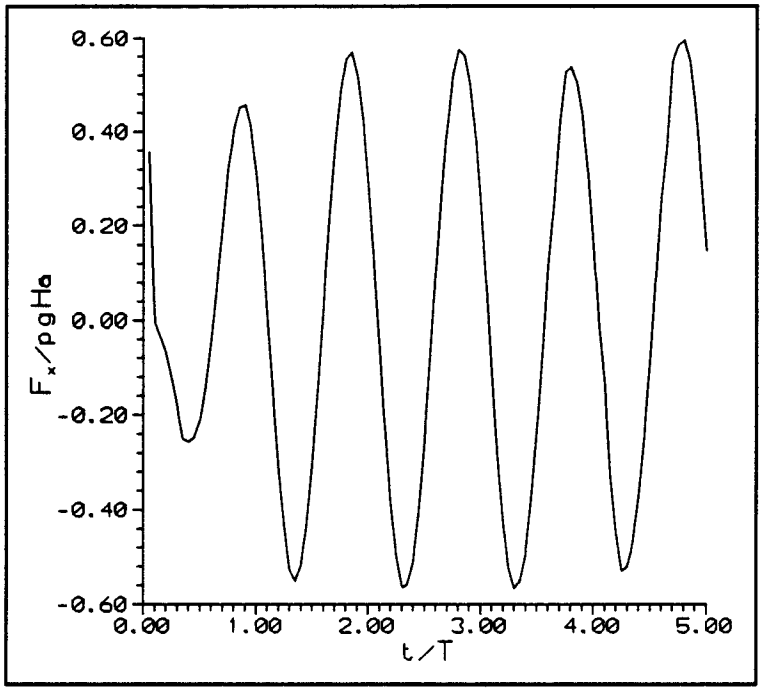

Figure 6.14 Horizontal Component of Wave Force on the Cylinder

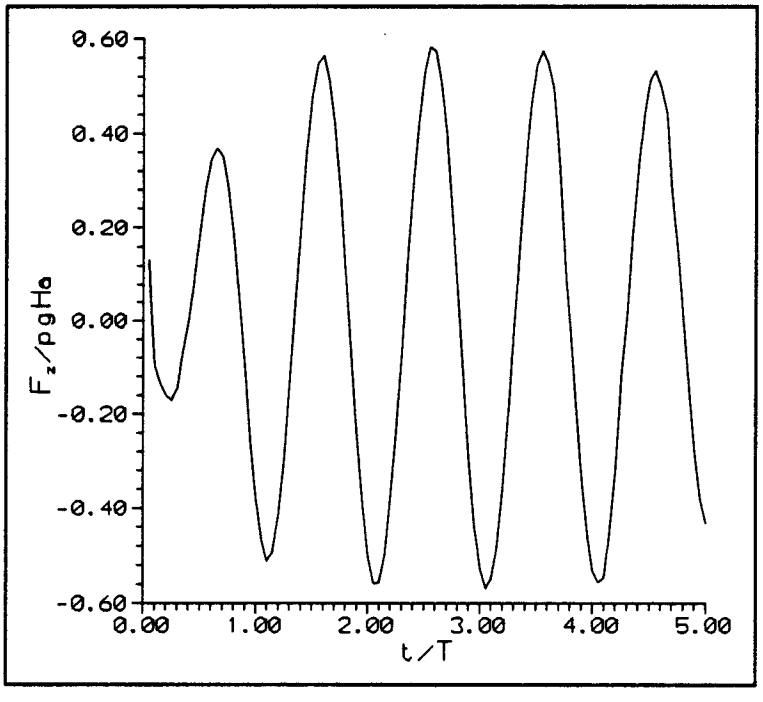

Figure 6.15 Vertical Component of Wave Force on the Cylinder

2.4.2). The horizontal and vertical components of force can then be computed from the pressures knowing the location and size of each element. The dimensionaless time histories of the resultant horizontal and vertical components on the axis of the cylinder are shown in Figures 6.14 and 6.15, respectively. The components have been non dimensionalized by ρgHa, where a is the radius of the cylinder. The time history of the magnitude of the total wave force is shown on Figure 6.16; the mean of the maximum dimensionaless force is 0.58. Figure 6.17 shows the dimensionaless force reported by Isaacson and Cheung, (1990) as a function of the wave period and the size of the cylinder (ka). The data presented in Figure 6.17 is based on experimental results of Vada (1987) and Chaplin (1984) and numerical results of Isaacson and Cheung (1990). The solid line is for a ratio of the depth of the cylinder axis below the water surface and the cylinder radius axis, h/a = 1.75 and the dashed line is for a h/a ratio of 2.0. For this example the wave period is 2 seconds, the water depth is 9 feet giving a wave number, k, of 0.3068, and a ka value of 0.46. The ratio of the depth of submergences of the cylinder to the cylinder radius is 2.00 and with a ka value of 0.46 the non-dimensionaless force would be 0.57. The value from this study 0.58 compares favorably to those presented in Figure 6.17.

It should be noted that according to Isaacson and Cheung (1990) the number of facets on the cylinder to accurately model the flow about, and the forces on, the cylinder is on the order of 50 facets. Their study was conducted in two-dimensions and they used an extremely large number of facets on both the

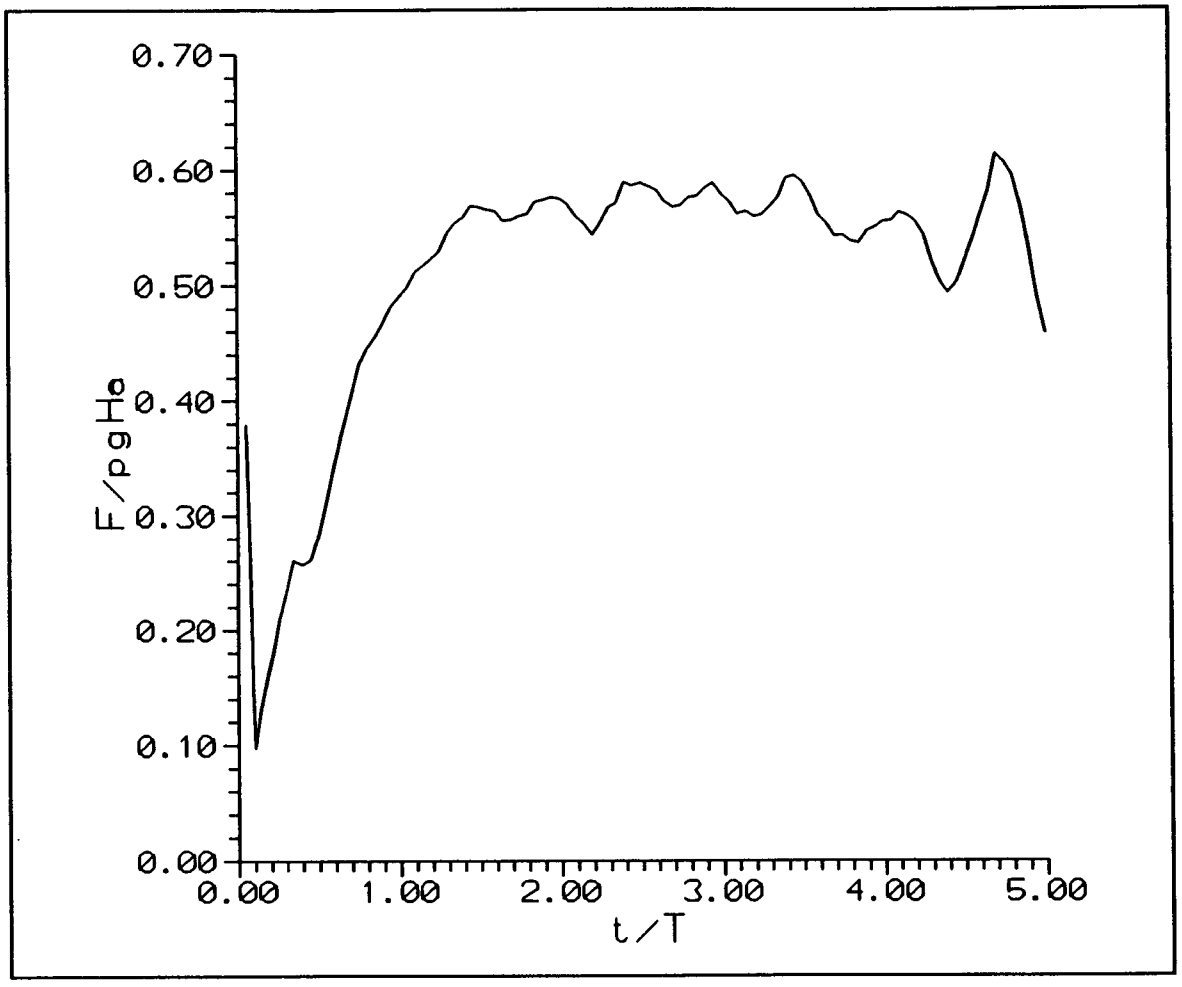

Figure 6.16 Magnitude of Total Wave Force on the Cylinder

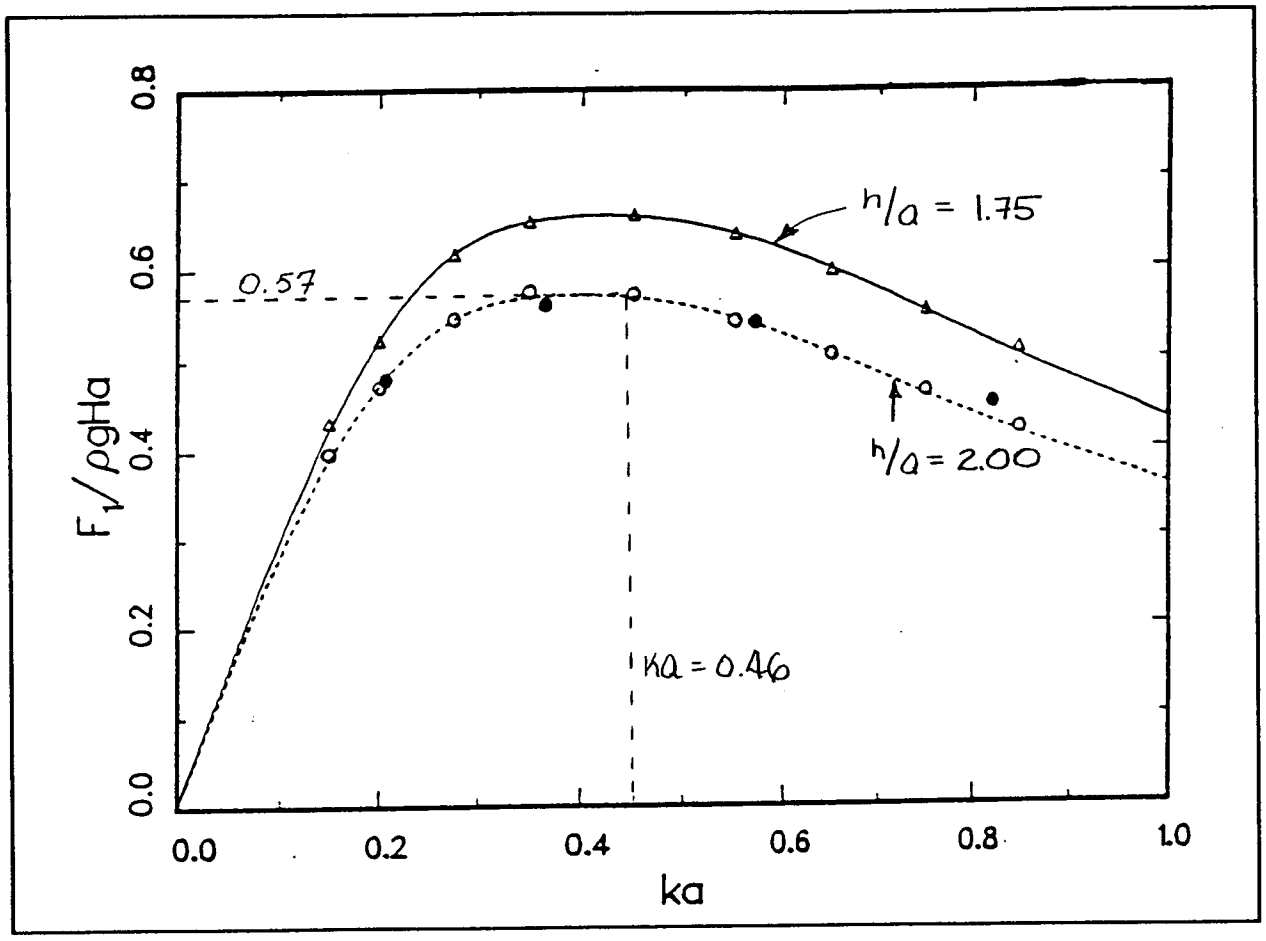

Figure 6.17 Wave Force as a Function of Wave Period, from Isaacson and Cheung (1990)

cylinder and the free surface. If this study were to try and duplicate the number of facets that they recommend the computational effort would be prohibitive. The ability of this study to reproduce the phase shift and the total wave force does not support the requirement (Isaacson and Cheung (1990)) of a large number of facets.

6.4 COUPLED BOUNDARY ELEMENT MODEL AND FINITE ELEMENT MODEL

The final example is a membrane interaction problem. The BEM has been verified in Sections 6.2 and 6.3; in particular, the ability of the model to predict the conditions on the free surface and the hydrodynamic loads on a rigid cylinder have been verified. This phase of the work involved comparison to results for two physical model tests conducted with a flexible membrane in the O.H. Hinsdale Wave Research Laboratory at Oregon State University.

Details of the experiment are given in Appendix C. Only a brief description will be given here along with experimental results needed to compare with numerical model results. The large two-dimensional wave channel (described earlier in Section 6.2) was used. A three-foot diameter cylindrical membrane made of 50 mil plasticized polyvinyl chloride fabric was clamped to circular steel flanges, which were attached to the side walls of the wave channel. The modulus of elasticity is approximately 8000 psi and the density of the material 0.05 lb/in^3. The cylinder was mounted horizontally at 6 feet above the channel floor and 113 feet from the wave board, see Figure 6.1. Three time histories of the water

surface were recorded using sonic profilers placed above, fore and aft of the cylinder. Displacements of the membrane were measured using three string pots placed at quarter points circumferentially around the cylinder, except at the bottom quarter point. All three string pots were located a fourth of the way across the channel. There was some concern that the string pots would affect the motion of the membrane; therefore point loads were added in the FEM to account for the string pots.

The majority of the wave channel is modeled as in the preceding sections (Sections 6.2 and 6.3). The cylinder is modeled using 36 eight-noded quadrilaterals in the BEM, see Figure 6.18. A FEM grid of only half of the cylinder (18 eight-noded quadrilaterals) was used and a symmetry condition was enforced half way across the channel. Figure 6.19 shows the FEM grid used to model the cylindrical membrane.

To account for the fluid mass enclosed by the fluid, lump masses were distributed at the nodes. The magnitudes of the lump masses were equivalent to the fluid mass enclosed by the membrane. To pre-stress the membrane the following boundary conditions were applied: the end attached to the steel flange was constrained both in the vertical direction and perpendicular to the membrane axis, an axial load was applied at the channel wall; and at the center of the channel where the symmetry condition was imposed, the membrane was constrained in the axial direction but free to move in the vertical direction and perpendicular to the axis. The FEM computes the location and velocities of the

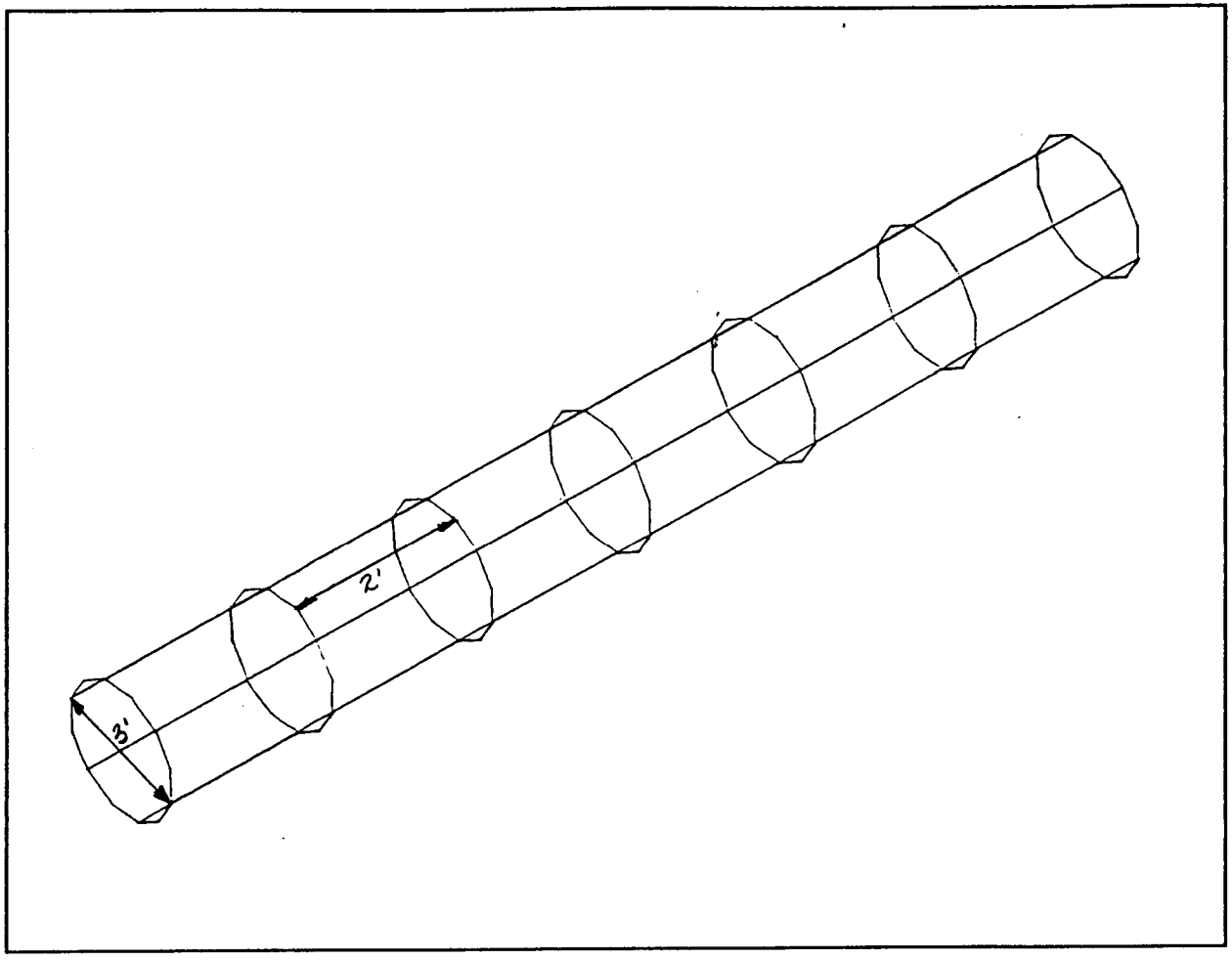

Figure 6.18 BEM Grid for the Cylindrical Membrane

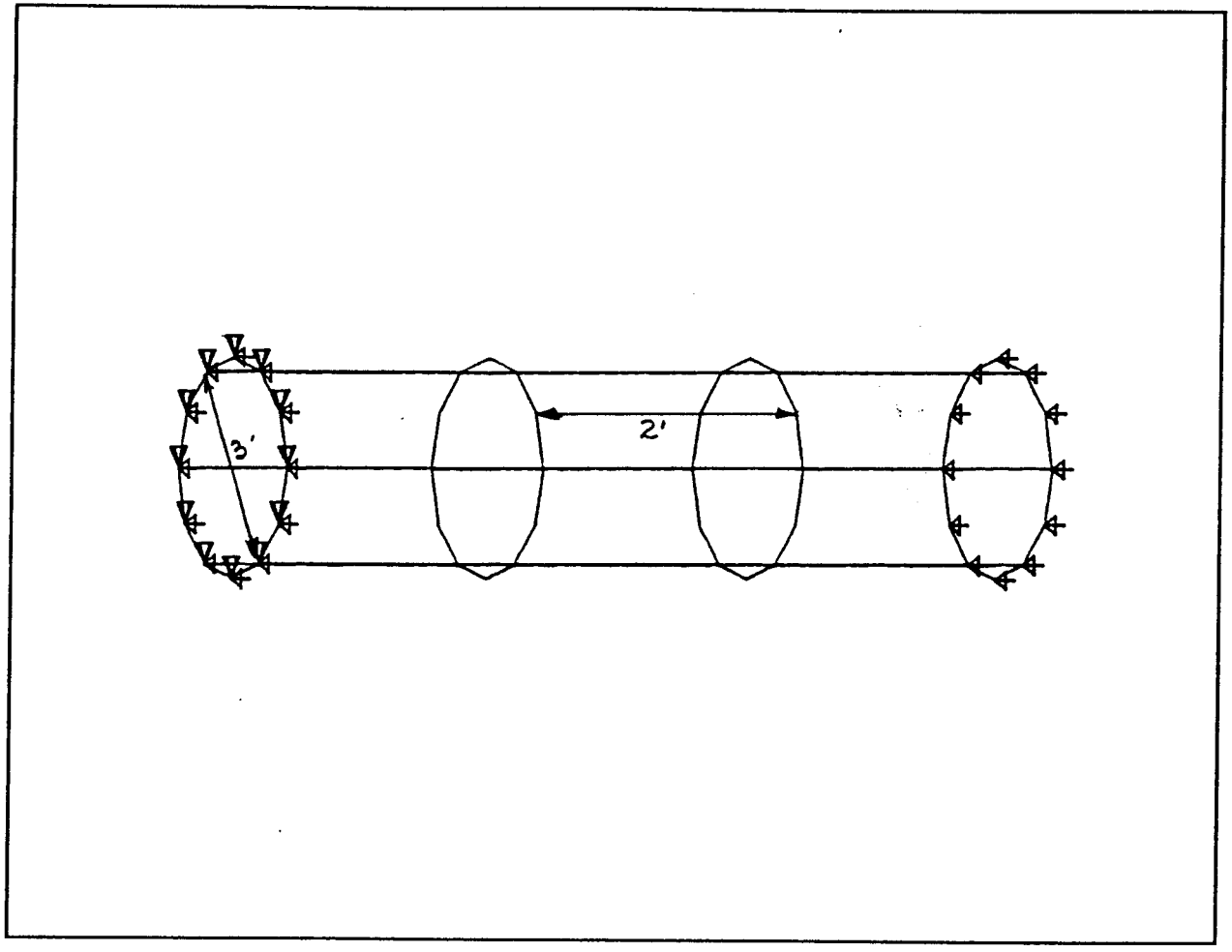

Figure 6.19 FEM Grid for the Cylindrical Membrane

membrane, these values are then used as in the BEM, with symmetry providing data for the full cylinder model. The BEM uses the locations and velocities of the membrane to set up the boundary element model and compute the location of the free water surface and the pressures on the membrane. The pressures are then fed back into the FEM to compute the new locations and velocities of the membrane nodes.

The fluid contained by the membrane could be modeled using the BEM and would require an additional coupling between the two BEMs and the FEM. Instead, in the data presented here the internal pressure is modeled as a constant and used as input into the FEM. The magnitude (10 psf above hydrostatic pressure) of the internal pressure is based on the internal pressure measured in the physical model tests. In the physical model tests the internal pressures were recorded and some anomalies were observed during the experiments. The internal pressure increased abruptly from the hydrostatic pressure when the membrane was first excited by a wave. Ohyama et al. (1989) noted that in their experiments on two-dimensional bottom mounted fluid-filled bags the internal pressure jumped at the onset of wave loading; they were unable to explain the increase. The internal pressures used as input in the numerical model were the mean pressures reached a few seconds into each run.

The first comparison made was to results for a 2 second incident wave with a half a foot wave height. Water surface elevations (non-dimensionalized by wave amplitude) along the channel (non-dimensionalized by wave length) are shown in

Figures 6.20 and 6.21. Figures 6.20 and 6.21 are a half of a wave period apart in time, after 8 and 9 seconds of simulation, respectively. In addition, the numerical results for the water surface elevation with no structure and with the rigid cylinder are shown. The centers of the rigid cylinder and the membrane cylinder are located at x/L = 0. Whereas the rigid cylinder had little effect on the wave profile (excluding the phase shift), the membrane cylinder alters the wave profile both in amplitude and in phase. Figures 6.22, 6.23 and 6.24, are the water surface elevation (non-dimensionalized by wave amplitude) versus time (non-dimensionalized by wave period) for three locations, fore, top and aft of the cylinder. Figure 6.22 is a half of a wave length fore of the cylinder, Figure 6.23 is on top of the cylinder and Figure 6.24 is a half of a wave length aft of the cylinder. The wave amplitude fore of the membrane cylinder is not noticeably altered (Figure 6.22) and the wave amplitude is reduced on top of and aft of the membrane cylinder (Figures 6.23 and 6.24).

Figures 6.25 and 6.26 show time histories of the non-dimensional water surface elevation across the channel half a wave length fore and aft of the structure, respectively. The water surface is symmetric about the wave channel centerline, thus only three histories, one foot, three feet and five feet from the channel wall, are shown in each figure. In all cases the water surface elevation towards the centerline is slightly higher than the water surface elevation towards the wall. The variation across the wave channel is less than ten percent and is similar to that shown in Figure 6.6.

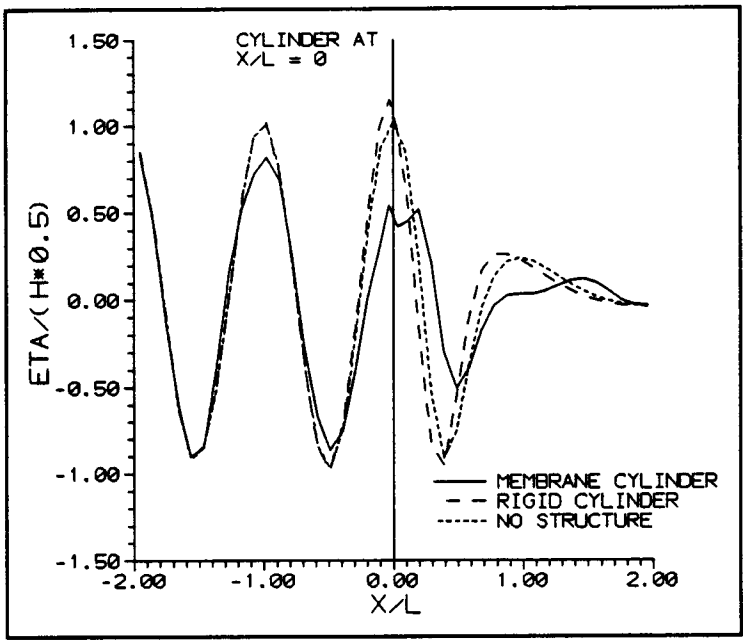

Figure 6.20 Water Surface Elevation Along the Wave Channel with the Membrane Cylinder

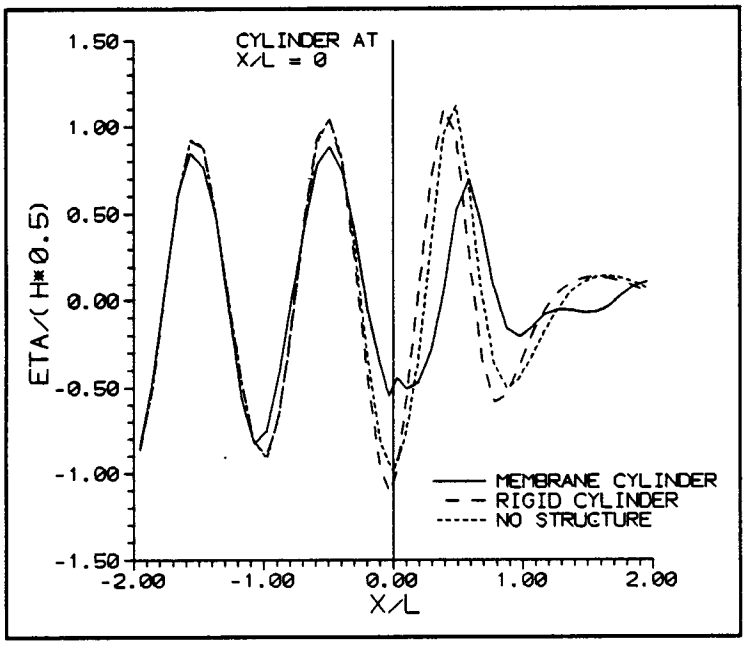

Figure 6.21 Water Surface Elevation Along the Wave Channel with the Membrane Cylinder

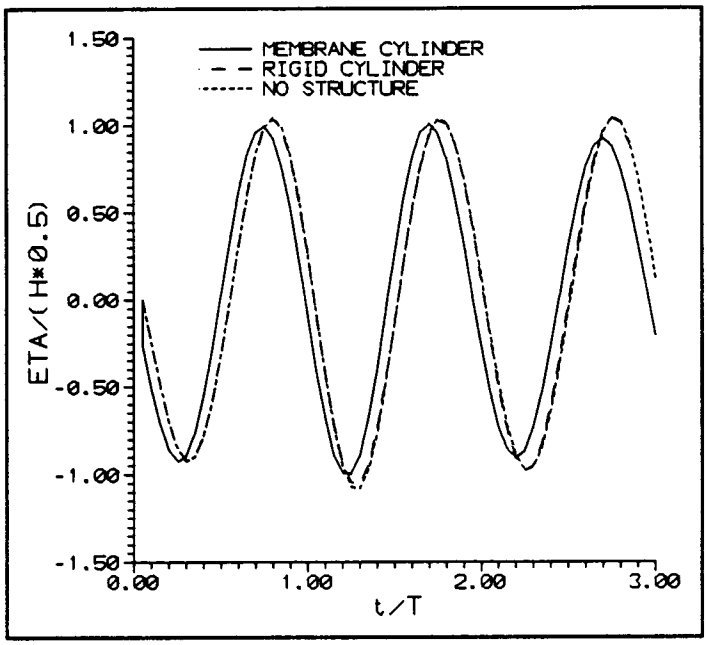

Figure 6.22 Water Surface Elevation a Half of a Wave Length Fore of the Cylinder

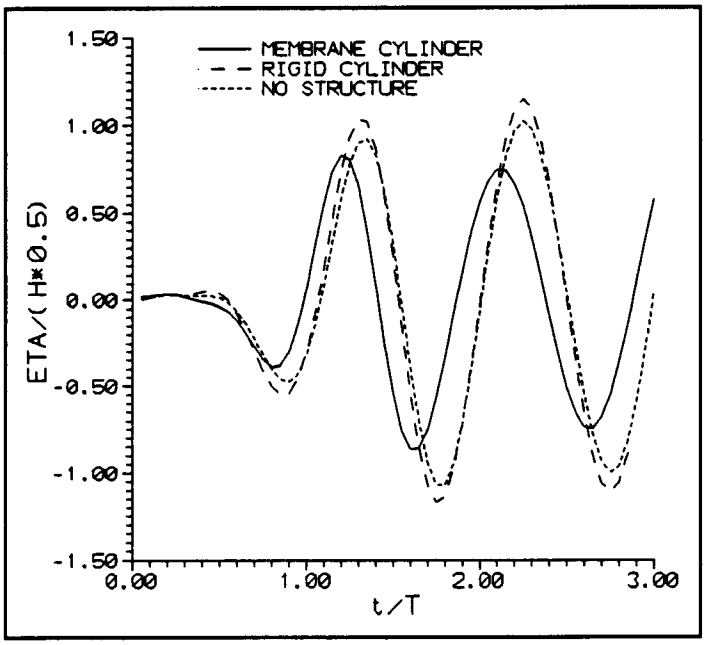

Figure 6.23 Water Surface Elevation on Top of the Cylinder

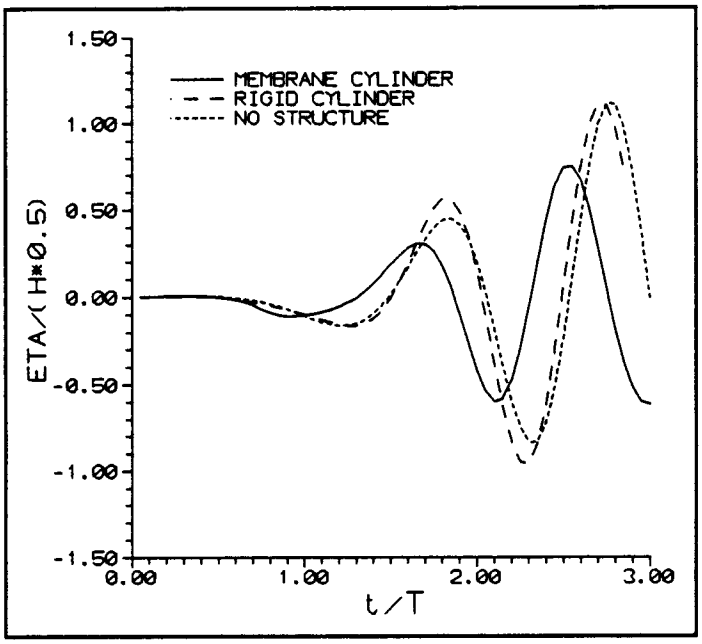

Figure 6.24 Water Surface Elevation a Half of a Wave Length Aft of the Cylinder

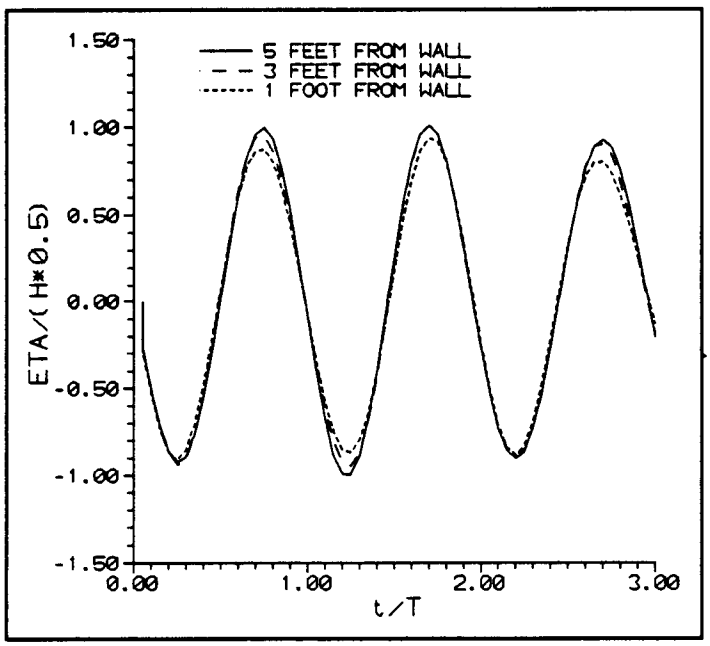

Figure 6.25 Variation in the Water Surface Elevation Across the Wave Channel a Half of a Wave Length Fore of the Cylinder

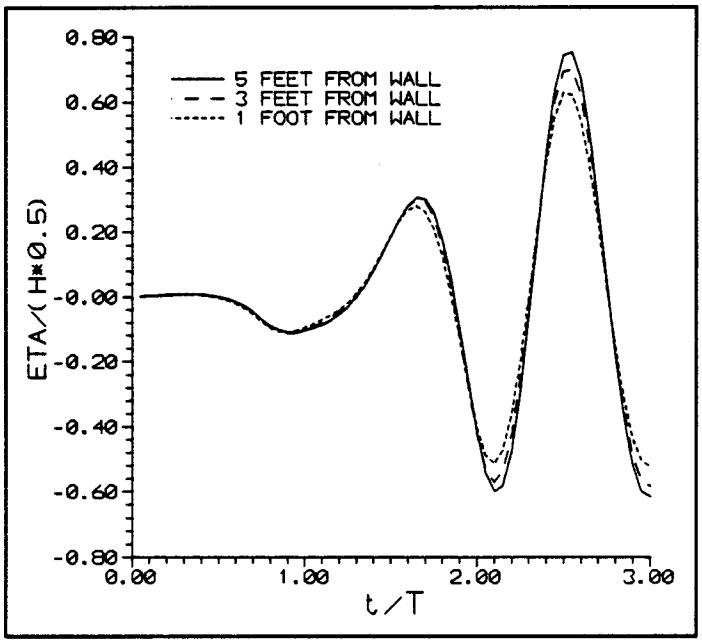

Figure 6.26 Variation in the Water Surface Elevation Across the Wave Channel a Half of a Wave Length Aft of the Cylinder

The wave condition, two second wave period and a half a foot wave height, shown in Figures 6.20-6.26 corresponds to Test Run Number 72 of the physical model. Figures 6.27-6.31 are the comparison of the numerical results and the physical model data. Each figure includes three graphs: graph a is the numerical results; graph b is the physical model data; and graph c superposes graphs a and b with a time shift of a quarter of a wave period applied to the model data. The same time shift was applied to all physical model data and was selected to give the best match around 6.0 on the non-dimensionalized time axis in Figure 6.28. The water surface elevation on top of the cylinder and aft of the cylinder are shown in Figures 6.27 and 6.28, respectively. The horizontal displacement (non-dimensionalized by the wave amplitude) fore of the cylinder is shown in Figure 6.29, the vertical displacement (non-dimensionalized by the wave amplitude) at the top of the cylinder is shown in Figure 6.30 and the horizontal displacement (non-dimensionalized by the wave amplitude) aft of the cylinder is shown in Figure 6.31.

The water surface elevation on top and aft of the cylinder are shown in Figures 6.27 and 6.28. It is interesting to note that the numerical model underpredicts the wave amplitude on top of the cylinder but overpredicts the wave amplitude aft of the cylinder. The numerical results appear more linear aft of the cylinder than the experimental data, see Figure 6.28. The difference between the numerical model results and the physical model data on top of the cylinder may in part be due to the narrow gap that forms between the free water surface and the

a)

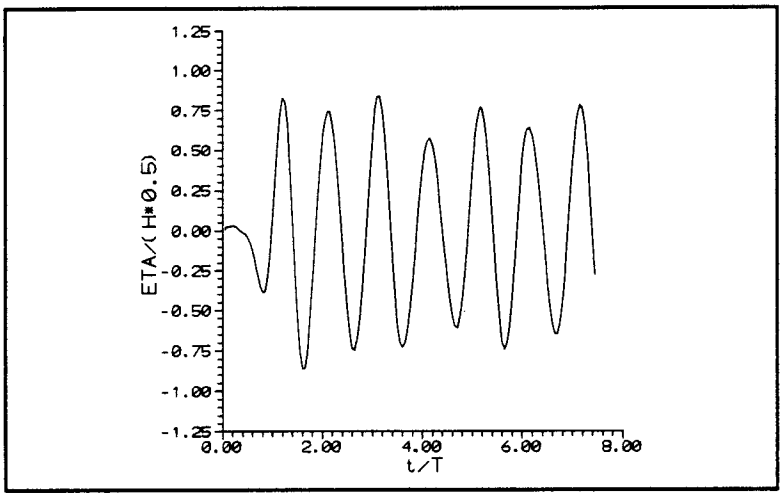

b)

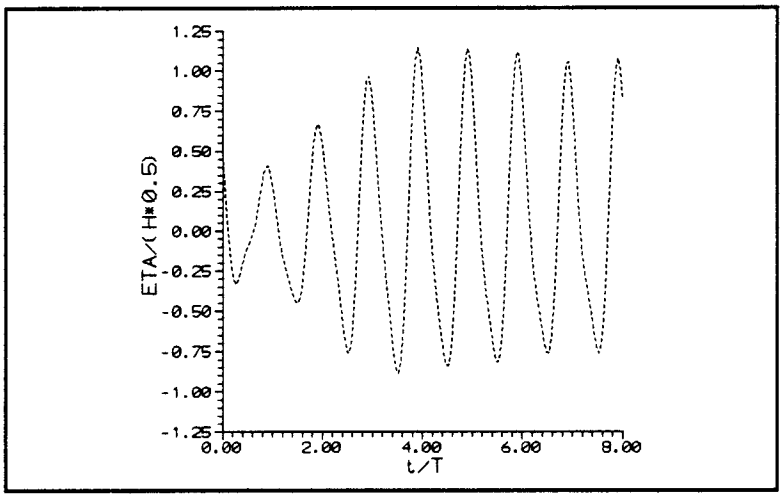

c)

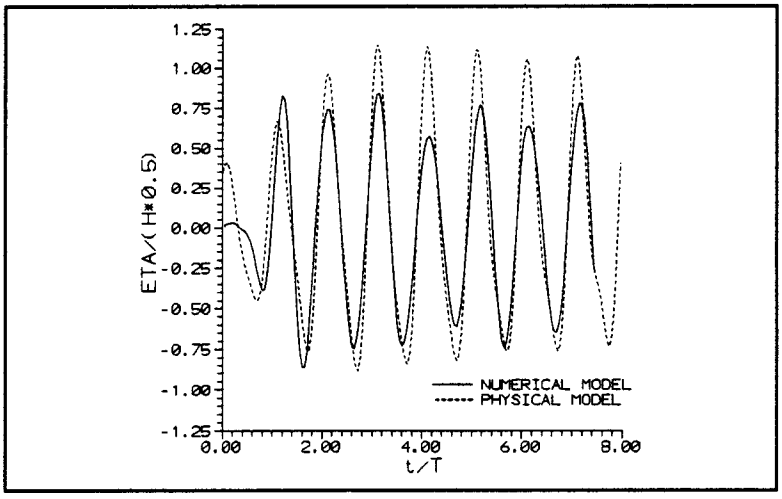

Figure 6.27 Water Surface Elevation on Top of the Cylinder, Numerical and Physical Model Results

a)

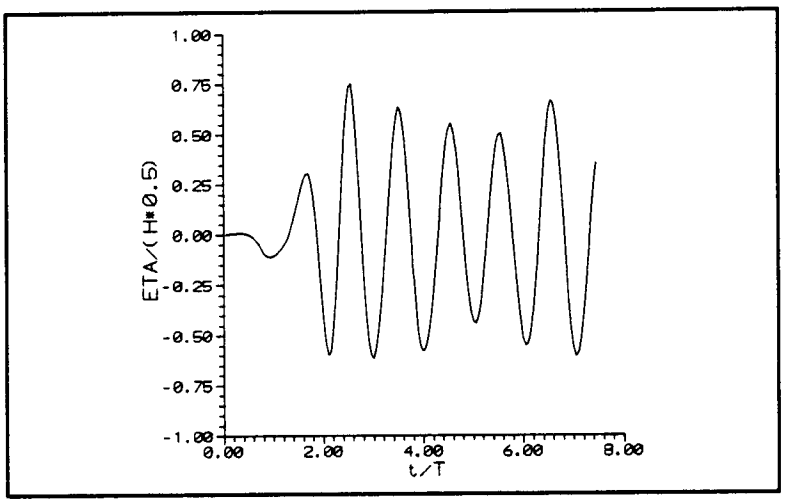

b)

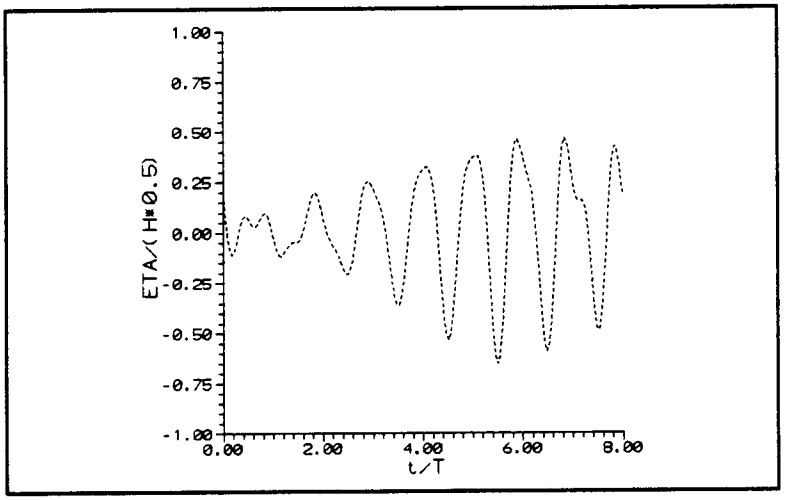

c)

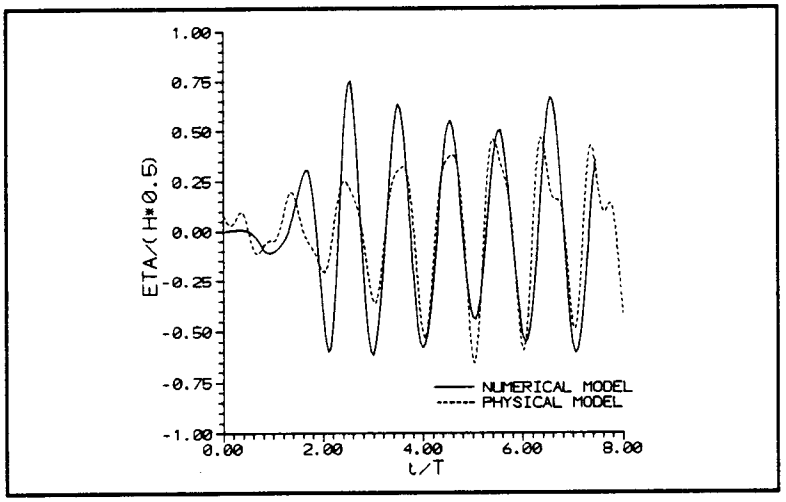

Figure 6.28 Water Surface Elevation a Half of a Wave Length Aft of the Cylinder, Numerical and Physical Model Results

a)

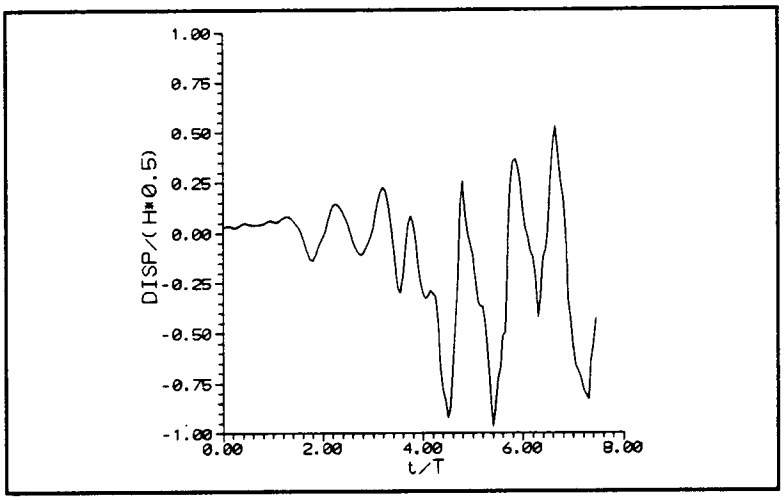

b)

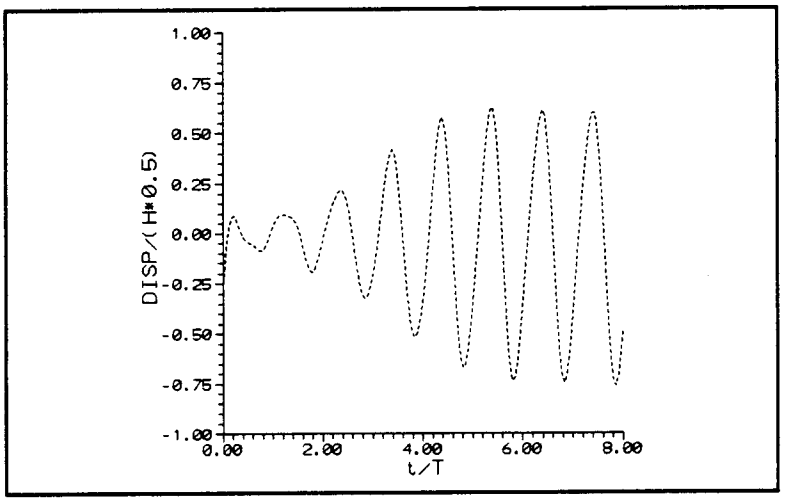

c)

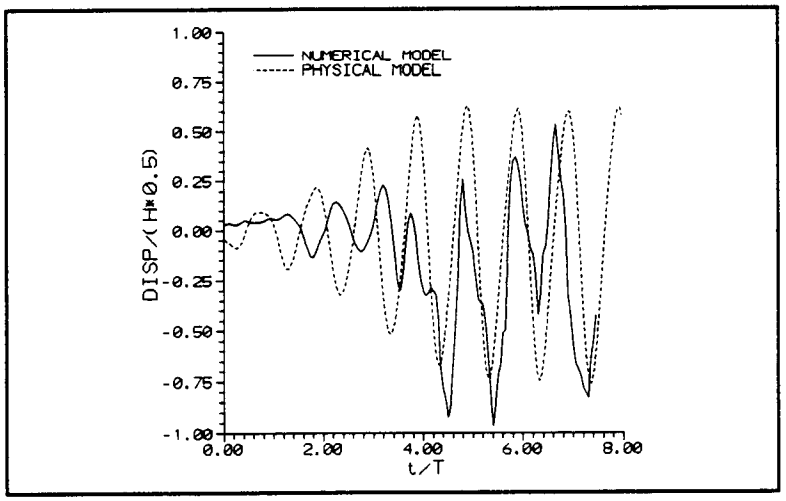

Figure 6.29 Horizontal Displacement Fore of Cylinder, Numerical and Physical Model Results

a)

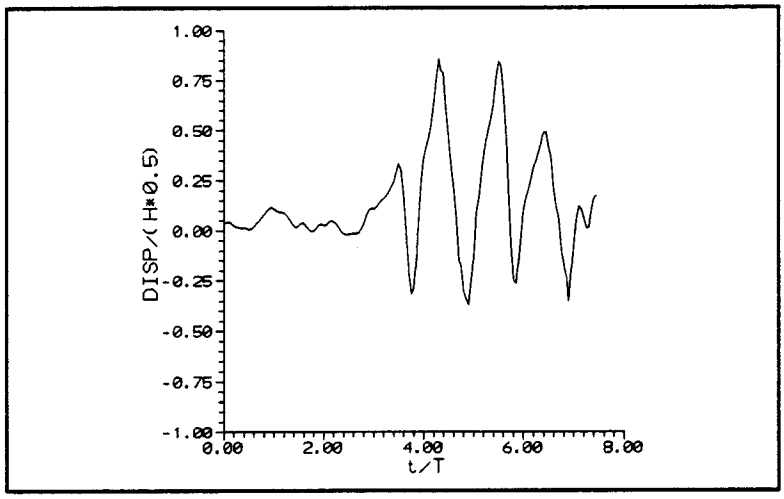

b)

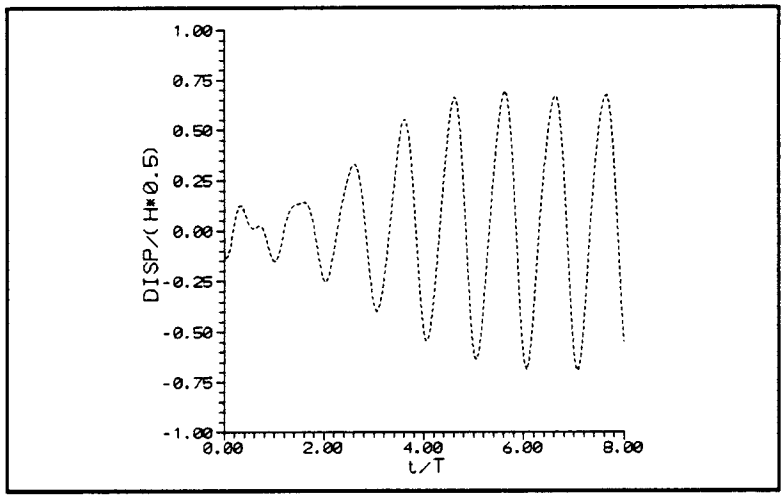

c)

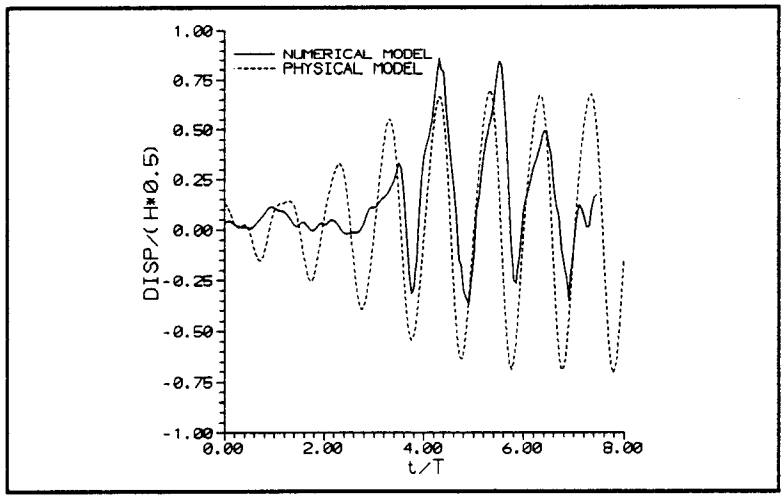

Figure 6.30 Vertical Displacement Top of Cylinder, Numerical and Physical Model Results

a)

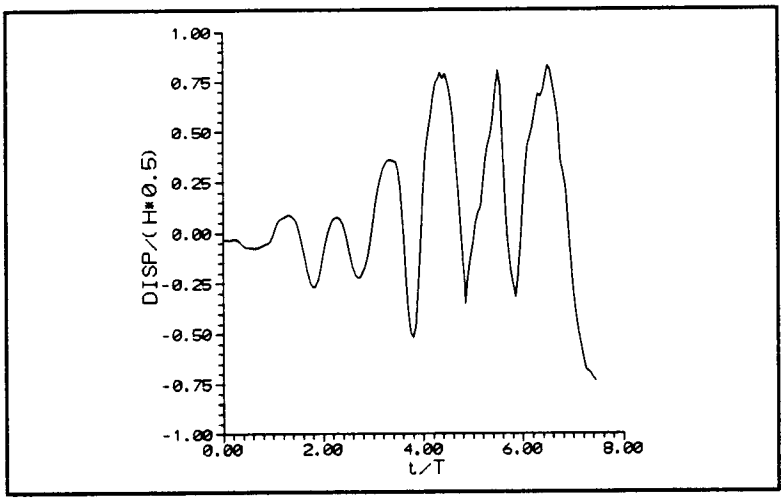

b)

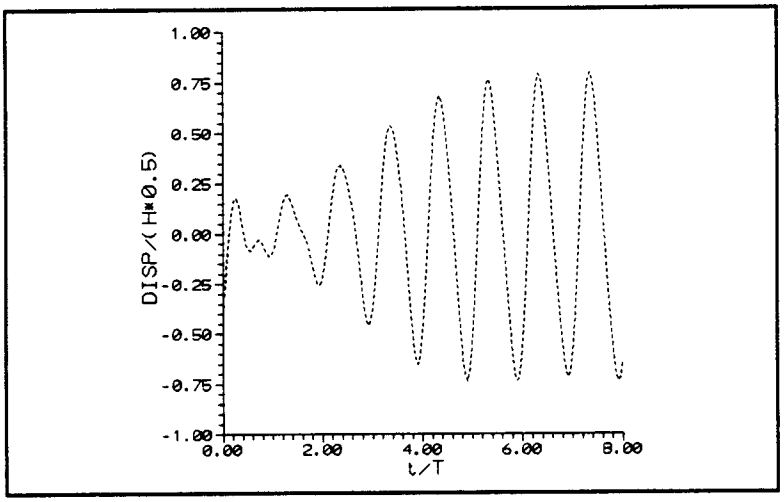

c)

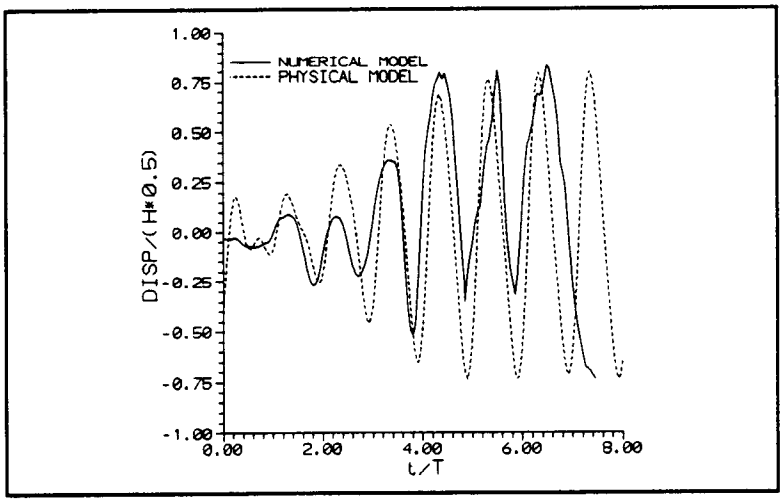

Figure 6.31 Horizontal Displacement Aft of Cylinder, Numerical and Physical Model Results

membrane. In the numerical algorithm iterations are performed at each time to locate both the free surface and the membrane. The error at each point (the difference between the current iteration and the previous iteration) is normalized by the current value at that point and the total error is the sum of all of the individual errors. Iterations are halted when a total error is less than a prescribed tolerance. When the membrane is close to the water surface, another error source may occur which is not evaluated in the numerical algorithm. That error is the relative difference between the free surface and the top of the membrane. Figures 6.20-6.22 show no apparent reduction in wave amplitude fore of the membrane cylinder when compared to numerical results without a cylinder and with a rigid cylinder. The wave amplitudes in those results appears affected only on top and aft of the membrane cylinder. In fact, it appears that the numerical model feels the affect of the cylinder sooner then the physical model.

The numerical model overpredicts the free water surface elevation when compared to the physical data but still provides a reasonable prediction of the transmission characteristics. The transmission coefficient for Run 72 was 0.154 (see Table C.3) and the numerical model predicts a transmission coefficient of 0.40. Upon examination of the physical model results, one observes that a marked change in the transmission coefficient occurs for the 2 second wave and 9 foot water depth, see Figure C.6. For the 2 second wave and 9 foot water depth the transmission coefficient ranged from 0.154 to 0.3, which is substantially lower than the other physical model results. The transmission coefficients are lower for

the 9 foot water depth when compared to the 10.5 foot water depth. The transmission coefficients for the 10.5 foot water depth are also at a minimum for the 2 second wave but the reduction is not as dramatic as that for the 9 foot water depth. The transmission coefficient of 0.4 predicted by the numerical model is larger than that of the physical model results but is reasonable when all of the physical data is considered.

The ability of the numerical model to reproduce the displacements of the membrane measured in the physical model are shown in Figures 6.29-6.31. The results are not as favorable as the results for the free water surface elevation. The displacements from the physical model appear sinusoidal and the displacements predicted by the numerical model are not sinusoidal and are not symmetric about the zero displacement value. In all cases the displacements are underpredicted in the numerical model. The under-prediction could be due to the lump masses applied in the numerical model. The lump masses are added to account for the internal mass contained by the membrane. The full internal mass contained by the membrane was applied at the corner nodes. The fluid mass acts over the full membrane surface and applying the full mass at corner nodes may place too much mass in the mass matrix of the FEM.

Another source of error in the numerical model is the internal pressure of the fluid contained by the membrane. The internal pressure was held constant, but should in fact vary sinusoidally. Figure 6.29, horizontal displacement fore of the cylinder, shows a bias in the data away from the center of the cylinder (membrane

displaces outward more than it displaces inward). Figure 6.30, vertical displacement, top of the cylinder, shows a bias away from the center. Figure 6.32 also shows a similar bias; the membrane seems to displaces outward more than inward. This corresponds to the fact that the internal pressure does not reduce in value and thus restricts the inward displacements.

It should be pointed out that an ideal fluid has been assumed in the development of the numerical model. Real fluid effects, such as form drag, are ignored. Real fluid effects may be a contributor to the structural loads seen by the membrane. These forces, if included could increase the predicted displacements. The wave length to diameter ratio for this experiment is approximately 7 and from Figure 1.3 the problem is approaching the area where real fluid effects need to be included. In the experiment, no real fluid effects were noted; large eddies behind the membrane were not observed. This could be because the free water surface aft of the membrane included high frequency waves and thus was not possible to visually discern wake formation aft of the cylinder. That is, real fluid effects could have been present but not visually detectable.

In order to evaluate the effectiveness of the new treatment of wave/membrane interaction developed in this work a comparison was made to results obtained with the earlier finite element model developed by Lo (1982) in which the hydrodynamics were roughly approximated including only the Froude-Krylof pressure. The horizontal displacements fore of the cylinder as predicted by the finite element model (Froude-Krylof pressure only) are shown in Figure 6.32.

The measured displacements are shown in Figure 6.33. The FEM over-predicts the displacements by a 100 percent. This should be compared to the results obtained in the new coupled model and shown in Figure 6.29. There an under-prediction of 25 percent was obtained. The over-prediction using Lo's (1982) model is probably due to inaccuracies in modelling the hydrodynamic pressure and the mass. In the FEM only the Froude-Krylof pressure is applied, i.e. the pressure that would exist if no structure were present. The pressure does not take in to account the fluid/structure interaction. In both the new model and the previous model lump masses have been added to the FEM grid to account for the internal fluid contained by the membrane. The membrane also moves the surrounding fluid and additional mass may be needed in Lo's model. In the coupled model, developed in the present work, the mass of the fluid surrounding the membrane is properly accounted for in the boundary element model. If, in addition, the internal fluid were modeled using the BEM, no lump masses would be required since the internal fluid mass would be accounted for in the BEM.

A second comparison to experimental results was made and numerical results were obtained corresponding to the physical model results for Test Run Number 67, in which the incident wave period was 1.5 seconds and the wave height was 0.5 feet. Figures 6.34 - 6.38 are the comparisons of the numerical results (solid line) and the physical model results (dashed line). No phase shift was applied to the model data. The numerical model results for the water surface elevation on top and aft of the cylinder compared favorably to the physical model

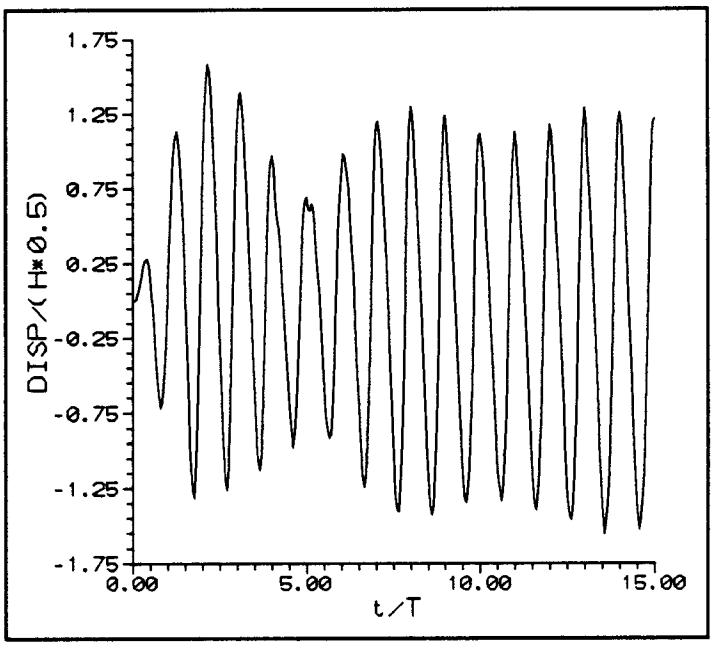

Figure 6.32 Horizontal Displacement Fore of Cylinder, FEM Model

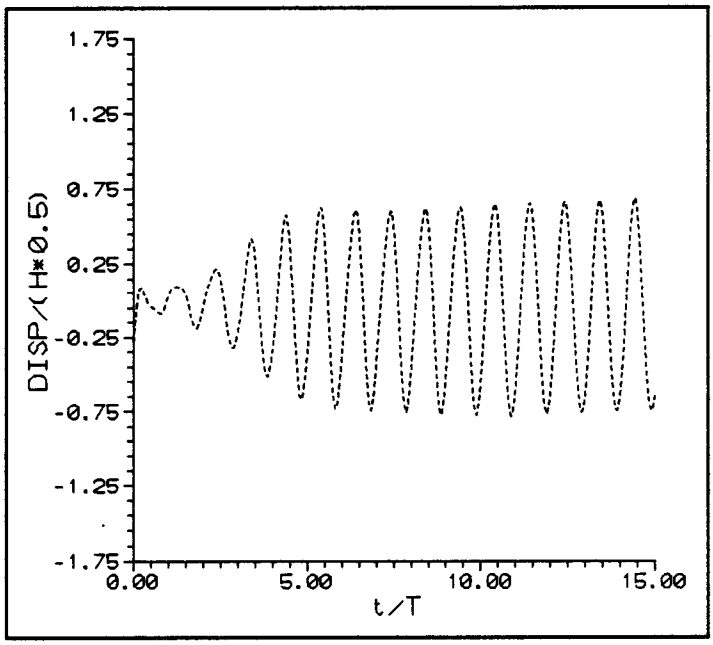

Figure 6.33 Horizontal Displacement Fore of Cylinder, Physical Model Results

data, Figures 6.34 and 6.35. The numerical model predicts the wave amplitude both on top and aft of the cylinder. There appears to be a phase shift between the numerical results and the physical model results for the water surface elevation on top of the cylinder, Figure 6.34. The phase shift does not appear aft of the cylinder, Figure 6.35.

The comparisons for the membrane displacements are shown on Figures 6.36-6.38. Figure 6.36 shows horizontal displacements fore of the cylinder; Figure 6.37 shows vertical displacements on top of the cylinder; and Figure 6.38 shows horizontal displacements aft of the cylinder. The numerical model overpredicts the displacements and the period of response. The period of wave forcing and the period of the physical model response are the same and half that of the fundamental period in the numerical model response. Upon evaluation of the numerical results, one sees that the model is trying to respond to the forcing period but only a very small response occurs. Is there a restriction or limitation in the FEM grid adopted?

To answer that question, the FEM was used to compute the natural periods of the membrane cylinder in a vacuum. The model used to compute the natural periods includes the mass of the internal fluid lumped at the corner nodes of each element. The first few modes are: two circumferential modes in the first longitudinal mode (2.01 seconds and 1.65 seconds) and two circumferential modes in the second longitudinal mode (1.62 seconds and 1.12 seconds). The fundamental period of the numerical model for the membrane is equivalent to the

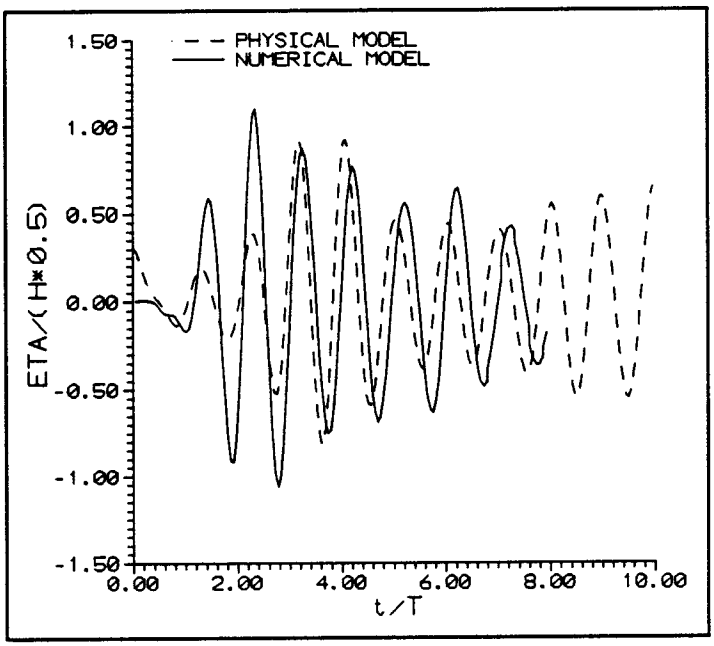

Figure 6.34 Water Surface Elevation on Top of the Cylinder, Numerical and Physical Model Results

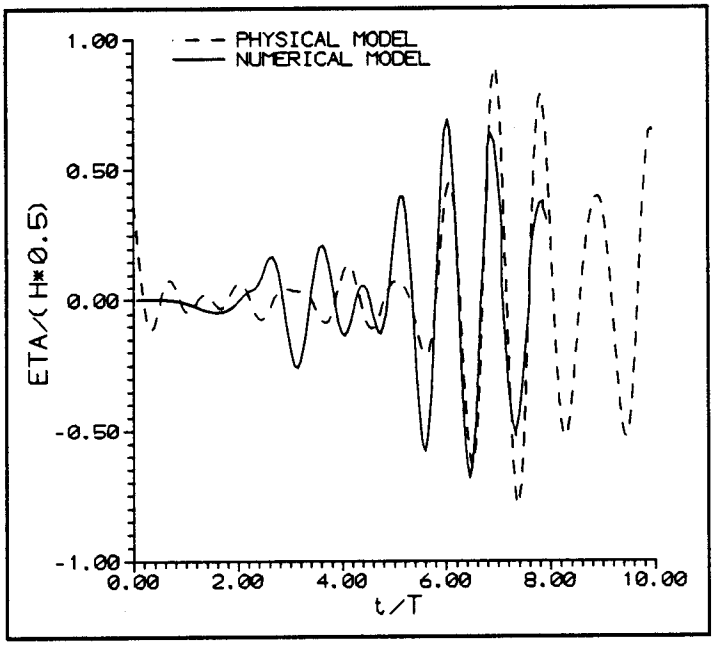

Figure 6.35 Water Surface Elevation Aft of the Cylinder, Numerical and Physical Model Results

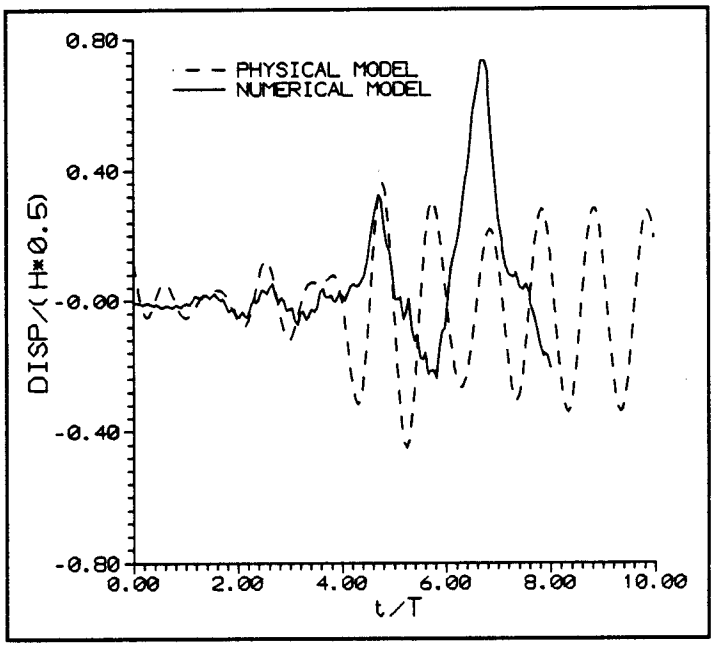

Figure 6.36 Horizontal Displacement Fore of the Cylinder, Numerical and Physical Model Results

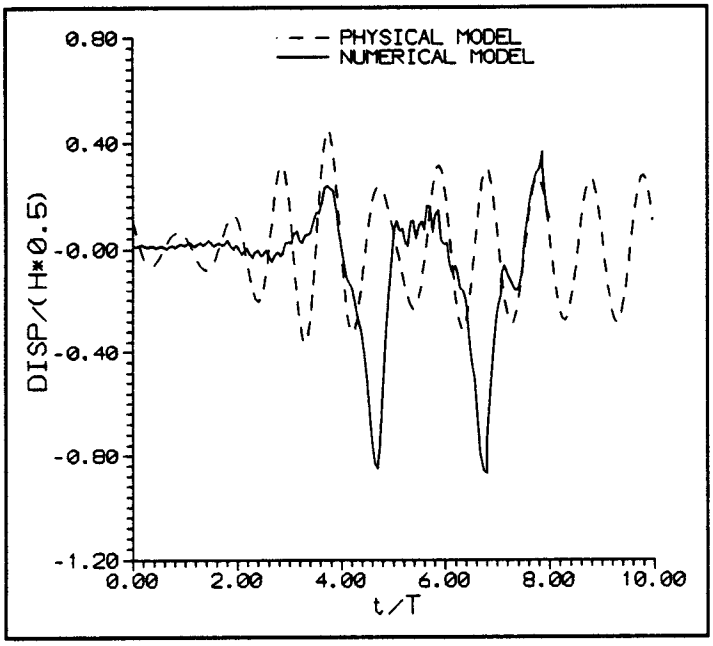

Figure 6.37 Vertical Displacement Top of the Cylinder, Numerical and Physical Model Results

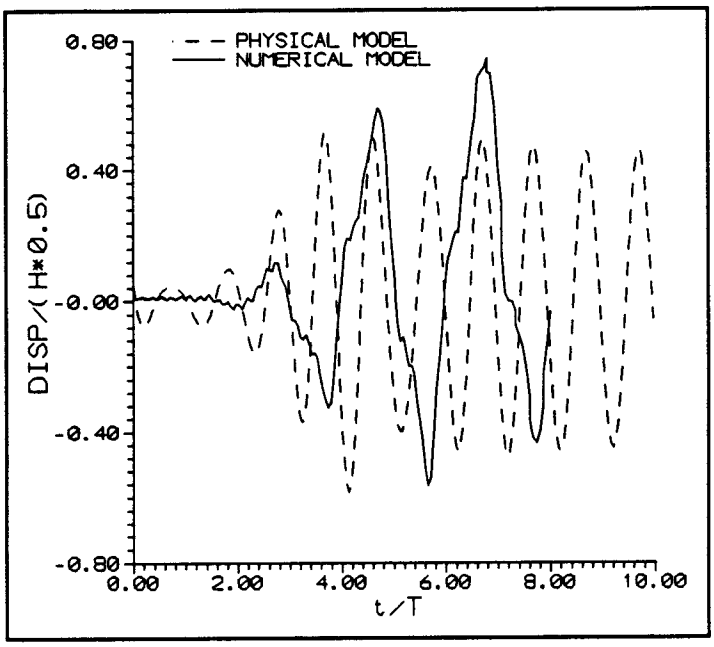

Figure 6.38 Horizontal Displacement Aft of the Cylinder, Numerical and Physical Model Results

forcing period of the first wave example (2.0 seconds) considered earlier in this section. The transmission and reflection coefficients reported in Appendix C confirm the fact that the physical model also has a fundamental period close to two seconds.

In the second example the forcing period of the waves is 1.5 seconds, which is close, but not exactly equal to, the second circumferential first longitudinal or the first circumferential second longitudinal modal periods of response for the membrane. Because of the means used to lump masses in the FEM code (at element corner nodes only), the effects of the fundamental circumferential and longitudinal modes are amplified while those of the higher modes are reduced. This may in part explain the irregular results displayed for the numerical model in Figures 6.36 to 6.38.

The free water surface elevation has been adequately predicted by the coupled model. However, numerical results for both Test Run Numbers 72 and 67 point out the importance of properly modeling the fluid contained by the cylindrical membrane to predict the membrane displacements. If the internal fluid were modeled using a BEM, the pressure of the internal fluid would vary with the wave loading and the internal fluid mass would be more accurately accounted for in the BEM.

CHAPTER 7 CONCLUSIONS

7.1 OBJECTIVE/ACCOMPLISHMENTS

The aim of the research was to develop a time-domain model of the wave/structure interaction of water wave waves and highly deformable membranes. This was accomplish by coupling an existing finite element model (FEM) of the response of the membrane, Lo (1982), with a boundary element model (BEM) of the fluid domain. The BEM was needed to improve the hydrodynamics of the FEM. Part of this work was development of the BEM, its coupling with the FEM and the necessary modifications to the FEM.

The BEM predicts water wave behavior in a wave channel with or without a structure present. Without a structure present, the numerical model was able to predict the water surface in a two-dimensional wave channel; see Section 6.2. Once the steady wave was established in the channel the error along the centerline of the channel was less than 5 percent and the variation across the channel was typically 8 percent. The interaction of a submerged rigid cylinder placed horizontally across a wave channel was modeled and the results compared to those obtained by Isaacson and Cheung (1988 and 1990). The water surface elevation profiles and the wave forces agreed well with their results, see Section 6.3. The ability of the coupled modeled to predict the fluid/structure interaction of water waves and highly deformable bodies was verified. The numerical model provides a model to predict the wave transmission characteristics of a fluid-filled

membrane, which was not obtainable from the previous developed model, Lo (1982). In addition, the coupled model slightly under-predicted the horizontal displacement (25 percent) whereas the finite element model greatly over-predicted the horizontal displacements (100 percent).

The BEM is numerically intensive and requires refined grids and long computational times. A BEM was implemented on a Cray YMP super computer. No attempt has been made to optimize the computer code, e.g. by developing out-of-core solvers and as a result the model can not be run on smaller machines. It is not clear whether out-of-core solvers would actually eliminate the need for a super computer, since the generation of the system of equations involves numerous computations. An out-of-core solver would not change the number of computations. The number of computations could be reduced if the fluid domain was modeled about an equilibrium position, thus requiring the [G] and [H] matrices (Section 3.3) to be computed only once. Then the major computational effort would be generating the right-hand side of the system of equations. In wave/rigid structure problems where linear wave theory is used, this is the approach taken. The boundary conditions at the water surface are assumed to apply at the still-water level. If an equilibrium position of the boundaries were used in a wave/deformable body interaction problem, i.e. linear deformations, more efficient computation would be achieved, but the accuracy of the coupling of the BEM and FEM would need to be evaluated.

7.2 FUTURE RESEARCH NEEDS

This research had the specific aim of developing a predictive tool for the wave/structure interaction of highly deformable bodies. Where the aim was accomplished, several areas for future research became apparent. The first is to develop a better understanding of the internal pressure of the fluid contained by the membrane. The second is additional experimental and parametric studies in a true three-dimensional application. The third research area is to improve the efficiency of the BEM. The fourth is to evaluate the level of approximations needed in the coupling of the BEM and the FEM. Additional research needs are listed in Appendix C.

7.2.1 Internal Fluid

During the physical model tests some, interesting phenomena were observed. One of those was the jump in internal pressure that occurred in the fluid contained by the membrane just as the wave reached the membrane. What causes the increase in pressure? One possible explanation is, when the fluid goes from zero acceleration to a finite acceleration a rapid change in pressure is required. Ohyama et al. (1989) noticed this same jump in the internal pressure in their experiments on a similar structure and are conducting research into why it occurs. If the internal fluid were to be modeled by the BEM, would the increased pressure be modeled? Is the increase in pressure a nonlinear effect, or is it associated with a pressure-dependent phase shift in the forces that act on the

cylinder?

If the jump in internal pressure is a nonlinear effect then care would need to be used when modeling this with the BEM. One of the terms in the dynamic boundary condition is Bernoulli constant and it is unclear how to compute its magnitude within the membrane. In the external fluid region, the boundary conditions on the free surface allow for the determination of the constant. There may be a missing boundary condition or constraint on the internal fluid that needs to be developed.

In the present study, lump mass has been added to the nodes of the membrane to account for the internal fluid enclosed by the membrane. If the BEM were used to model the internal fluid, the mass of the internal fluid would be accounted for and lump masses in the FEM would not be required.

7.2.2 Experimental Work and Parametric Studies

Additional two-dimensional experiments are required to validate the model and to evaluate the practicality of using membranes as wave barriers. Data, both numerical and experimental, needs to be collected on transmission coefficients for various membrane structures, different sizes, water depths, and amounts of submergence. Experimental work and numerical model development is also needed on wave transmission when wave breaking is one method of wave dissipation.

The present model describes a three-dimensional system. However,

insufficient data (numerical or experimental) has been collected to validate the application of the model or to evaluate edge effects. In practical applications these will be three-dimensional in nature even if the wave field is long-crested and the angle of attack is perpendicular to the structural axis.

7.2.3 Improve Efficiency

As stated, the BEM, and to some extent the FEM, were developed to model the time domain relationship of the nonlinear interaction of water waves and highly deformable membranes. Little effort was taken to insure that the model would be efficient. The relatively smaller computational effort required by the FEM as compared to the BEM suggests that any effort to improve the efficiency of the combined model should concentrate on the BEM. One area that could be improved in the BEM is the utilization of the vector capability of the super computer. It is not likely that the BEM would ever run efficiently on a non-vector machine; thus, improving the vectorization of the code could reduce computational effort. Improvements could also be made in the exchange of data between the BEM and the FEM, but as stated earlier, the BEM requires the majority of the computational effort.

The number of elements and nodes could be reduced if a flat and level bottom boundary were assumed. This would enable Green's Function to account for the bottom boundary using the method of images, Isaacson (1982). Using this other form of Green's Function the bottom boundary would not need to be

gridded. If linear wave theory were assumed and the boundaries were assumed to act at an equilibrium position, another form of Green's Function could be used that accounts for the boundary conditions on the free water surface, the bottom boundary, and the far field boundary, Yeung (1975). This could affect the accuracy of the coupling between the BEM and FEM.

Another way to reduce the number of elements and grid points is to model the fluid domain in two-dimensions. This would require methods of incorporating the three-dimensional effects of the membrane motion into the coupling. If the fluid were modeled in two-dimensions the resulting coupled model would run on much smaller machines.

The model constructed in this study is in three-dimensions because of the three- dimensional motions of the membrane. To properly account for the hydrodynamics, the fluid domain should be modeled in three-dimensions. A fully three-dimensional model has developed in this study may not be practical due to computer requirements.

7.2.4 Evaluate Levels of Approximation in Coupling

The coupling of the fluid domain and the membrane occurs through the pressure exerted on the membrane. The pressure is dependent on the position and velocity of the membrane and thus an iterative procedure has been used to couple the loading. To further complicate the problem the pressure exerted on the membrane is nonconservative, i.e., the direction in which the pressure is

dependent on the rotations of the membrane and is constantly changing. Various reduced levels of accuracy in the coupling can be achieved by approximations. How accurate does the coupling have to be to adequately predict the response of the membrane and the free water surface?

Approximations that should be investigated include:

- use pressures from *a prior* time step without correction for motions of the membrane
- assuming the mean position of membrane when calculating the pressure
- reforming the membrane and the fluid models into two-dimensional problems

CHAPTER 8 BIBLIOGRAPHY

Banerjee, P.K. and Butterfield, R., Boundary Element Methods in Engineering Science, McGraw-Hill, London, 1981.

Bender, W.J. Jr., "Behavior of a Membrane Floating Breakwater," Masters Thesis, Department of Civil Engineering, Oregon State University, Corvallis, Oregon, 1989.

Berger, B.S., "Dynamic Response of an Infinite Cylinder Shell in an Acoustic Medium," Journal Applied Mechanics, Vol 36 No 2, June 1969, pp. 342-345.

Brebbia, C.A., The Boundary Element Method For Engineers, John-Wiley & Sons, New York, 1978.

Brevig, P., Greenhow, M. and Vinje, T., "Extreme Wave Forces on Submerged Wave Energy Devices," Applied Ocean Research, Vol 4 No 4, 1982, pp. 219-225.

Broderick, L.L. and Leonard, J.W., "Selective Review of Boundary Element Modeling For the Interaction of Deformable Structures with Water Waves," Engineering Structures, Vol 12, October 1990, pp. 269-276.

Chakrabarti, S.K., Hydrodynamics of Offshore Structures, Computations Mechanics Publication, Springer-Verlag, New York, 1987.

Chaplin, J. R., "Nonlinear Forces on a Horizontal Cylinder Beneath Waves," Journal of Fluid Mechanics, Vol 147, 1984, pp. 449-464.

Cox, J.V., "A Preliminary Study on Finite Element Hosted Coupling with the Boundary Element Method," Naval Civil Engineering Laboratory, NCEL Technical Note (N-1783), Port Hueneme, California, April 1988.

Cummings, W.E., "The Impulse Response Function and Ship Motions," David Taylor Model Basin Report, No 1661, Washington, D.C., 1962.

Frederiksen, H.D., "Wave Attenuation by Fluid Filled Bags," ASCE Journal of the Waterway, Harbors and Coastal Engineering Division, February 1971, pp. 73-90.

Friedman, M.B. and Shaw, R.P., "Diffraction of a Plane Shock Wave by an Arbitrary Rigid Cylindrical Obstacles," Journal Applied Mechanics, Vol 29 No 1, March 1962, pp. 40-46.

Geers, T.L., "Transient Response Analysis of Submerged Structures," Finite Element Analysis of Transient Nonlinear Structural Behavior, Ed. by Belytschko, T. et al., AMD-Vol-14, ASME, New York, N.Y., 1975.

Geers, T.L., "Residual Potential and Approximate Methods For Three-Dimensional Fluid-Structure Interaction Problems," ASME Journal of Acoustics, Vol 49 No 5, May 1971, pp. 1505-1510.

Green, A.E. and Adkins, J.E., Large Elastic Deformations, Oxford University Press, London, 1960.

Guenther, R.B., and Lee, J.W., Partial Differential Equations of Mathematical Physics and Integral Equations, Prentice Hall, New Jersey, 1988.

Han, P.S. and Olson, M.D., "Interactive Analysis of Wind-Loaded Pneumatic Membrane Structures," Computers and Structures, Vol 25 No 5, 1987, pp. 699-712.

Han, P.S., "Iterative Nonlinear Analysis of Wind-Loaded Pneumatic Membrane Structures," PhD Dissertation, The University of British Columbia, 1986.

Han, P.S., Olson, M.D., and Johnston, R.L., "A Galerkin Boundary Element Formulation With Moving Singularities," Engineering Computation, Vol 1, 1984, pp. 282-286.

Haywood, J.H., "Response of an Elastic Cylindrical Shell to a Pressure Pulse," Quarterly Journal of Mechanics and Applied Mathematicals, Vol 11, Part 2, 1958, pp. 129-141.

Hildebrand, F.B., Introduction to Numerical Analysis, Dover Publications, Inc., New York, 1974.

Huang, H., "An Exact Analysis of the Transient Interaction of Acoustic Plane Waves with a Cylindrical Elastic Shell," Journal Applied Mechanics, Vol 37 No 4, Dec. 1970, pp. 1091-1106.

Hudspeth, R.T., Class Notes from Wave Forces, Department of Civil Engineering, Oregon State University, Corvallis, Oregon, 1988.

Isaacson, M. and Cheung, K.-F., "Time-Domain Solution for Second Order Wave Diffraction," ASCE Journal of Waterway, Port, Coastal, and Ocean Engineering, Vol 116 No 2, March/April, 1990, pp. 191-210.

Isaacson, M. and Cheung, K.-F., "An Efficient Time-Domain Solution to Nonlinear Wave Force Predictions," Procs. Ocean Structural Dynamics Symposium '88, Oregon State University, Corvallis, Oregon, September 13-14, 1988, pp. 407-421.

Isaacson, M., "Nonlinear-Wave Effects on Fixed and Floating Bodies," Journal of Fluid Mechanics, Vol 120, 1982, pp. 267-281.

Iwagaki, Y., Asano, T. and Honda, T., "Computation Effects of Pneumatic Breakwaters and Other Types of Breakwaters on Wave Damping," Coastal Engineering, Vol 3, 1978, pp. 2172-2189.

Kerper, D.R., "Behavior of a Compliant Wave-Current Barrier," Masters Thesis, Department of Civil Engineering, Oregon State University, Corvallis, Oregon, 1988.

Kuich, "Starting to Work with Boundary Elements," Boundary Element Techniques in Computer Aided Engineering, Ed. by Brebbia, Martinus Nijoff Publishers, Dordrecht, 1984, pp. 141-158.

Leonard, J.W., Tension Structures, McGraw-Hill, New York, 1988.

Leonard, J.W. and Lo, A., "Nonlinear Dynamics of Cable-Reinforced Membranes," Procs. of Building Structures, Structural Congress '87, Orlando, August, 1987.

Lo, A., "Nonlinear Dynamic Analysis of Cable and Membrane Structures," PhD Dissertation, Oregon State Univeristy, Corvallis, Oregon, 1982.

Masuda, K. and Kato, W., "Hybrid BEM for Calculating Nonlinear Wave Forces on 3-Dimensional Bodies," Boundary Elements, Ed. by Brebbia, C.A. et al., Springer-Verlag, Berlin, 1983, pp. 209-215.

McIver, M. and McIver, P., "Second-Order Wave Diffraction by a Submerged Circular Cylinder," Journal of Fluid Mechanics, Vol 219, 1990, pp. 519-529.

Mei, C.C., "Numerical Methods in Water-Wave Diffraction and Radiation," Annual Review of Fluid Mechanics, 1978, pp. 393-416.

Milgram, J.H., "Forces and Motions of a Flexible Floating Barrier," Journal of Hydronautics, Vol 5 No 2, 1971, pp. 41-51.

Modi, V.J. and Misra, A.L., "Response of an Inflatable Offshore Platform to Surface Wave Excitations," Journal of Hydronautics, Vol 14 No 1, 1980.

Nakayama, T. and Washizu, K., "The Boundary Element Method Applied to the Analysis of Two-Dimensional Nonlinear Sloshing Problems," International Journal For Numerical Methods in Engineering, Vol 17, 1981, pp. 1631-1646.

Ohyama, T., Tanaka, M., Kiyokawa, T., Uda, T. and Murai, Y., "Transmission and Reflection Characteristics of Waves Over a Submerged Flexible Mound," Coastal Engineering in Japan, Vol 32 No 1, 1989, pp 53-68.

Sarpkaya, T. and Isaacson, M., Mechanics of Wave Forces on Offshore Structures, Van Nostrand Reinhold Company, New York, 1981.

Sclavounous, P.D., "Radiation and Diffraction of Second-Order Surface Waves by Floating Bodies," Journal of Fluid Mechanics, Vol 196, 1988, pp. 65-91.

Seymour, R.J., "Tethered Float Breakwater: A Temporary Wave Protection for Open Ocean Construction," Proceedings 8th Offshore Technology Conference, Vol 2, 1976, pp. 253-264.

Shaw, R.P., "Boundary Integral Equation Methods Applied to Water Waves," ASME Procs. Applied Mechanics Conference, Troy, New York, June 23-25, 1975, pp. 7-14.

Shaw, R.P. and Friedman, M.B., "Diffraction of Pulses by Deformable Cyclindrical Obstacles of Arbitrary Cross Section," ASME Proceeding of the Fourth US National Congress of Applied Mechanics, N.Y., 1962, pp. 371-379.

Shen, S.F., "Finite Element Methods in Fluid Mechanics," Annual Review of Fluid Mechanics, Vol 10, 1978, pp. 393-416.

→ Sollitt, C.K., Lee, C.P. and McDougal, W.G., "Mechanically Coupled Buoyant Flaps: Theory and Experiment," Proceeding of the 20th International Conference on Coastal Engineering, Taipei, Taiwan, 1986, pp. 2445-2459.

Tanaka, M., Ohyama, T., Kiyokawa, T., Uda, T., and Omata, A., "Wave Control by Flexible Underwater Mound," Offshore Technology Conference, Houston Texas, May 7-10, 1990, pp. 551-558.

Tang, W., Transforming Domain into Boundary Integrals in BEM, Ed. by Brebbia, C.A. and Orszag, S.A., Springer-Verlag, Berlin, 1988.

Vada, T., "A Numerical Solution of the Second-Order Wave-Diffraction Problem for a Submerged Cylinder of Arbitrary Shape," Journal of Fluid Mechanics, Vol 174, 1987, pp. 23-37.

Williams, A.N. and Geiger, P.T., "Buoyant Flexible Breakwater," Research Report No, UHCE88-12, Cullen College of Engineering, University of Houston, Houston Texas, 1988.

Yamamoto, T., Yoshida, A. and Ijima, T., "Dynamics of Elastically Moored Floating Objects," Applied Ocean Research, Vol 2 No 2, 1980, pp. 85-92.

Yeung, R.W., "The Transient Heaving Motion of Floating Cylinders," Journal of Engineering Mathematics, Vol 16, 1982, pp. 97-119.

Yeung, R.W., "A Hybrid Integral-Equation Method for Time-Harmonic Free-Surface Flow," Procs. 1st International Conference on Numerical Ship Hydrodynamics, Gaithersburg, Maryland, Ocotber 1975, pp. 581-607.

Yuan, S.W., Foundations of Fluid Mechanics, Prentice-Hall, Inc. New Jersey, 1967.

Zienkiewicz, O.C. and Taylor, R.L., The Finite Element Method, McGraw-Hill, England, 1989.

Zienkiewicz, O.C., Lewis, R.W., and Stagg, K.G., Numerical Methods in Offshore Engineering, John Wiley & Sons, New York, 1978.

Zienkiewicz, O.C. and Bettes, P., "Infinite Elements in the Study of Fluid-Structure Interaction Problem," Proceeding of the 2nd International Symposium on Computing Methods in Applied Science and Engineering, Versailles, France, 1975, pp. 133-172.

APPENDICES

APPENDIX A ALGORITHMS

A time-domain numerical model of the fluid structure interaction of water waves and highly deformable bodies was developed and verified. The main thrust of this effort was the development of a time-domain boundary element model (BEM) of the fluid domain. The BEM was then coupled with an existing finite element model (FEM) of membrane structures, Lo (1982). The FEM has a simplistic hydrodynamic load capability but is based on Froude-Krylov forces, Sarpkaya and Isaacson (1981). The framework for the FEM formed the basic framework for the BEM and the coupled FEM and BEM.

Figure A.1 is the initialization flow chart of all of the models. The geometry, material properties and constraints are read. Then the various types of loads are inputted; constant, time dependent and wave loading. Then depending on the solution being sought a variety of options are available: linear static configurations of a tension structure, SOLVE1; nonlinear static configuration of a tension structure, SOLVE2; time-domain dynamic analysis of tension structure, SOLVE3; and the wave diffraction problem, BEM.

Figures A.2 and A.3 are descriptions of the BEM, which can be used independently of the tension structure FEM model. The BEM can be used to model the diffraction problem of water waves with rigid structures, see Section 6.3. The BEM is also used as a load model for the FEM code. This is shown in Figure A.4 where the load vector can be computed from a Froude-Krylov

approximation (FEM) or a solution to the diffraction problem (BEM).

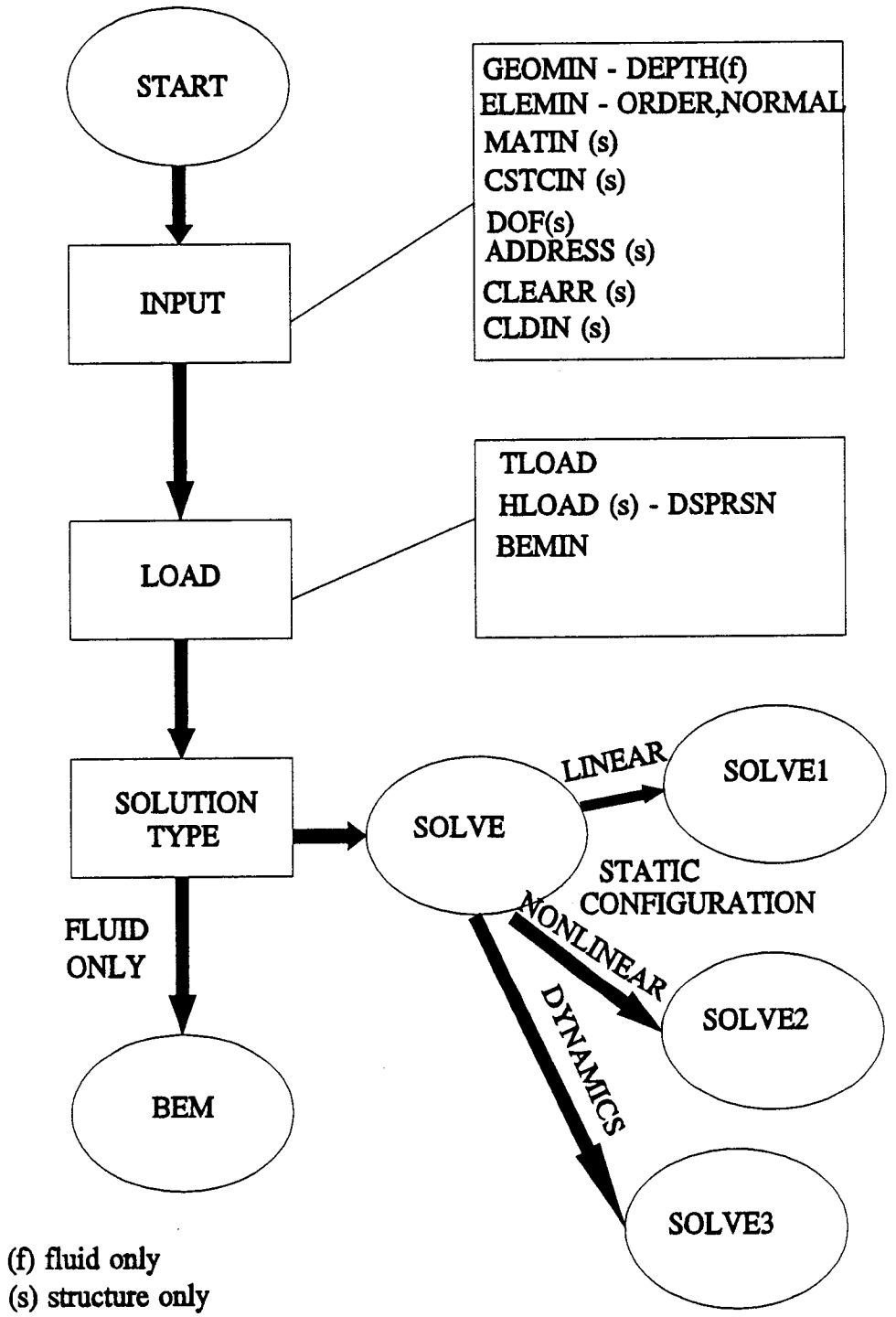

Figure A.1 Flow Chart of Coupled Model

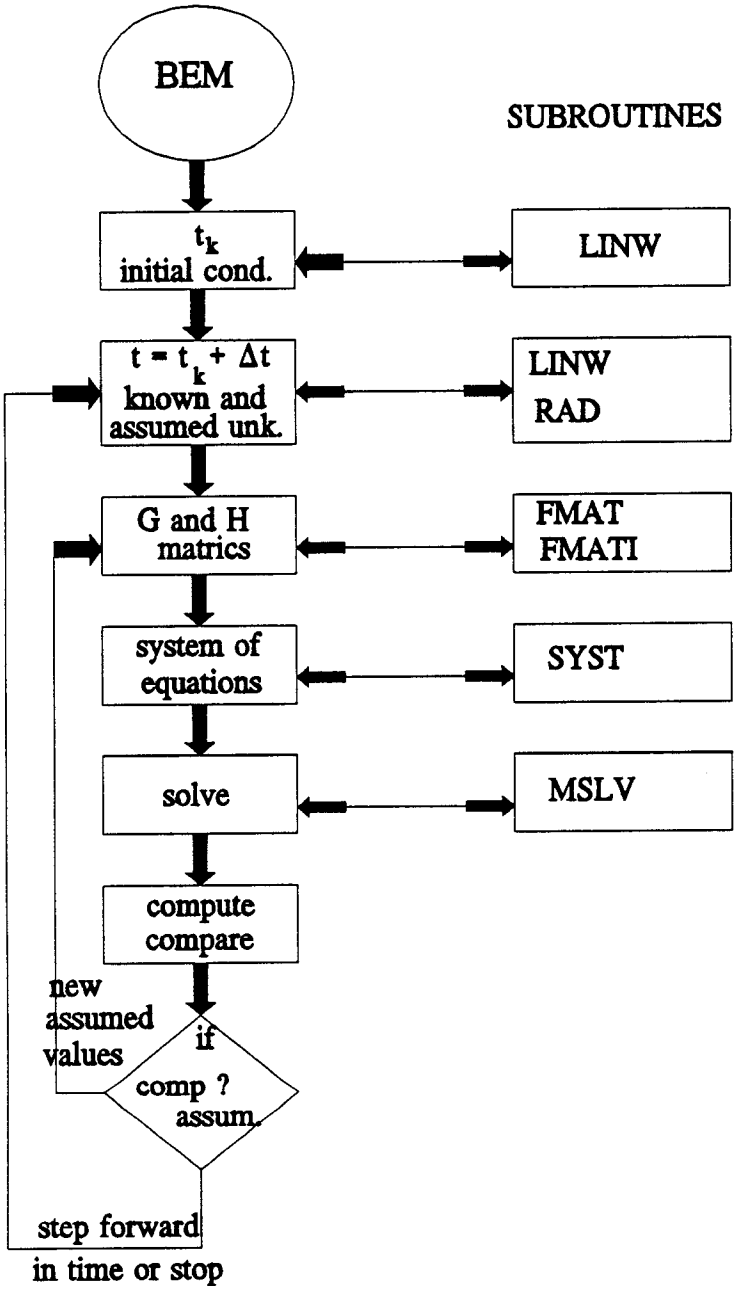

Figure A.2 Flow Chart of BEM

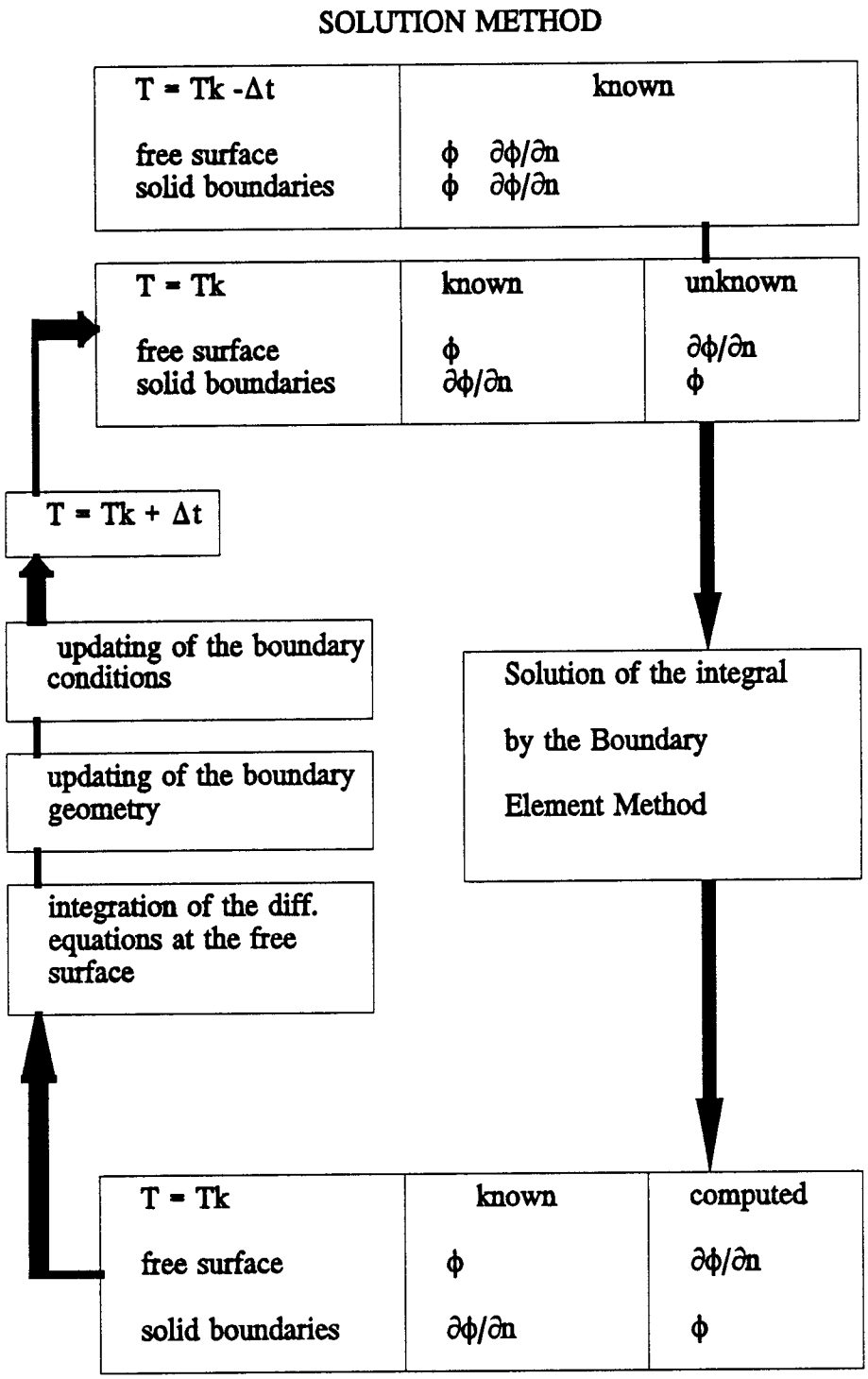

Figure A.3 BEM Algorithm

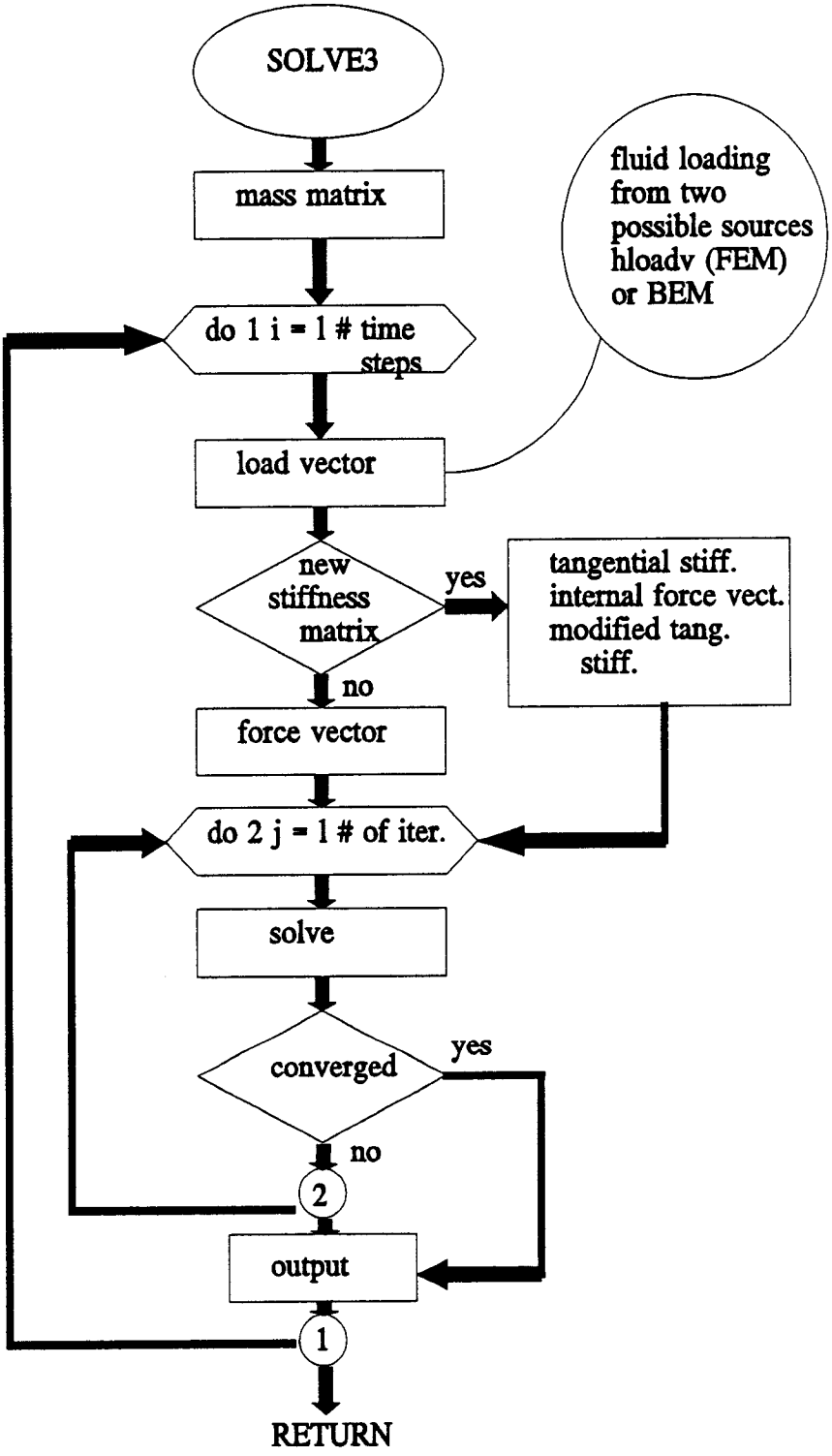

Figure A.4 Dynamic Analysis Algorithm

APPENDIX B LITERATURE REVIEW

Selective review of boundary element modelling for the interaction of deformable structures with water waves

L.L. Broderick and J.W. Leonard

Oregon State University, Corvallis, OR 97333, USA
(Received April 1989; revised September 1989)

A review was conducted of the use of the boundary element method as a solution technique for the nonlinear interaction of deformable structures and finite amplitude waves. The review concentrated on those areas in which modelling difficulties are anticipated: boundaries, waves, time domain analysis, fluid – structure interaction and a coupled finite element and boundary element model. Very little information was uncovered on the nonlinear fluid – structure interaction, although it is anticipated that the fluid domain would be modelled with a boundary element model and the structure would be modelled with a finite element model. The boundary element method appears to be a viable solution technique for the nonlinear interaction of deformable structures and finite amplitude waves.

Keywords: boundary elements, waves, nonlinearities, dynamics, wave/structure interaction, deformable structure

This work focuses on available methods for numerical analysis of the interaction of highly deformable bodies and water waves in the time domain. The problem under study is shown in *Figures 1* and *2* in a continuous space with coordinates x_i, $i = 1, 2, 3$. A three-dimensional deformable body of arbitrary shape, B, is placed in a fluid domain, F. The fluid domain is subject to long-crested finite amplitude waves (two-dimensional sea state with an arbitrary direction, θ). These 'nonlinear' waves will induce large rigid body motions and large deformations in B. The interaction of B with the waves will cause modifications in the wave field by diffraction, reflection, transmission and wave generation. This change in the wave field will produce additional changes in the motion of B. Not only are the structural motions and waves nonlinear, the coupled interaction is nonlinear.

Obviously an analytical solution to this problem is impracticable due to the nonlinear interactions and the irregular geometry. The Finite Element Method (FEM) would be a logical starting point, but another less developed approach is the Boundary Element Method (BEM). References using FEM will not be cited. This paper explores the potential use of BEM to model nonlinear fluid – structure interactions. In particular this review will provide guidance in developing a numerical model to model nonlinear interactions.

The BEM has been used in a variety of applications and there are several areas where difficulties could arise. This review has concentrated on the following potential difficulties:

- *boundaries*—boundaries at infinity and adaptable boundaries that can move with the free surfaces and boundary surfaces
- *time domain*—time domain analysis versus frequency domain analysis (the majority of the literature is in the frequency domain)
- *waves*—modelling the free surface for linear wave theory (small amplitude wave height) and nonlinear wave theory (finite amplitude wave height)
- *fluid – structure interactions*—the nonlinear coupled action and reaction of the fluid and structure
- *coupled FEM and BEM*—structure modelled using FEM and the fluid modelled using BEM. The question arises as to how to couple the two modelling techniques.

Each of the areas mentioned above has its own section and there is a preliminary section on BEM, where the BEM technique is described and compared with FEM. It should be noted that most of the references cited in the sections on boundaries, waves, time domain and fluid/structure interaction are those articles that involve water waves. References 70–89 relate to the general topics but are in other engineering disciplines. These articles, although not cited in the various sections, served as valuable insights into BEM.

0141-0296/90/040269-08

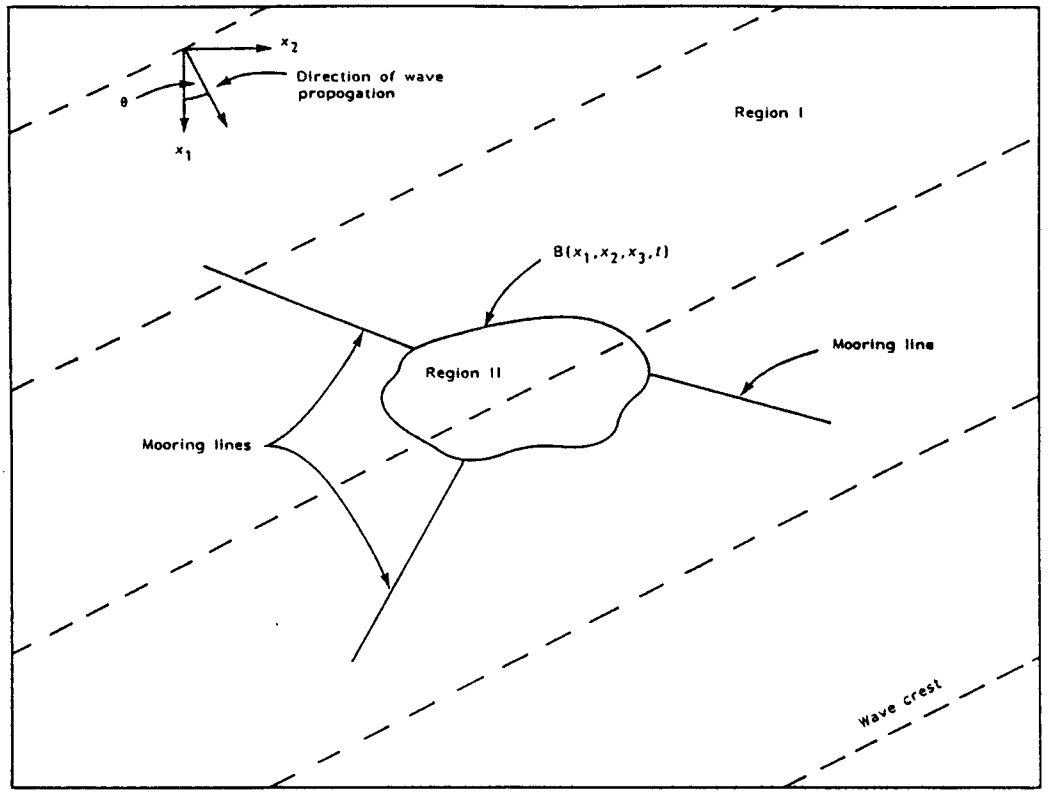

Figure 1 Plan view

Boundary element method

The building block for most engineering systems is an infinitesimally small element where the relationships between the major variables can be assumed, thus creating a series of differential equations. In the case of finite element or finite difference methods, the differential equations are left in this form[1]. These equations are approximated discretely over the domain by functions which fully or partially satisfy the boundary conditions. This is accomplished by discretizing the domain and then simultaneously solving the systems of equations while imposing the boundary conditions.

In the boundary element method (BEM) an attempt is made to integrate the differential equations prior to discretizing the domain. These equations, called boundary element integrals, exactly satisfy the conditions in the domain. Boundary element integrals only involve variables on the boundaries, which means that only the boundaries need to be discretized. The solution variables will then vary continuously throughout the domain, and all approximations of geometry will occur on the boundaries.

BEM utilizes the principle of superposition and thus is only applicable to linear systems or those nonlinear systems that can be approximated in an incremental sense using linear systems. Because of the 'linear systems' requirement the domain must be homogeneous. If the domain is not homogeneous, the domain must be divided into regions such that each region is homogeneous, or can be approximated as a homogeneous domain.

There are two major classes of BEM, indirect and direct[1,2]. The indirect method starts with a solution that satisfies the governing equations in the space domain but has unknown coefficients. The coefficients are evaluated by imposing the boundary conditions in some sense, like least squares. Generally the solution used is the unit singular solution of the differential equations and the unknown coefficients are the specific densities over the boundaries. Once the coefficients are determined the values of the physical variables can be determined using a simple integration procedure. Alternatively, in the direct method the physical variables are the unknown functions appearing in the integral equations. The direct method is generally presented in terms of Green's identity. Both the indirect and the direct method can be equated to the weighted residual formulation[2].

In BEM there are two approximations made to obtain the boundary values: (1) integrating in a piecewise manner; and (2) solving the integral in a weighted residue sense (on the boundary). The integration can be extremely difficult to perform because the functions tend to be singular. The singular nature of the functions does

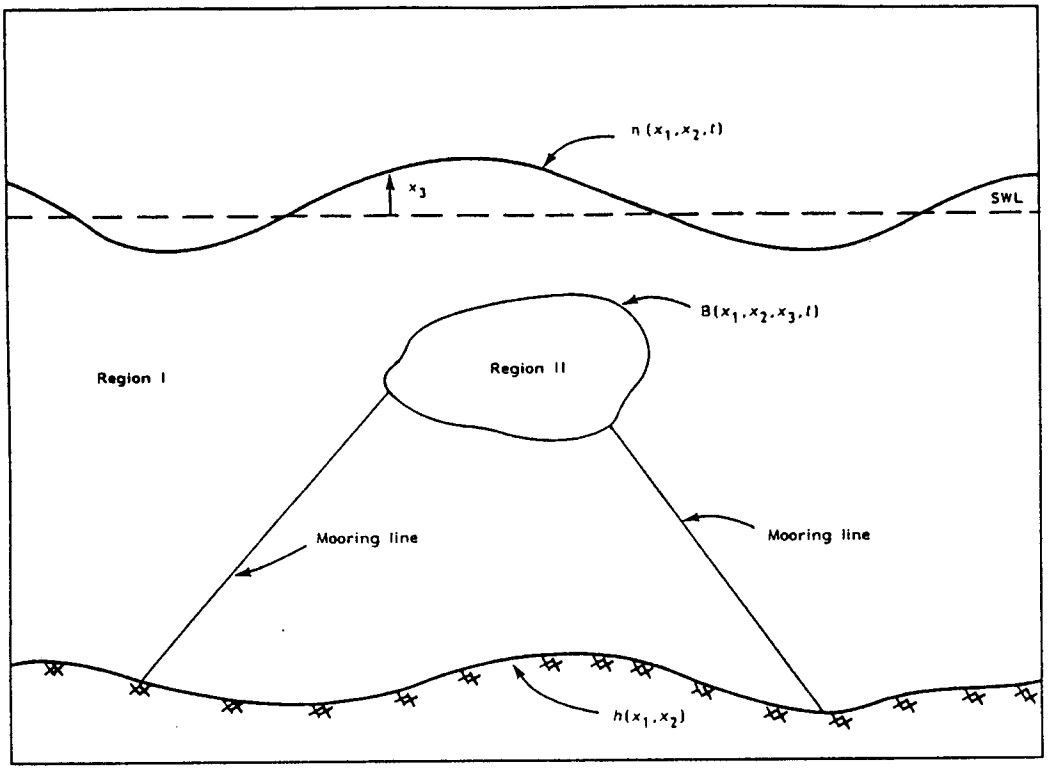

Figure 2 Profile

allow BEM to effectively model problems with high gradients.

In general the advantages and disadvantages of BEM are as follows[3].

Advantages

- For homogeneous material, only the boundary needs to be discretized.
- Infinite boundaries are easier to model in BEM than in FEM.
- The order of nodes and elements is not critical to the efficiency of the computer solution.
- Once a solution for the boundary is established, solving for any interior point is straightforward.

Disadvantages

- Off-the-shelf computer codes are not yet commonly available.
- The solution matrix is fully populated.
- Internal forces other than those that can be related to a surface integral cannot be applied.
- If the surface area to volume ratio is large, the solution technique will not be economical.
- If the material is non-homogeneous the inner region will need to be discretized.

References 1–17 provide general information on formulations and numerical procedures used in the BEM.

Boundaries

There are three types of boundaries in the interaction of waves and a deformable structure: the bottom boundary, the radiation boundaries and the interface boundaries. The interface boundaries can be further broken down to the type of interface, namely, air/water or structure/water. In this study three possible interfaces were considered: the air/water interface (free surface), the deformable structure/water interface and the wave maker/water interface. The wave maker/water interface may not exist, depending on the procedure used to input waves in a numerical model. Implied in the following definitions of boundary conditions is that the governing field equation for the fluid domain is the Laplace equation:

$$\nabla^2\Phi = 0 \tag{1}$$

where Φ is the velocity potential and the velocity vector ∇ is equal to $-\partial\Phi/\partial x_i$.

The bottom boundary is the easiest of the boundaries to deal with as long as the sea floor is assumed to be rigid and impermeable. In addition, the sea floor is

assumed to be neither accreting nor eroding. With these assumptions the bottom boundary conditions can be writtten as:

$$\frac{\partial \Phi}{\partial n} = 0 \tag{2}$$

where n is the unit normal. This states that the velocity component normal to the sea floor is zero.

In the BEM formulation the sea floor does not have to be at a constant elevation but the degree that it can vary depends on the computer resources available. The more elements that the sea floor is divided into, the more accurate the representation of the numerical model, but the computer cost will increase accordingly. There is a balance that must be reached between representing nature and available computing resources.

The radiation condition is an artificial boundary that is imposed on the numerical model because the domain of the model does not extend to infinity. The radiation boundary conditions must ensure a unique solution and a solution that is nearly the solution that would exist if the artificial boundary were not there. This condition forces all propagating waves to be outgoing. In the case of linear waves and a *frequency domain analysis* the radiation condition is the well-known Sommerfield condition[18] which specifies an outgoing scattered wave with radial decay:

$$r^{1/2}\left(\frac{\partial \Phi}{\partial r} \mp ik\Phi\right) = 0 \qquad \text{as } r \to \pm\infty \tag{3}$$

where $k = 2\pi/L$, $i = \sqrt{-1}$ and $r = (x^2 + z^2)^{1/2}$. Equation (3) has been modified for *time domain analysis* and written as:

$$\frac{\partial \Phi}{\partial t} + C\frac{\partial \Phi}{\partial r} = 0 \tag{4}$$

where C is the wave celerity[19]. There are still problems associated with the Orlanski condition in determining the phase velocity at the boundaries at each instant in time[20].

One approach that has been used to avoid the problem of defining an appropriate radiation boundary condition in the time domain is to place the far field boundary a sufficient distance from the body. Any scattered waves generated by the interaction will only travel a short distance over the duration of the test. Thus the values of the potential and the normal velocity at the far field boundary are dependent only on the incident wave field[21].

The free surface boundaries have the following boundary conditions: the water and the air or structure must stay in contact, and no interchange of material across the interface is allowed. The air/water interface has two boundary conditions, one kinematic and one dynamic. The kinematic boundary condition is[18]:

$$-\frac{\partial \Phi}{\partial x_3} = \frac{\partial \eta}{\partial t} - \frac{\partial \Phi}{\partial x_1}\frac{\partial \eta}{\partial x_1} - \frac{\partial \Phi}{\partial x_2}\frac{\partial \eta}{\partial x_2} \quad \text{on } x_3 = \eta \tag{5}$$

where η is the free water surface. The dynamic boundary condition is[18]:

$$\eta = \frac{1}{g}\left(Q(t) + \frac{\partial \Phi}{\partial t} - \frac{1}{2}\bar{Q}^2\right) \quad \text{on } x_3 = \eta \tag{6}$$

where g is the acceleration due to gravity and Q is the Bernoulli's constant. The structure/water interface has two boundary conditions, one kinematic and the other dynamic. The kinematic boundary condition is[18]:

$$-\nabla\Phi = \bar{v} \cdot n_B \qquad \text{on} \quad B \tag{7}$$

where $\bar{v}$ is the velocity of the structure and n_B = unit normal to the surface. The dynamic boundary condition is actually stated in a dynamic equilibrium equation of motion for a deformable body[22]. For additional information and references on the free surface interfaces see the sections on Waves and Fluid/structure interaction.

Another difficulty that will develop in the formulation of boundary conditions for the interaction of deformable structures and waves is the wet/dry element. The deformable structure can pierce the surface and at various times different amounts of the structure will be underwater or out of the water. This will further complicate the forces on the structure which change with time. The bookkeeping required to keep track of the location of the water/air/structure interface will be critical[23,24].

Variable depth bottom boundary

In References 25–29 the degree to which the sea floor was allowed to vary depended on the discretization of the sea floor. The limiting factor to the discretization is the computer available to perform the work. A balance must be reached between the number of elements and resources. It should be noted that in References 25–29 the bottom depth becomes constant at the outer boundaries where a radiation boundary is matched.

Radiation boundary

The radiation boundary tends to be solved in two ways, either assuming an eigenvalue expansion in the fluid domain exterior to the radiation boundary, or solving the Sommerfield radiation condition in the frequency domain. Either method can be equated to the other. If the problem being solved is in the time domain, the Orlanski or a modified version of the Orlanski condition is used. The eigenvalue expansion method is used in References 26, 28–30. References 20, 25, 27, 31–37 use the Sommerfield or Orlanski radiation condition.

Needed BEM work on boundary

- Making sure that the radiation condition selected ensures that the far field is unaffected by the structure/fluid interaction.
- How to handle the wet/dry elements. Some work has been done on 'adaptable' meshes for BEM[23,24].

Waves

Waves are disturbances on the air/water interface that serve as the exciting force for the deformable structure.

The boundary conditions on the interface were given as equations (5) and (6) in the previous section. Solving for the wave height, η, is difficult because the surface coordinate, x_3, is following η and the position of η is unknown. To get around this, the amplitude of the wave is often considered to be small and η is referenced to the still water level (SWL), $x_3 = 0$. This linearizes the boundary conditions, but it requires the wave heights to be small (linear wave theory). The assumption of small wave heights is applicable in numerous situations but there are times when finite amplitude waves are necessary. There are several methods used to describe nonlinear waves: Stokes (2nd and 3rd) higher order waves, Dean's stream function, transformal mapping and cnoidal waves just to name a few[18]. Which method is better depends on the water depth and wave period of interest; even then, which method is the best is still open to debate.

Table 1 summarizes what various authors have done in order to model waves in a BEM. Across the top the divisions are based on the BEM method used: indirect, direct or weighted residual. (For discussion on classifications see the section on BEM.) Vertically the divisions are based on the type of waves modelled: linear, nonlinear or special type of waves. The references for the various categories shown in *Table 1* are listed in the footnote. There were no references found for categories N_1, N_3, S_1 and S_3.

It would be desirable to have one method that can be used to model both linear and nonlinear waves. There are distinct advantages to using the same method and one of those advantages is in model verification. Data sets exist that involve linear waves. These data sets could be used to verify a numerical model. If the linear wave portion of the numerical code is validated and the same method is used to generate nonlinear waves, there will be some confidence in the results. If different methods are used, no confidence in the nonlinear portion of the model can be derived from the linear portion. *Table 1* suggests that the direct method is the most promising to use for both linear and nonlinear waves.

In addition to the methods described above, there is another way to disturb the air/water interface. One of the boundaries can be a wave maker (structure/water interface). A wave maker type problem would serve as one of the verification tests to prove the validity of a numerical code. For additional information on the structure/water interface see the section on Fluid/structure interaction.

Table 1 Classification of BEM methods for water wave problems

	Indirect	Direct	Weighted
Linear	L_1	L_2	L_3
Nonlinear	N_1	N_2	N_3
Special	S_1	S_2	S_3

Category L_1 (indirect-linear): References 9, 32, 38–43
Category L_2 (direct-linear): References 9, 26–29, 34, 36, 37, 44
Category L_3 (weighted residue-linear): Reference 45
Category N_1 (indirect-nonlinear): no references available
Category N_2 (direct-nonlinear): References 20, 21, 26, 37, 46, 47
Category N_3 (weighted residue-nonlinear): no references available
Category S_1 (indirect-special): no references available
Category S_2 (indirect-special): References 33, 48–50
Category S_3 (weighted residue-special): no references available

Not represented in *Table 1* are those methods that involve the complex potential and transformal mapping. References 51–54 used BEM with the complex potential to successfully model finite amplitude waves. Longuet-Higgins and Cokelet[54] first used the mixed Eulerian Lagrangian method for nonlinear free surface problems, assuming potential flow. They were confined to two-dimensional flows because the physical plane was transformed to the complex plane. Dommermuth and Yue[53] developed a numerical method to model three-dimensional (axisymmetric) nonlinear free surface problems. They used a mixed Eulerian Lagrangian formulation based on the work by Longuet-Higgins and Cokelet but kept the problem in the physical plane. Taking advantage of axisymmetry, Rankine ring sources were used in a Green's theorem boundary integral formulation to solve the field equation. The free surface was then updated in time following Lagrangian points. They presented three examples: (1) the growth and collapse of a vapour cavity near the free surface; (2) the heaving of a floating vertical cyclinder starting from rest; and (3) the heaving of an inverted vertical cone. This method of a mixed formulation appears to provide very accurate results. Dommermuth *et al.*[52] have verified a numerical model of steep waves in a two-dimensional wave tank and compared results with laboratory data.

Time domain analyses

A majority of the effort reported on water waves and BEM has been done in the frequency domain. For the nonlinear dynamic interaction of waves and deformable structures, a time domain analysis is necessary. Several of the references cited in the References section introduce time domain analysis in BEM modelling. The references cited below all deal with water waves and BEM.

Various techniques were employed to solve the time domain problem: most authors used a time marching procedure. Brevig *et al.*[46] used a nonlinear time stepping procedure to reduce computer time but yet maintain convergence. The first three time steps were done using the Runge–Kutta method and then Hammering-corrector method. Nakayama[48] and Washizu *et al.*[35] used a finite difference scheme in their time analyses (similar to a Newton Raphson approach). Isaacson[21] used a time differencing scheme in his time marching analysis. Sen and Pawlowski[37] considered both linear and nonlinear waves and used a fourth order Adams–Bashforth–Moulton scheme. In the articles by Salmon *et al.*[27] and Lennon *et al.*[33] the problem was defined such that time appears explicitly in the boundary conditions which allows for a non-iterative solution. Jagannathan[20] used the method described by Longuet-Higgins and Cokelet[54] of Lagrangian marker particles. The integration over time was done using the non-iterative Adam's predictor–corrector method. Yeung[56] used Volterra's method to derive a time-dependent integral equation associated with the fluid motion. It is a

time marching process in that the results at t_c are dependent on the results for $t < t_2$.

Reference 26 also gives information on time domain analysis.

Fluid-structure interactions

The interaction of finite amplitude waves and deformable structures involves the coupling of two dynamic models. One model is a diffraction radiation model to compute the hydrodynamic loadings on the structure. The other model is a dynamic structural model that uses the hydrodynamic loads to predict stresses and geometrical changes in the structure. The coupling of the two models is done through the boundary conditions on the fluid/structure interface. The boundary conditions are: the velocity of the fluid and the structure are the same at contact points, and the pressure exerted on the structure by the fluid is balanced by the pressure exerted on the fluid by the structure. The kinematic boundary conditions have been stated in equation (7); the dynamic boundary condition is the dynamic equilibrium equation of motion for the deformable body (see, for example, Lo[22]).

For deformable structures, the pressure is equated at various points around the structure. In the case of floating rigid bodies, the pressure is integrated over the body to obtain resultants at the centre of gravity, and forces exerted by the fluid and the structure are equated. If the waves in the numerical model are generated by a numerical wave maker both types of condition will exist. The deformable structure will require the equating of pressure and the wave maker will require the equating of forces.

The following is a summary of several articles that deal with the interaction of floating bodies and waves using BEM.

Yeung[29] solved the two-dimensional problem of a floating body of arbitrary geometry. The bottom elevation can vary in the region of interest, but must approach a constant depth in the outer regions (not necessarily the same depth). This body is rigid and is not restrained with mooring lines. Linear wave theory is used. Yeung[56] then extended this work to the time domain using Volterra's method and an unsteady Green's function.

Masuda and Kato[34] solved a similar problem to that described by Yeung. They extended their results to three-dimensional bodies in two-dimensional seas. They also used finite amplitude wave theory.

Yamamoto *et al.*[46] solved a similar problem to that of Yeung, namely, a two-dimensional body of arbitrary shape. The bottom elevation is allowed to vary in the area of interest but must reach a constant where the radiation boundary condition is applied. The floating body is restrained by elastic mooring lines.

Brevig *et al.*[46] were interested in computing the maximum forces on submerged wave energy devices. They used nonlinear wave theory with a time marching process to bring the wave to the point of breaking. The problem was solved in two dimensions.

Isaacson[21] developed a method for calculating the interaction of steep ocean waves with a fixed or floating structure of arbitrary shape. The problem involves nonlinear wave theory and a time marching process.

Sclavounous[37] studied the second order radiation and diffraction of surface waves by floating bodies. This was accomplished by deriving a second order Green's function using an explicit sum- and difference frequency method.

These articles are typical of what is documented in the literature. Only one reference was located that dealt with deformable structures and waves (Lo[22]) and in that model the structure was modelled using FEM. The fluid domain is ideally suited for boundary elements and the nonlinearity associated with structural motions may require finite element modelling.

FEM–BEM models

To model the fluid/structure interaction between finite amplitude waves and a deformable body, a coupled FEM and BEM model might be used. The fluid domain could be modelled using BEM and the structure modelled using FEM.

When coupling the two modelling techniques there are three basic approaches: (1) an iterative process between the two models; (2) a BEM-hosted model; or (3) a FEM-hosted model (Cox[58]). The first approach is inefficient and should only be used if the second or third approach cannot be done. The choice between approach (2) or (3) depends on the make-up of the total domain of the problem.

A successful example of an iterative approach was presented by Han[59], who developed a numerical model to study the nonlinear interaction of wind-loaded pneumatic membrane structures. The membrane was modelled using a FEM and the medium surrounding the membrane was modelled using BEM. It is anticipated that the nonlinear interaction of water waves and deformable structures can be analysed in a similar manner.

If the problem is dominated by a region where FEM is used, a FEM-hosted model should be used. In a FEM-hosted model the BEM subdomain is treated as one or several finite elements. In this approach the boundary integral equations are the equivalent stiffness of the subdomain and can be assembled into the FEM. The stiffness can be obtained by a variational approach or a direct approach. In the variational approach the stiffness relationship is derived from a boundary variational equation. In the direct approach the boundary element equations are manipulated into a stiffness form. Generally in FEM models the system of equations is symmetric and banded, which is efficient to solve numerically. Thus care should be taken to keep the resulting stiffness matrix symmetric and banded. While it is possible to create symmetric and banded matrices using the direct method (Brebbia[2]), it is more straightforward to use the variational approach to do so.

In the case where the domain is dominated by BEM, the FEM subdomain becomes a boundary element region, and equilibrium and compatibility are approximately enforced along the interface. This is similar to breaking up a non-homogeneous domain into several homogeneous domains. This method will result in equations that are non-symmetric, which are not as efficiently solved as symmetric and banded matrices. The choice of which method, BEM or FEM, should be the host depends on which region predominates.

Care must be taken when using a coupled model to ensure that fictitious gaps between the elements do not affect the results. These numerical gaps are due to the

way that BEM satisfies the boundary condition. In the BEM formulations the governing equations are satisfied exactly in the domain but the boundary conditions are only approximately satisfied. The shape functions used for the BEM do not constrain the displacement field, but are merely an approximation of the boundary values for integration. See Cox[58] for recommendations as to how to avoid or minimize the problem.

In References 30, 32, 34 and 58–69 BEM has been combined with other modelling techniques. Most of the references involve BEM coupled with FEM but there are examples where BEM is coupled with other techniques, such as finite difference. Arnold and Noye[44] provide a general reference on this subject.

Conclusions

The boundary element method is a viable solution technique for modelling the nonlinear interaction of deformable structures and water waves. The BEM is ideally suited to the fluid domain while a FEM model is more suited to modelling the structure. This would require a coupled FEM and BEM model. As with any solution technique, difficulties will arise and care must be taken to ensure accurate results.

Acknowledgement

This material is based upon work supported by the USN Office of Naval Research under the University Research Initiative (URI) Contract No. N00014-86-K-0687.

References

1 Banerjee, P.K. and Butterfield, R. *Boundary Element Methods in Engineering Science*, McGraw-Hill, London, 1981
2 Brebbia, C.A. *The Boundary Element Method For Engineers*, John Wiley & Sons, New York, 1978
3 Kuich, G. 'Starting to work with boundary elements', in *Boundary Element Techniques in Computer-Aided Engineering* (Ed C.A. Brebbia), Martinus Nijhoff Publishers, Boston, 1984
4 Banerjee, P.K. and Shaw, R.P. *Developments in Boundary Element Element Methods—2*, Applied Science Publishers, London, 1982
5 Banerjee, P.K. and Butterfield, R. *Developments in Boundary Element Methods—1*, Applied Science Publishers Ltd, London, 1979
6 Brebbia, C.A. and Noye, B.J. *Proc. Boundary Element Technol Conf. BETECH 85, Adelaide, Australia*, Springer-Verlag, Berlin, 1985
7 Brebbia, C.A. *Topics in Boundary Element Research, Volume 2: Time-Dependent and Vibration Problems*, Springer-Verlag, Berlin, 1985
8 Brebbia, C.A. *Boundary Element Techniques in Computer-Aided Engineering*, Martinus Nijhoff Publishers, Boston, 1984
9 Brebbia, C.A., Telles, J.C.F. and Wrobel, L.C. *Boundary Element Techniques Theory and Applications in Engineering*, Springer-Verlag, Berlin, 1984
10 Brebbia, C.A. *Topics in Boundary Element Research Volume 1: Basic Principles and Applications*, Springer-Verlag, Berlin, 1984
11 Brebbia, C.A., Futagami, T. and Tanaka, M. *Boundary Elements*, Springer-Verlag, Berlin 1983
12 Brebbia, C.A. *Progress in Boundary Element Methods Volume 1*, John Wiley & Sons, New York, 1981
13 Glowinski, R. and Lions, J.L. *Computing Methods in Applied Sciences and Engineering, 1977, 1*, Springer-Verlag, Berlin, 1979
14 Hromadka, T.V. *The Complex Variable Boundary Element Method*, Lecture Notes in Engineering (Eds C.A. Brebbia and S.A. Orszag), Springer-Verlag, Berlin, 1984
15 Ingham and Kelmanson *Boundary Integral Equation Analysis of Singular, Potential, and Biharmonic Problems*, Springer-Verlag, Berlin, 1984
16 Liggett, J.A. and Liu, P.L.F. *The Boundary Integral Equation Method For Porous Media Flow*, George Allen & Unwin, London, 1983
17 Tang, W., *Transforming Domain into Boundary Integrals in BEM*, Springer-Verlag, Berlin, 1988
18 Sarpkaya, T. and Isaacson, M. *Mechanics of Wave Forces on Offshore Structures*, Van Nostrand Reinhold Company, New York, 1981
19 Orlanski, I. 'A simple boundary condition for unbounded hyperbolic flows', *J. Computational Phys.* 1976, 21, 251–269
20 Jagannathan, S. 'Simulation of two-dimensional nonlinear free surface flows', *Proc. Ocean Structural Dynamics Symposium, OSDS '86, Corvallis, OR, 9–11 September 1986*, 130–144
21 Isaacson, M. 'Nonlinear-wave effects on fixed and floating bodies', *J. Fluid Mech.* 1982, 120, 267–281
22 Lo, A. 'Nonlinear dynamic analysis of cable and membrane structures', *PhD Dissertation*, Oregon State University, 1982
23 Mullen, R.L. Rencis, J.J. 'Adaptive mesh refinement techniques for boundary element methods', in *Advanced Topics in Boundary Element Analysis* (Eds T.A. Cruse, A.B. Pifko and H. Armen), AMD-Vol 72, ASME, New York, 1985, 235–255
24 Weeks, G.E. and Cost, T.L. 'An algorithm for automatically tracking ablating boundaries', *Int J for Num. Meth in Engng* 1979, 14, 441–449
25 Mei, C.C. and Chen, H.S. 'A hybrid element method for steady linearized free-surface flows', *Int. J. for Num. Meth. in Engng* 1976, 10, 1153–1175
26 Nagata, S. and Ijima, T. 'Numerical analysis of transient, finite amplitude motion of a moored, submerged cylinder', in *Boundary Elements* (Eds C.A. Brebbia *et al.*), Springer-Verlag, Berlin, 1983, 239–248
27 Salmon, J.R., Liu, P.L.-F. and Liggett, J.A. 'Integral equations method for linear water waves', *J. Hydraulics Div., ASCE* 1980, HY12, 1995–2010
28 Yamamoto, T., Yoshido, A. and Ijima, T. 'Dynamics of elastically moored floating objects', *Appl. Ocean Res.* 1980, 2, No. 2, 85–92
29 Yeung, R.W. 'A hybrid integral-equation method for time-harmonic free-surface flow', *Proc. 1st International Conference on Numerical Ship Hydrodynamics, Gaithersburg, Md, October 1975*, 581–607
30 Shaw, R.P. 'Boundary integral equation methods applied to water waves', *Proc. Applied Mechanics Conference, Troy, NY, 23–25 June 1975*, ASME, 7–14
31 Bettess, P. and Zienkiewicz, O.C. 'Diffraction and refraction of surface waves using finite and infinite elements', *Int J. for Num. Meth. in Eng* 1977, 11, 1271–1290
32 Huang, M.C. 'Boundary finite element method in wave diffraction analysis', *Proc. Ocean Structure Dynamics Symposium, OSDS '84, Corvallis, OR, 1984*, 491–503
33 Lennon, G.P., Liu, P.L-F. and Liggett, J.A. 'Boundary integral solutions of water wave problems', *J. Hydraulics Div., ASCE* 1982, 108, HY8, 921–931
34 Masuda, K. and Kato, W. 'Hybrid BEM for calculating nonlinear wave forces on the 3-dimensional bodies', *Boundary Elements* (Eds C.A. Brebbia *et al.*), Springer-Verlag, Berlin, 1983, 209–215
35 Mei, C.C. 'Numerical methods in water-wave diffraction and radiation', *Ann. Rev. Fluid Mech.* 1978, 393–416
36 Naftzger, R.A. and Chakrabarti, S.K. 'Scattering of waves by two-dimensional circular obstacles in finite water depths', *J. Ship Res.* 1979, 23, No. 1, 32–42
37 Sen, D. and Pawlowski, J.S. 'Simulation of unsteady propagation of steep waves by boundary element method', *Proc. 7th International Conference on Offshore Mechanics and Arctic Engineering, OMAE*, 1988, 181–190
38 Garrison, C.J. 'Hydrodynamic loading of large offsbore structures: three-dimensional source distribution methods', in *Numerical Methods in Offshore Engineering* (Eds O.C. Zienkiewicz, R.W. Lewis and K.G. Stagg), John Wiley & Sons, New York, 1978, 87–140
39 Garrison, C.J. 'Hydrodynamics of large objects in the sea part II: motion of free-floating bodies', *J. Hydronautics* 1975, 9, No. 2, 58–63
40 Garrison, C.J., 'Hydrodynamics of large objects in the sea part I—hydrodynamic analysis', *J. Hydronautics* 1974, 8, No. 1, 5–12
41 Huang, M.C., Chen, B.S. and Shaw, J.J. 'Boundary element method in wave diffraction/radiation analysis: two dimensional vertical problem', *Proc. National Science Council Part A: Physical Science and Engineering*, 10, No. 3, Taipei, Taiwan, July 1986, 298–312
42 Newman, J.N. 'Distributions of sources and normal dipoles over a quadrilateral panel', *J Engng Math* 1986, 20, 113–126
43 Williams, B.A. 'Analysis of wave/object interaction using distributed source element of linearly varying strengths', *Masters Thesis*, Naval Postgraduate School, Monterey, CA, June 1977
44 Arnold, R.J. and Noye, B.J. 'Boundary element and finite difference techniques for simulating oscillations in closed basins', *Proc. Boun-*

dary Element Technol Conf, BETECH 85, Adelaide, Australia (Eds C.A. Brebbia and B.J. Noye) Springer-Verlag, Berlin, 1985, 31–43

45 Au, M.C. and Brebbia, C.A. 'Water waves analysis', in *Topics in Boundary Element Research Volume 1: Basic Principles and Applications* (Ed C.A. Brebbia), Springer-Verlag, Berlin, 1984, 97–122

46 Brevig, P., Greenhow, M. and Vinje, T. 'Extreme wave forces on submerged wave energy devices', *Appl. Ocean Res.* 1982, 4, No. 4, 219–225

47 Molin, B. 'Second-order diffraction loads upon three-dimensional bodies', *Appl. Ocean Res.* 1979, 1, No. 4, 197–202

48 Nakayama, T. 'Boundary element analysis of nonlinear water wave problems', *Int. J. for Num. Meth. in Engng* 1983, 19, 953–970

49 Nakayama, T. and Washizu, K. 'The boundary element method applied to the analysis of two-dimensional nonlinear sloshing problems', *Int. J. for Num. Method. in Engng* 1981, 17, 1631–1646

50 Soh, W.K. 'Computer study of solitary waves travelling over submerged obstacles', in *Proc. Boundary Element Technology Conference, BETECH 85, Adelaide, Australia*, (Eds C.A. Brebbia and B.J. Noye), Springer-Verlag, Berlin, 1985, 45–57

51 Baker, G.R., Meiron, D.I. and Orzag, S.A. 'Generalized vortex methods for free-surface flow problems', *J. Fluid Mech.* 1982, 123, 477–501

52 Dommermuth, D.G., Yue, D.K.P., Lin, W.M., Rapp, R.J., Chan, E.S. and Melville, W.K. 'Deep-water plunging breakers: a comparison between potential theory and experiments', *J Fluid Mech.* 1988, 189, 423–442

53 Dommermuth, D.G. and Yue, D.K.P. 'Numerical simulation of nonlinear axisymmetric flows with a free surface', *J. Fluid Mech.* 1987, 178, 195–219

54 Longuet-Higgins, M.S. and Cokelet, E.D. 'The deformation of steep surface waves on water I. A numerical method of computation', *Proc. Roy. Soc. London A* 1976, 350, 1–26

55 Washizu, K., Nakayama, T., Ikegawa, M., Tanaka, Y. and Aduchi, T. 'Some finite element techniques for the analysis of nonlinear sloshing problems', in *Finite Elements in Fluids—Volume 5* (Eds R.H. Gallagher, J.T. Oden, O.C. Zienkiewicz, T. Kawai, and M. Kawahara), John Wiley, 1984, 357–376

56 Yeung, R.W. 'The transient heaving motion of floating cylinders', *J. Engng Maths* 1982, 16, 97–119

57 Sclavounous, P.D. 'Radiation and diffraction of second-order surface waves by floating bodies', *J. Fluid Mech.* 1988, 196, 65–91

58 Cox, J.V. 'A preliminary study on finite element hosted coupling with the boundary element method', *NCEL Technical Note (N-1783), Naval Civil Engineering Laboratory*, Port Hueneme, CA, April 1988

59 Han, P.S. 'Interactive nonlinear analysis of wind-loaded pneumatic membrane structures', *PhD Dissertation*, The University of British Columbia, 1986

60 Eatock Taylor, R. and Zietsman, J. 'A comparison of localized finite element formulations for two-dimensional wave diffraction and radiation problems', *Int. J. for Num. Meth. in Engng* 1981, 17, 1355–1384

61 Liggett, J.A. and Liu, P.L.F. 'Application of boundary element methods to fluid mechanics', *Topics in Boundary Element Research Volume 1: Basic Principles and Applications* (Ed C.A. Brebbia), Springer-Verlag, Berlin, 1984, 78–96

62 Margulies, M. 'Combination of the boundary element and finite element methods', *Progress in Boundary Element Methods Volume 1* (Ed C.A. Brebbia), John Wiley & Sons, 1981, 258–288

63 Mariem, J.B. and Hamdi, M.A. 'A new boundary finite element method for fluid–structure interaction problems', *Int. J. for Num. Meth. in Engng* 1987, 24, 1251–1267

64 Mathews, I.C. 'Numerical techniques for three dimensional steady state fluid structure interaction', *Proc. Boundary Element Technol. Conf., BETECH 85, Adelaide, Australia*, (Eds C.A. Brebbia and B.J. Noye), Springer-Verlag, Berlin, 1985, 59–82

65 Shaw, R.P. 'An outer boundary integral equation applied to transient wave scattering in inhomogeneous medium', *J. Appl. Mech.* 1975, 147–152

66 Shugar, T.A. and Cox, J.V. 'A study of coupling boundary and finite element methods in 2 dimensional elastostatics', Naval Civil Engineering Laboratory, Port Hueneme, CA, October 1984

67 Zielinski, A.P. and Zienkiewicz, O.C. 'Generalized finite element analysis with T-complete boundary solution functions', *Int. J. for Num. Meth. in Engng* 1985, 21, 509–528

68 Zienkiewicz, O.C., Kelly, D.W. and Bettess, P. 'Marriage a la mode—the best of both worlds (finite elements and boundary integrals)', in *Energy Methods in Finite Element Analysis* (Eds R. Glowinski, E.Y. Rodin, and O.C. Zienkiewicz, John Wiley & Sons, New York, 1979

69 Zienkiewicz, O.C., Kelly, D.W. and Bettess, P. 'The coupling of the finite element method and boundary solution procedures', *Int. J. for Num. Meth. in Engng* 1977, 11, 355–375

70 Bando, K. and Sonu, C.J. 'Development and verification of numerical models for floating breakwaters', US Army Waterways Experiment Station, Coastal Engineering Research Center, Vicksburg, MS, 1986

71 Belytschko, T. and Geers, T.L. *Computational Methods for Fluid–Structure Interaction Problems*, AMD-Vol 26, ASME, New York, 1977

72 Belytschko, T. and Hughes T. *Volume I Computational Methods for Transient Analysis*, North Holland, Amsterdam, 1983

73 Belytschko, T. *et al. Finnite Element Analysis of Transient Nonlinear Structure Behavior*, AMD-Vol 14, ASME, New York, 1975

74 Bushnell, D. 'A strategy for the solution of problems involving large deflections, plasticity and creep', *Int. J. for Num. Meth. in Engng* 1977, 11, 683–708

75 Cox, J.V. and Shugar, T.A. 'A recursive integration technique for boundary element methods in elastostatics', *Advanced Topics in Boundary Element Analysis* (Eds T.A. Cruse *et al.*), AMD-Vol 72, ASME, New York, November 1985

76 DeRuntz, J.A. and Geers, T.L. 'Added mass computation by the boundary integral method', *Int. J. for Num. Meth. in Engng* 1978, 12, 531–549

77 Heise, U. 'Dependence of the round-off error in the solution of boundary integral equations on a geometric scale factor', *Computer Methods in Applied Mechanics and Engineering*, 62, North-Holland, 1987, 115–126

78 Kirk, C.L. *Dynamic Analysis of Offshore Structures*, Gulf Publishing Company, Houston, 1982

79 Lachat, J.C. and Watson, J.O. 'Effective numerical treatment of boundary integral equations: a formulation for three-dimensional elastostatics', *Int. J. for Num. Meth. in Engng* 1976, 10, 991–1005

80 Lee, C.H. 'Removal of irregular frequencies using the modified integral equation', *Proc. Third International Workshop on Water Waves and Floating Bodies, Swope Center, Woods Hole, MA, 10–13 April 1988*

81 Leonard, J.W., Huang, M.C. and Hudspeth, R.T. 'Hydrodynamic interference between floating cylinders in oblique seas', *Appl. Ocean Res.* 1983, 5, No. 3, 158–166

82 Noblesse, F. 'Alternative integral representations for the green function of the theory of ship wave resistance', *J. Engng Maths* 1982, 16, 241–265

83 Noblesse, F. 'The Green function in the theory of radiation and diffraction of regular waves by a body', *J. Engng Maths* 1982, 16, 137–169

84 Oussett, Y. and Sayhi, M.N. 'Added mass computations by integral equation methods', *Int. J. for Num. Meth. in Engng* 1983, 19, 1355–1373

85 Park, K.C., Felippa, C.A. and DeRuntz, J.A. 'Stabilization of staggered solution procedures for fluid–structure interaction analysis', *Computational Methods for Fluid–Structure Interaction Problems* (Eds T. Belytschko *et al.*) AMD-Vol 26, ASME, New York, 1977

86 Telles, J.C.F. 'A self-adaptive co-ordinate transformation for efficient numerical evaluation of general boundary element integrals', *Int. J. for Num. Meth. in Engng* 1987, 24, 959–973

87 Wepf, D.H., Wolf, J.P. and Bachmann, H. 'Hydrodynamic-stiffness matrix based on boundary elements for time-domain dam–reservoir–soil analysis', *Earthquake Engng and Struct. Dyn.* 1988, 16, 417–432

88 Zienkiewicz, O.C., Kelly, D.W. and Bettess, P. 'The Sommerfield (radiation) condition of infinite domains and its modelling in numerical procedures', *Computing Methods in Applied Sciences and Engineering, 1977, I* (Eds R. Glowinski and J.L. Lions), Springer-Verlag, Berlin, 1979

89 Zienkiewicz, O.C., Lewis, R.W. and Stagg, k.G. *Numerical Methods in Offshore Engineering*, John Wiley & Sons, New York, 1978

APPENDIX C FLEXIBLE CYLINDER EXPERIMENT

C.1 INTRODUCTION

To verify the coupled boundary element model (BEM) and the finite element model (FEM) of the nonlinear interaction of water waves and deformable bodies, a large-scale physical model test was conducted in the large wave channel at the O.H. Hinsdale Wave Research Laboratory at Oregon State University. A membrane cylinder was placed horizontally in the wave tank. Waves were then generated that induced motions in the cylinder, which in turn affected the waves. The deformations of the free surface were recorded above, fore, and aft of the cylinder. Displacements of the membrane were physically recorded with string pots as well as visually recorded on video tape. The internal pressure of the fluid enclosed by the membrane was also recorded. The resulting data allows for the verification of the coupled model by comparing the predicted deformations of the free surface and displacements of the membrane to those measured in the physical model.

C.2 TEST SETUP

The large wave channel in the O.H. Hinsdale Wave Research Laboratory is 342 feet long, 12 feet wide, and 15 feet deep. A hinged-flap waveboard, hydraulically driven and servo-controlled, can generate random and monochromatic waves up to five feet high. This channel provides a facility to

validate theoretical wave models with large scale experiments in an environment with minimal Reynolds Number distortion.

The three-foot-diameter cylinder was placed horizontally across the tank and rigidly attached to the side walls, see Figures C.1 and C.2. The center of the cylinder was located 113 feet from the wave board and 6 feet above the floor. The membrane material was plasticized polyvinyl chloride (pvc) with a thickness of 50 mil. The modulus of elasticity is approximately 8000 psi and the density of the material 0.05 lb/in^3. The material comes in rolls approximately 6 feet wide. To form cylinder, two 4.8 X 12 foot sections were attached using glue. The seams were heat-sealed and appeared to be fairly air-tight. The seams were at the top and bottom of the cylinder when placed in the wave channel.

The cylinder shape was formed by clamping the membrane over circular steel flanges that were rigidly attached to the side walls of the tank. To insure that the membrane did not slide off of the steel flanges, a one inch strip of the membrane was glued around the edge of the flange to give the clamps something to seat against. (During the trial the strips had not been glued to the flanges and the membrane did come off the flanges.)

The steel flanges were equipped with hose fittings at the top and bottom. One of the fittings on the bottom of the flange allowed the inside of the cylinder to be filled with water as the water level was raised in the tank. This same fitting allowed the internal pressure to be varied before the start of a test by adding water. During a run this fitting was sealed, allowing no change in the internal

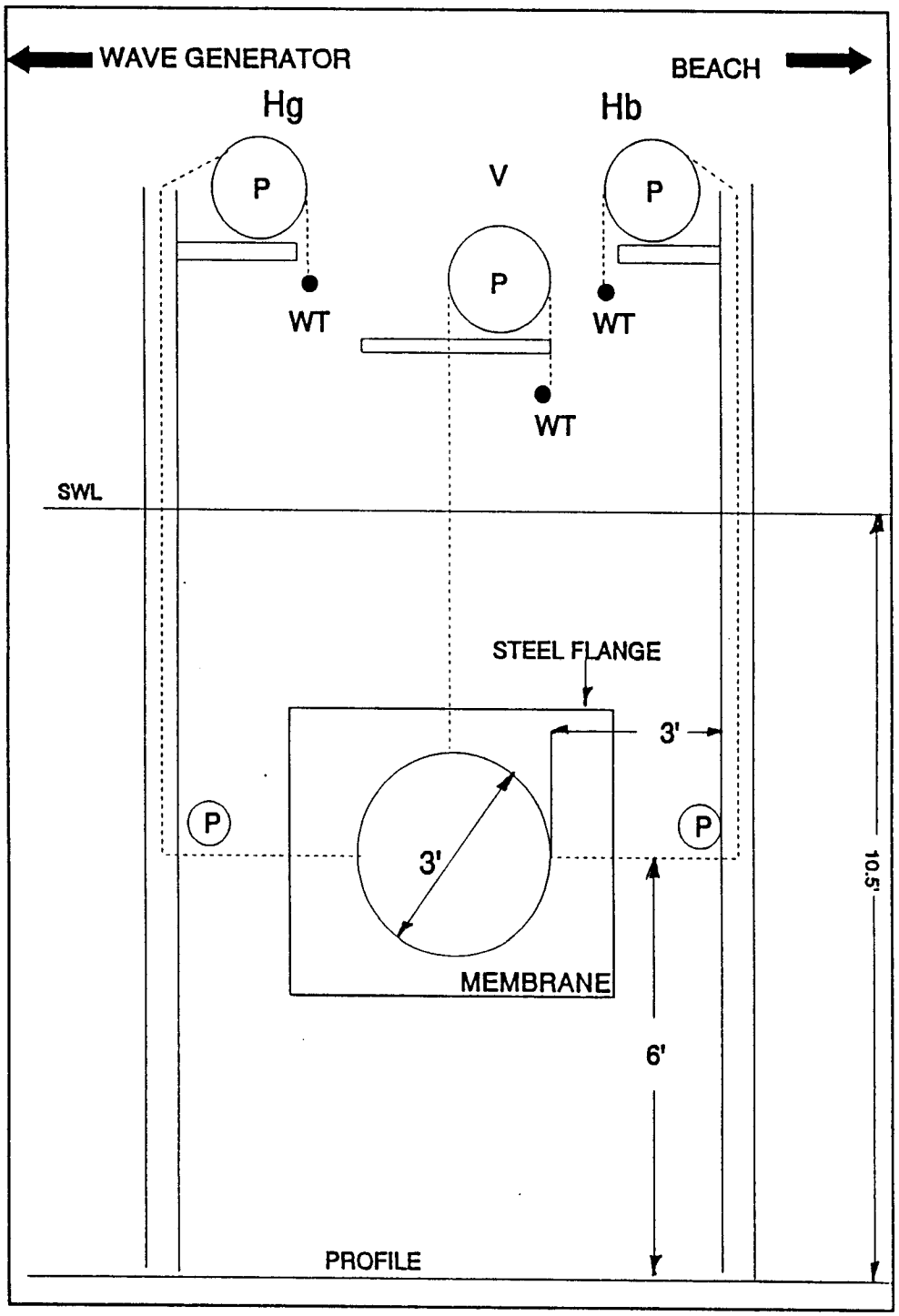

Figure C.1 Profile of Flexible Cylinder Experiment

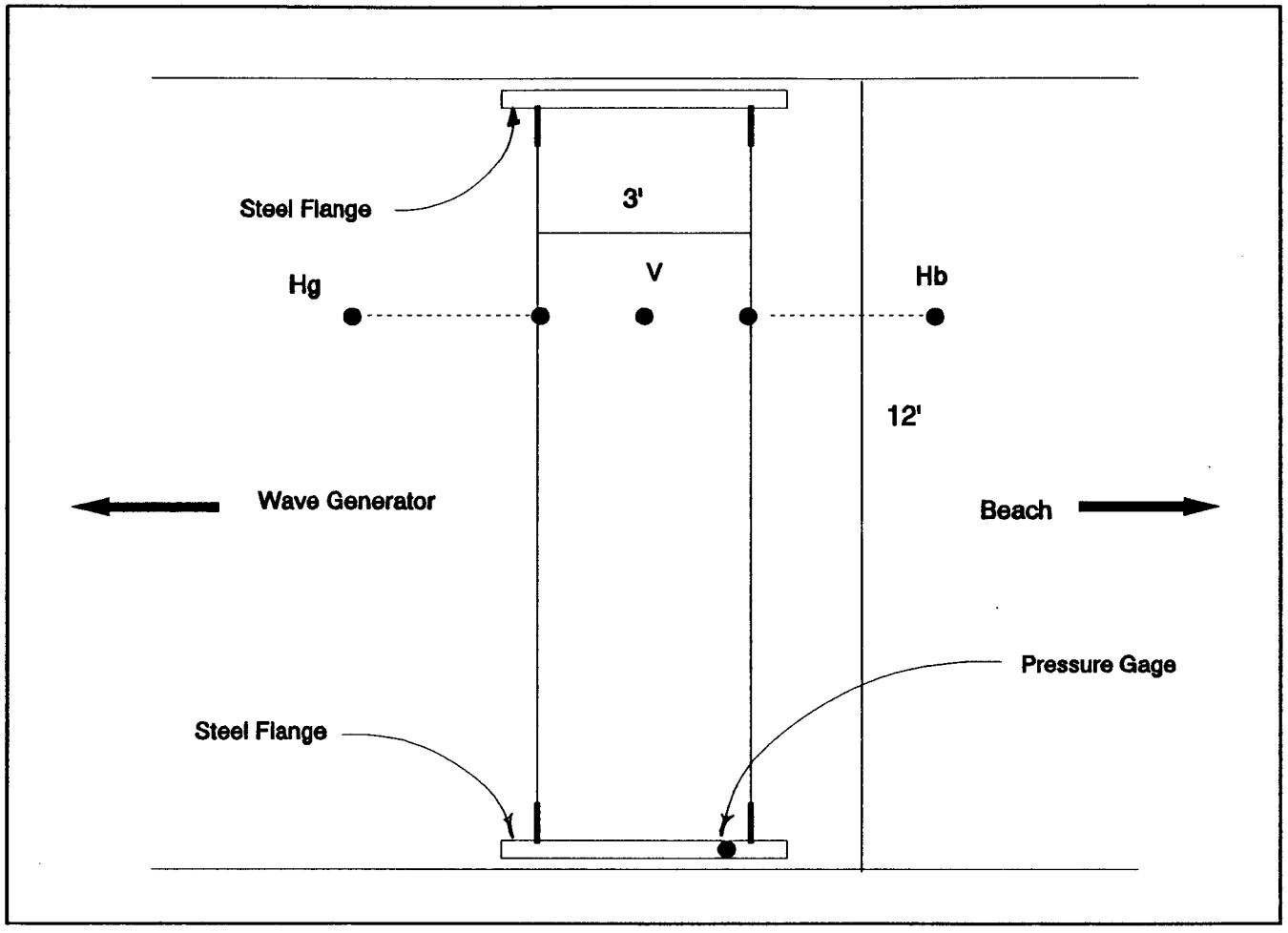

Figure C.2 Plan View of Flexible Cylinder Experiment

volume of fluid. A pressure transducer was placed in one of the fittings located at the top of the cylinder to record the internal pressure of the fluid enclosed in the membrane.

The center line of the cylinder was 6 feet off the tank floor, see Figure C.1. Two water levels were tested, 9 feet and 10.5 feet, which gave a submergence of 1.5 feet and 3, feet respectively. Monochromatic waves were generated with wave periods ranging from 1.5 seconds to 6 seconds. Random waves were also generated at both water depths. Wave heights varied from a couple of inches to over a foot. Sonic profilers were used to record the free surface above, fore, and aft of the cylinder. String pots and piano wire were used to measure the displacement of the membrane at three locations around the cylinder, see Figures C.1 and C.2. Various weights were tried on the end of the string pots to see if the point force affected the displacements; there was no noticeable effect. The displacement measurements were taken at the quarter point across the tank.

C.3 DATA COLLECTION

Seven channels of data were collected; Figure C.3 is a sample output of the raw data. The data was then edited and the appropriate scale factor applied, producing plots similar to Figure C.4. A sample header file is shown in Table C.1. Included in the header file are: test number, date and time of test, wave period, wavemaker span, water depth, and sampling rate. Various data analysis

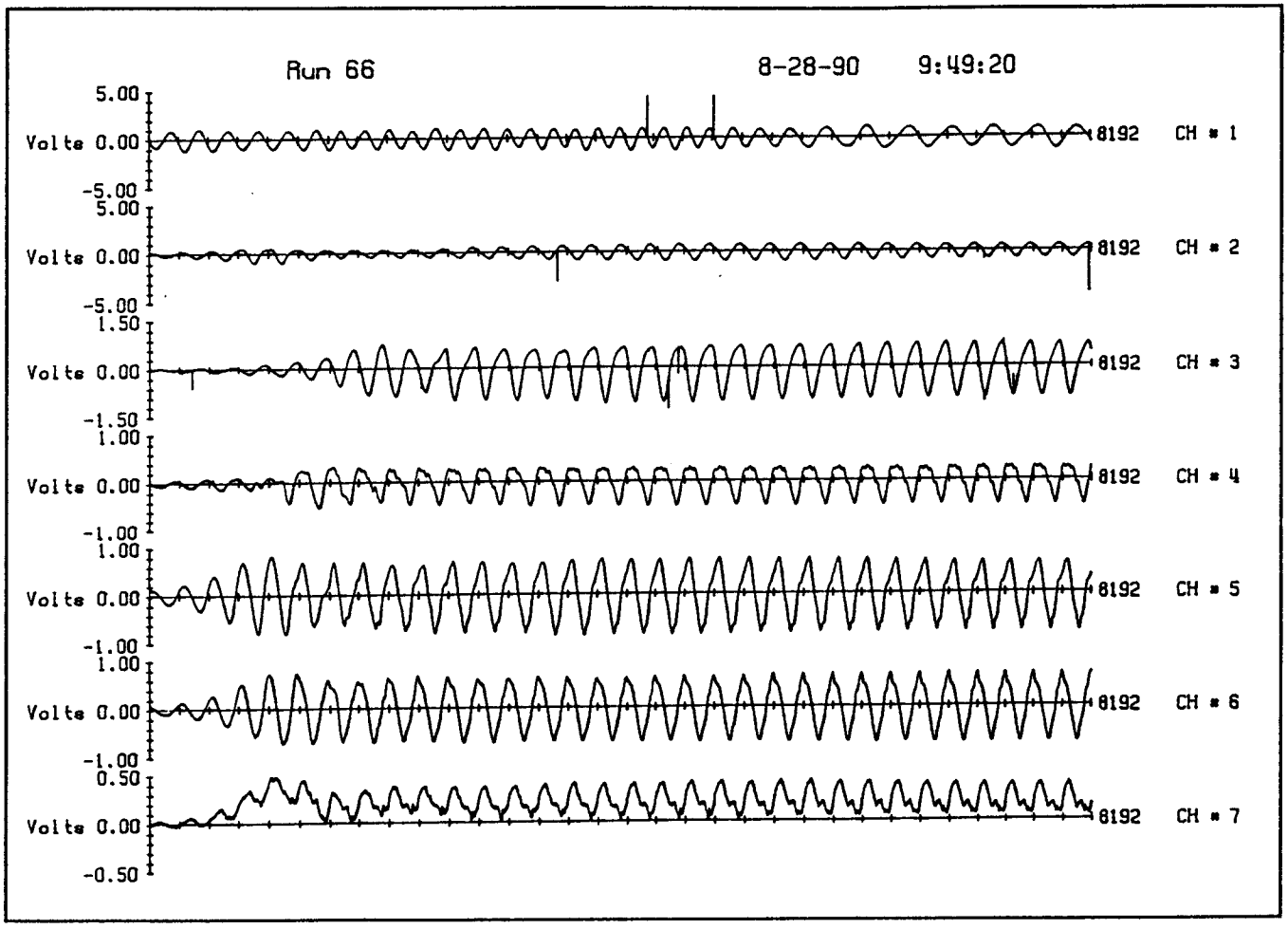

Figure C.3 Raw Data Run 66

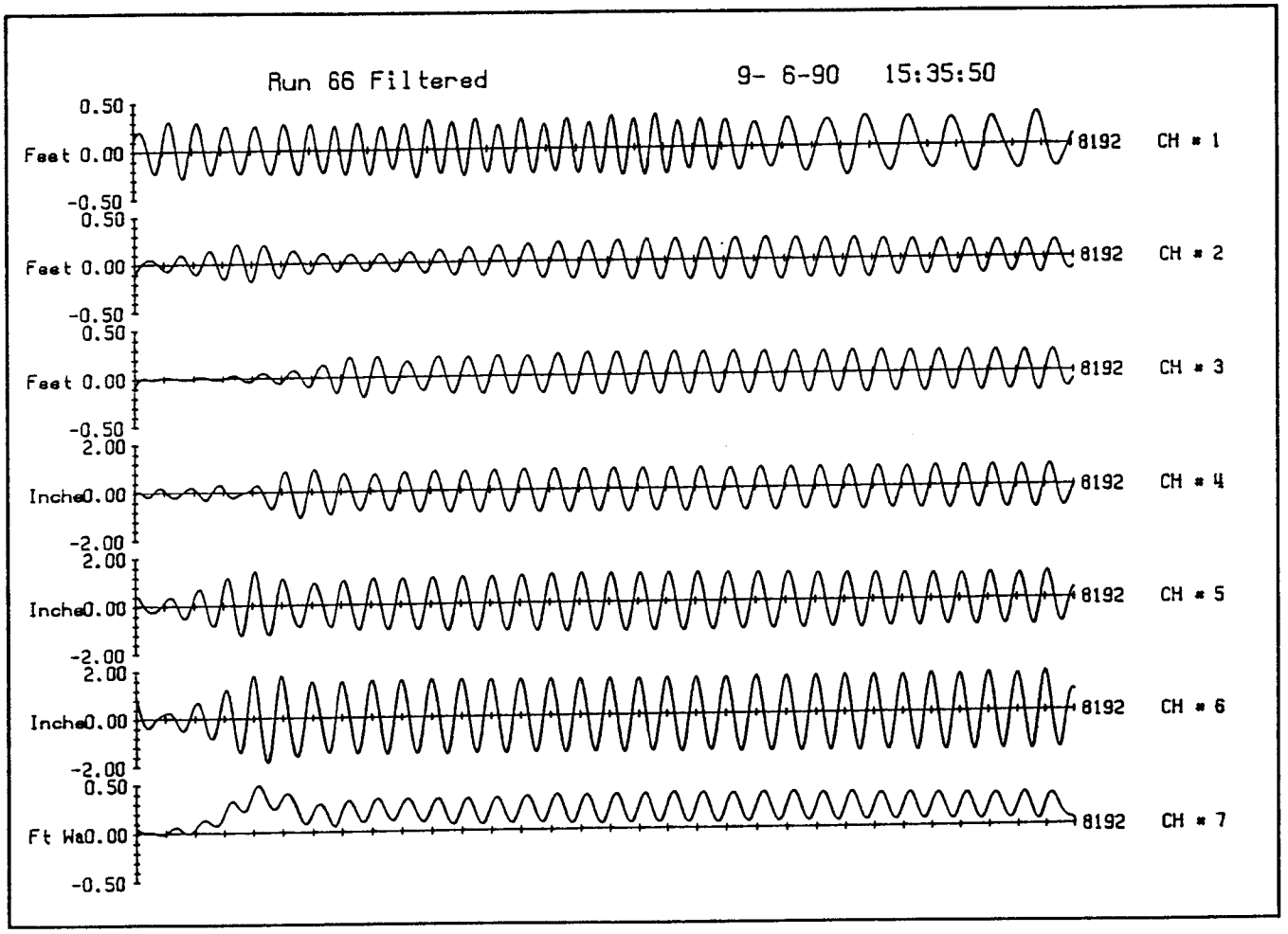

Figure C.4 Filtered Data Run 66

programs (provided by David Standley, staff member of the O.H. Hinsdale Wave Research Laboratory) were run on the data and provided a variety of information, see sample output in Table C.2. Table C.3 is a summary of the data collected for all 93 runs.

Originally, the plan had been to measure the displacements of the membrane by video techniques. Two video cameras, one mounted vertically under the center of the cylinder and one mounted 20 feet in front of the cylinder at an angle of 30 degrees, recorded the membrane's motion. The string pots were added because it was not clear how accurate the cameras would be in measuring the displacements. The video tapes do add qualitative information to the wave/structure interaction.

An attempt was made to strain gauge the membrane and this appeared to work during the trial. However, when the membrane was placed back into the wave tank for the experiment, the strain gauges ceased to operate, most likely because the in water-tight seals leaked.

C.4 INITIAL RESULTS

The reflection and transmission coefficients were computed for the monochromatic runs. The results are shown in Figures C.5 and C.6. In most wave barrier tests, the sum of the reflection coefficient and the transmission coefficient is one, implying conservation of energy. In this experiment, the coefficients added up to approximately one for most wave periods, but for the two

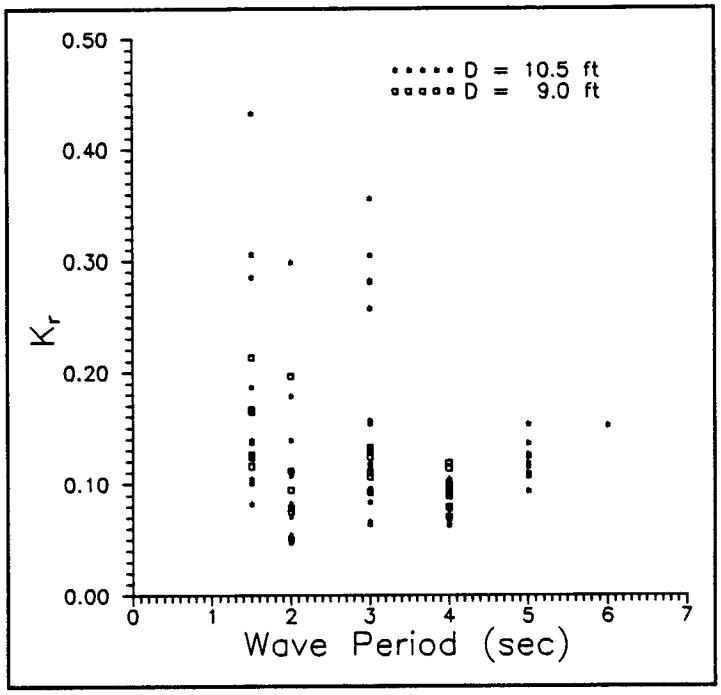

Figure C.5 Reflection Coefficient

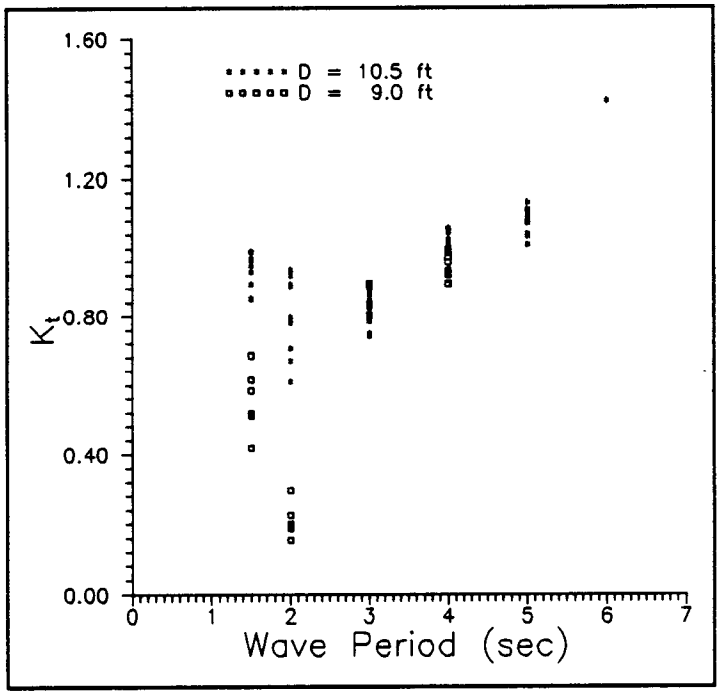

Figure C.6 Transmission Coefficient

second wave periods the coefficients added up to less than one. In the case of the 9 foot water depth, the coefficients added up to substantially less than one approximately 0.3. Obviously, the waves are transferring energy into the membrane and in fact, for that case the membrane was undergoing motions perpendicular to the wave crest. Is it possible that at a wave period of 2 seconds the membrane becomes a wave maker in the cross-tank direction? The sonic profilers were placed at the center line of the tank and may have missed the cross-wave energy.

C.5 FUTURE APPLICATION OF THE DATA SET

Only a few of the runs were used to verify the numerical model, even though a large data set of information has been collected. The following is a preliminary list of analyses that should be conducted on this data set:

- Evaluate the jump in internal pressure that occurs as the membrane is loaded. Compare the increase in the internal pressure to the starting pressure. Does the period of excitation affect the increase in internal pressure?
- Factor into the analysis the starting internal pressure. Is the membrane cylinder more effective as a wave barrier the stiffer the cylinder?
- Compare the maximum displacements of the cylinder to the wave height. How does the internal pressure affect this?
- Evaluate the phase information between the various channels of data.

- Develop a procedure to utilize the random wave data collected.

Table C.1 Header File Run 66

Test identification .....(80 char). : Cylindrical Membrane
Run identification .....(40 char). : Run 66
Investigator ID .....(40 char). : Laurie Broderick
Date of test .....(20 char). : 28-Aug-90
Time of test .....(20 char). : 09:41
Name of Raw data file .....(32 char). : Run.066
Name of Zeroes file .....(32 char). : Zero.066
Name of Spectrum file .....(32 char). : Spec.066
Name of Time series file ..(32 char). : Ts.066
Name of listing file .....(32 char). : List.066
Number of data channels .....(I). : 7
Number of points in zeroes file .(I). : 256
Number of points in data file ...(I). : 8192
Starting block to reduce .....(I). : 1
Number of points to reduce .....(I). : 8192
Wave height channel number .....(I). : 1
Phase reference to channel # ....(I). : 2
Random wave = 1, Periodic wave = 0 .. : 0
Random wave spectrum type (40 char).. :
Delta-T (Seconds) .....(F). :
Frequency (Hz) .....(F). : .667
Number of points per period .....(I). : 256
Estimated wave height (Ft).....(F). : 1.00000
Span (wavemaker setting) .....(F). : 60.00000
Towing speed (Ft/Sec) .....(F). : .00000
Water Depth at wave board (Ft) ..(F). : 12.00000
Water Depth at test section .....(F). : 9.00000
Deans Case Number .....(10 char). :
Material or Fabric type ...(40 char). :
Number of channels to reduce.....(I). : 7

Channel number .....(I). : 1
Channel identifier .....(80 char). : Incident Wave
Transducer identifier .....(40 char). : Eta 1
Calibration slope .....(F). : -.26667
Calibration intercept .....(F). : .00000
Physical units .....(10 char). : Feet
Filter cut-off frequency (Hz)....(F). : 1.00000
Rockland filter freqency (Hz)....(F). : 0.00000
Marsh-McBirney time constant TAU.(F). : .00000

Table C.1 Header File Run 66

Channel number .....(I). : 2
Channel identifier .....(80 char). : Wave At Model
Transducer identifier .....(40 char). : Eta 2
Calibration slope .....(F). : -.26667
Calibration intercept .....(F). : .00000
Physical units .....(10 char). : Feet
Filter cut-off frequency (Hz)....(F). : 1.00000
Rockland filter freqency (Hz)....(F). : 0.00000
Marsh-McBirney time constant TAU.(F). : .00000

Channel number .....(I). : 3
Channel identifier .....(80 char). : Transmitted Wave
Transducer identifier .....(40 char). : Eta 3
Calibration slope .....(F). : -.26667
Calibration intercept .....(F). : .00000
Physical units .....(10 char). : Feet
Filter cut-off frequency (Hz)....(F). : 1.00000
Rockland filter freqency (Hz)....(F). : 0.00000
Marsh-McBirney time constant TAU.(F). : .00000

Channel number .....(I). : 4
Channel identifier .....(80 char). : Horiz G String Pot
Transducer identifier .....(40 char). : Horiz G String Pot
Calibration slope .....(F). : 2.50000
Calibration intercept .....(F). : .00000
Physical units .....(10 char). : Inches
Filter cut-off frequency (Hz)....(F). : 1.00000
Rockland filter freqency (Hz)....(F). : 20.00000
Marsh-McBirney time constant TAU.(F). : .00000

Channel number .....(I). : 5
Channel identifier .....(80 char). : Vertical String Pot
Transducer identifier .....(40 char). : Vertical String Pot
Calibration slope .....(F). : 1.66667
Calibration intercept .....(F). : .00000
Physical units .....(10 char). : Inches
Filter cut-off frequency (Hz)....(F). : 1.00000
Rockland filter freqency (Hz)....(F). : 20.00000
Marsh-McBirney time constant TAU.(F). : .00000

Table C.1 Header File Run 66

Channel number .....(I). : 6
Channel identifier .....(80 char). : Horiz B String Pot
Transducer identifier .....(40 char). : Horiz B String Pot
Calibration slope .....(F). : 2.50000
Calibration intercept .....(F). : .00000
Physical units .....(10 char). : Inches
Filter cut-off frequency (Hz)....(F). : 1.00000
Rockland filter freqency (Hz)....(F). : 20.00000
Marsh-McBirney time constant TAU.(F). : .00000

Channel number .....(I). : 7
Channel identifier .....(80 char). : Pressure
Transducer identifier .....(40 char). : Pressure
Calibration slope .....(F). : 1.00000
Calibration intercept .....(F). : .00000
Physical units .....(10 char). : Ft Water
Filter cut-off frequency (Hz)....(F). : 1.00000
Rockland filter freqency (Hz)....(F). : 20.00000
Marsh-McBirney time constant TAU.(F). : .00000

Table C.2 Sample Computer Output Run 66

```
          9- 6-1990     16:18:36.17

          OSU WRF time series data reduction  (29-Jul-88 version)

                              Cylindrical Membrane

 Run identification ..................... : Run 66

 Investigator ........................... : Laurie Broderick

 Data collection date ................... : 28-Aug-90            09:41
 Header information file name ......... : hdr.066
 Raw data file name ..................... : Run.066
 Raw data zeroes file name ............. : Zero.066
 Spectrum output file name ............. : Spec.066
 Clean time series output file name ... : Ts.066
 Depth at waveboard (Ft) ............... =   12.00000
 Depth at test section (Ft) ............ =    9.00000
 Number of data channels collected .... =   7
 Number of data points collected ...... =  8192
 Number of data points reduced ........ =  8192
 Starting block (256 points/block) .... =     1
 Wave period (Sec) ..................... =    1.49925
 Wave maker frequency (Hz) ............. =     .66700
 Wavemaker span (0. to 1000.) ......... =   60.00000
 Estimated wave height (Ft) ............ =    1.00000
 Deans case number ..................... =
 Number of points per period ........... =  256
 It took    7.20 seconds for an FFT of 8192 points.
-------------------------------------------------------
 Channel #   1  Feet         Incident Wave


     Time series statistics before filtering
             Mean ....... =        .0155
             Mean square  =        .0370

       20 Largest amplitudes:

   Freq      Amplitude       Freq      Amplitude       Freq      Amplitude

   .85459      .116536       .45856      .092902       .87544      .091929
   .83375      .076839       .47941      .069707       .66700      .061885
   .43772      .061386       .70869      .054095       .50025      .051231
   .62531      .049284       .75037      .043343       .79206      .043081
   .41688      .040708       .56278      .038928       .89628      .038320
   .54194      .035004       .77122      .034934       .60447      .032488
   .72953      .029771       .68784      .029457

 Energy from the spectrum before filtering =     3.69921E-02
 Energy from the spectrum after filtering  =     3.68190E-02
 Ratio (Percent) ....................... =  99.53

 Energy from the spectrum after filtering  =     3.68190E-02
 Variance of time series ............... =     3.68189E-02
 Ratio (Percent) ....................... = 100.00
 Difference ............................ =     6.33299E-08
```

Table C.2 Sample Computer Output Run 66

```
Channel #   2  Feet        Wave At Model

    Time series statistics before filtering
            Mean ....... =        .0089
            Mean square  =        .0156

      20 Largest amplitudes:

  Freq      Amplitude      Freq      Amplitude      Freq      Amplitude

  .66700      .158170      .64616      .056773     1.33400      .021167
  .70869      .019341      .75037      .018659      .72953      .016973
  .62531      .016424      .68784      .016178      .77122      .016161
  .79206      .011521      .81291      .007154     1.35484      .006307
  .54194      .004750     2.00100      .004571      .56278      .004359
 1.41737      .003850     1.37569      .003829      .83375      .003741
  .52109      .003727     1.39653      .003669

Energy from the spectrum before filtering =     1.55875E-02
Energy from the spectrum after filtering  =     1.52282E-02
Ratio (Percent) ......................... =  97.69

Energy from the spectrum after filtering  =     1.52282E-02
Variance of time series ................. =     1.52282E-02
Ratio (Percent) ......................... = 100.00
Difference .............................. =     1.49012E-08
-------------------------------------------------------------
Channel #   3  Feet        Transmitted Wave

    Time series statistics before filtering
            Mean ....... =        .0098
            Mean square  =        .0191

      20 Largest amplitudes:

  Freq      Amplitude      Freq      Amplitude      Freq      Amplitude

  .66700      .173775      .64616      .046380     1.33400      .035050
  .68784      .029911      .70869      .024558      .72953      .023493
  .62531      .021681      .75037      .015822     1.35484      .014732
 1.31316      .011922      .60447      .011130     1.29231      .010586
  .81291      .010069      .83375      .009214      .56278      .008762
  .58363      .008594      .02084      .007254      .54194      .007109
  .50025      .006375      .52109      .006167

Energy from the spectrum before filtering =     1.90693E-02
Energy from the spectrum after filtering  =     1.80504E-02
Ratio (Percent) ......................... =  94.66

Energy from the spectrum after filtering  =     1.80504E-02
Variance of time series ................. =     1.80504E-02
Ratio (Percent) ......................... = 100.00
Difference .............................. =     7.45058E-09
```

Table C.2 Sample Computer Output Run 66

```
Channel #   4  Inches      Horiz G String Pot


    Time series statistics before filtering
            Mean ....... =       -.0529
            Mean square  =        .3792

      20 Largest amplitudes:

  Freq      Amplitude      Freq      Amplitude      Freq      Amplitude

  .66700      .745674    1.33400      .221807      .64616      .207259
  .62531      .139361     .60447      .107717      .68784      .102580
 2.00100      .095803     .58363      .082512      .75037      .072560
  .70869      .072130     .72953      .071796      .77122      .063946
  .56278      .051125    1.31316      .049839      .79206      .046251
 1.47991      .041770    3.33500      .041704     1.29231      .031262
 4.00200      .029125     .87544      .028276

Energy from the spectrum before filtering =     3.79222E-01
Energy from the spectrum after filtering  =     3.40340E-01
Ratio (Percent) ......................... =  89.75

Energy from the spectrum after filtering  =     3.40340E-01
Variance of time series ................. =     3.40340E-01
Ratio (Percent) ......................... = 100.00
Difference .............................. =     1.78814E-07
------------------------------------------------------------
Channel #   5  Inches      Vertical String Pot


    Time series statistics before filtering
            Mean ....... =        .0104
            Mean square  =        .6223

      20 Largest amplitudes:

  Freq      Amplitude      Freq      Amplitude      Freq      Amplitude

  .66700     1.067597    1.33400      .143380      .64616      .138019
  .79206      .083038     .77122      .079387     2.00100      .070894
  .81291      .070824     .75037      .069194      .72953      .058574
  .70869      .056912     .83375      .049457      .68784      .046589
 3.33500      .044849    1.31316      .044628      .60447      .038798
  .58363      .037884    1.29231      .035910      .56278      .033546
 1.47991      .030757    1.27147      .030559

Energy from the spectrum before filtering =     6.22289E-01
Energy from the spectrum after filtering  =     6.01521E-01
Ratio (Percent) ......................... =  96.66

Energy from the spectrum after filtering  =     6.01521E-01
Variance of time series ................. =     6.01521E-01
Ratio (Percent) ......................... = 100.00
Difference .............................. =    -5.96046E-08
```

Table C.2 Sample Computer Output Run 66

```
Channel #   6  Inches      Horiz B String Pot


    Time series statistics before filtering
            Mean ..... =       -.0029
            Mean square  =      1.1626

      20 Largest amplitudes:

  Freq      Amplitude      Freq      Amplitude      Freq      Amplitude

  .66700    1.471096       .77122     .116355       .75037     .112456
  .62531     .109074       .79206     .108916      1.33400     .103476
  .64616     .099068       .72953     .098822       .70869     .092421
  .60447     .090246      2.00100     .086693       .81291     .086228
  .68784     .085632       .58363     .071430      3.33500     .056624
  .83375     .053625       .56278     .050277      1.31316     .041305
 4.00200     .040438      1.47991     .033973

Energy from the spectrum before filtering =     1.16260E+00
Energy from the spectrum after filtering  =     1.14207E+00
Ratio (Percent) ......................... =  98.23

Energy from the spectrum after filtering  =     1.14207E+00
Variance of time series ................. =     1.14207E+00
Ratio (Percent) ......................... = 100.00
Difference .............................. =    -4.76837E-07
------------------------------------------------------------
Channel #   7  Ft Water    Pressure


    Time series statistics before filtering
            Mean ..... =        .1996
            Mean square  =      .0141

      20 Largest amplitudes:

  Freq      Amplitude      Freq      Amplitude      Freq      Amplitude

  .66700     .124348      1.33400     .042654       .08337     .035470
  .10422     .035411       .12506     .033983       .06253     .033716
  .04169     .030353       .64616     .028350       .14591     .027392
  .02084     .025095      1.31316     .020767       .16675     .011955
 2.66800     .011112      1.29231     .010819       .60447     .009799
 2.00100     .009339      3.33500     .009176       .58363     .009107
  .68784     .009093       .22928     .009072

Energy from the spectrum before filtering =     1.40517E-02
Energy from the spectrum after filtering  =     1.23579E-02
Ratio (Percent) ......................... =  87.95

Energy from the spectrum after filtering  =     1.23579E-02
Variance of time series ................. =     1.23579E-02
Ratio (Percent) ......................... = 100.00
Difference .............................. =     1.21072E-08
```

Table C.3 Flexible Cylinder Data

DATE	TIME	RUN #	d	wt	pressure	T	SPAN	K_r	K_t
Aug 23 1990	11:03	1	10.5'	8 oz		1.5	40	0.4322	0.9710
	11:10	2	10.5	8		1.5	40	0.2847	0.9280
	11:22	3	10.5	8		1.5	60	0.1365	0.9880
	11:31	4	10.5	8		1.5	60	0.1004	0.8930
		1a	10.5	8		1.5	40		
		3a	10.5	8		1.5	60		
		1b	10.5	8		1.5	40		
	13:50	5	10.5	8	0.342	1.5	70	0.1387	0.8930
	14:14	6	10.5	8	0.550	1.5	70	0.1863	0.8930
	14:24	7	10.5	8	0.460	2.0	40	0.1386	0.9190
	14:34	8	10.5	8	0.370	2.0	40	0.1784	0.9340
	14:43	9	10.5	8	0.333	2.0	60	0.0472	0.7960
	14:52	10	10.5	8	0.670	2.0	60	0.1109	0.8860
	15:00	11	10.5	8	0.540	2.0	70	0.2980	0.7880
	15:09	12	10.5	8	0.468	2.0	70	0.0483	0.7050
	15:18	13	10.5	8	0.730	2.0	80	0.1073	0.7030
	15:27	14	10.5	8	0.592	2.0	80	0.0523	0.6080
	15:36	15	10.5	8	0.518	3.0	50	0.2802	0.8280
	15:46	16	10.5	8	0.444	3.0	50	0.1532	0.8330
	15:56	17	10.5	8	0.403	3.0	90	0.0918	0.8730

Table C.3 Flexible Cylinder Data

DATE	TIME	RUN #	d	wt	pressure	T	SPAN	K_r	K_t
Aug 23 1990	16:06	18	10.5	8	0.333	3.0	90	0.2820	0.848
	16:15	19	10.5	8	0.738	3.0	130	0.3558	0.861
	16:25	20	10.5	8	0.555	3.0	130	0.1560	0.846
	16:36	21	10.5	8	0.471	3.0	150	0.0833	0.824
	16:46	22	10.5	8	0.721	3.0	150	0.2568	0.830
Aug 24 1990	08:24	23	10.5	8	0.487	4.0	160	0.0986	0.935
	08:36	24	10.5	8	0.755	4.0	160	0.0785	1.054
	08:47	25	10.5	8	0.570	4.0	110	0.0929	1.058
	08:54	26	10.5	8	0.530	4.0	110	0.1040	1.012
	09:01	27	10.5	8	0.492	4.0	200	0.0651	1.025
	09:10	28	10.5	8	0.410	4.0	200	0.0709	1.000
	09:19	29	10.5	8	0.385	4.0	230	0.0623	1.025
	09:27	30	10.5	8	0.750	4.0	230	0.0800	1.043
	09:37	31	10.5	8	0.610	5.0	110	0.1095	1.096
	09:46	32	10.5	8	0.550	5.0	110	0.0932	1.042
	09:54	33	10.5	8	0.480	5.0	160	0.1090	1.085
	10:05	34	10.5	8	0.444	5.0	160	0.1075	1.033
	10:15	35	10.5	8	0.390	5.0	220	0.1185	1.012
	10:24	36	10.5	8	0.725	5.0	220	0.1359	1.074
	10:31	37	10.5	8	0.650	5.0	280	0.1060	1.088

Table C.3 Flexible Cylinder Data

DATE	TIME	RUN #	d	wt	pressure	T	SPAN	K_r	K_t
Aug 24 1990	10:42	38	10.5	8	0.540	5.0	280	0.1233	1.132
	10:51	39	10.5	8	0.500	5.0	320	0.1258	1.112
	11:00	40	10.5	8	0.440	5.0	320	0.1528	1.071
Aug 27 1990	08:27	41	10.5	8	0.583	6.0	200	0.1515	1.421
	08:37	42	10.5	8	0.460	3.0	90	0.9580	0.790
	08:51	43	10.5	4	0.833	3.0	90	0.1175	0.794
	09:12	44	10.5	4	0.540	3.0	90	0.1128	0.796
	09:22	45	10.5	4	0.470	3.0	90	0.1171	0.784
	09:35	46	10.5	4	0.410	3.0	150	0.3044	0.751
	09:49	47	10.5	8	0.930	1.5	40	0.1042	0.992
	09:59	48	10.5	8	0.990	1.5	60	0.3055	0.945
	11:10	49	10.5	8	0.870	1.5	80	0.0819	0.850
	11:19	50	10.5	8	1.000	2.0	60	0.0540	0.894
	11:29	51	10.5	8	1.010	2.0	80	0.0824	0.778
	11:39	52	10.5	8	1.020	2.0	100	0.0707	0.669
	11:55	53	10.5	8	0.980	3.0	130	0.0638	0.7824
	13:44	54	10.5	8	0.940	3.0	150	0.0657	0.7507
	13:56	55	10.5	8	1.000	4.0	160	0.1024	1.047
	14:02	56	10.5	8	1.050	4.0	230	0.0772	1.015
	14:10	57	10.5	8	1.050	5.0	220	0.1239	1.107

Table C.3 Flexible Cylinder Data

DATE	TIME	RUN #	d	wt	pressure	T	SPAN	K_r	K_t
Aug 27 1990	14:20	58	10.5	8	1.030	5.0	320	0.1146	1.130
	14:45	59	10.5	8	1.070	R			
	14:59	60	10.5	8	1.070	R			
	15:23	61	10.5	8	1.000	R			
	15:46	62	10.5	8	0.940	R			
Aug 28 1990	09:11	63	9.0	8	0.540	1.5	40	0.1261	0.6137
	09:21	64	9.0	8	0.430	1.5	40	0.2134	0.684
	09:32	65	9.0	8	0.730	1.5	60	0.1236	0.5101
	09:43	66	9.0	8	0.600	1.5	60	0.1664	0.584
	09:53	67	9.0	8	0.530	1.5	80	0.1157	0.419
	10:04	68	9.0	8	0.750	1.5	80	0.1642	0.605
	11:17	69	9.0	8	0.740	2.0	60	0.0756	0.300
	11:27	70	9.0	8	0.600	2.0	60	0.1961	0.2252
	11:38	71	9.0	8	0.560	2.0	80	0.0947	0.194
	11:49	72	9.0	8	0.480	2.0	80	0.1114	0.154
	12:02	73	9.0	8	0.780	2.0	100	0.0786	0.187
	12:14	74	9.0	8	0.650	2.0	100	0.0507	0.199
	13:42	75	9.0	8	0.800	3.0	90	0.1102	0.886
	13:53	76	9.0	8	0.680	3.0	90	0.1060	0.895
	14:05	77	9.0	8	0.610	3.0	110	0.0924	0.8022

Table C.3 Flexible Cylinder Data

DATE	TIME	RUN #	d	wt	pressure	T	SPAN	K_r	K_t
Aug 28 1990	14:16	78	9.0	8	0.560	3.0	110	0.1320	0.804
	14:27	79	9.0	8	0.710	3.0	130	0.1291	0.836
	14:39	80	9.0	8	0.630	3.0	130	0.1235	0.831
	14:50	81	9.0	8	0.560	4.0	120	0.0793	0.9208
	14:58	82	9.0	8	0.540	4.0	120	0.0909	0.892
	15:06	83	9.0	8	0.490	4.0	160	0.0704	0.895
	15:15	84	9.0	8	0.820	4.0	160	0.0780	0.927
	15:23	85	9.0	8	0.730	4.0	200	0.0958	0.970
	15:31	86	9.0	8	0.670	4.0	200	0.1139	0.922
	15:44	87	9.0	8	0.620	4.0	240	0.0884	0.998
Aug 29 1990	08:27	88	9.0	8	0.630	4.0	240	0.1184	0.989
	08:37	89	9.0	8	0.510	4.0	280	0.1003	0.991
	08:46	90	9.0	8	0.440	4.0	280	0.0939	0.955
	09:11	91	9.0	8	0.620	R			
	09:33	92	9.0	8	0.690	R			
	09:51	93	9.0	8	0.670	R			